

Visualization of Porosity in Carbon Fiber Reinforced Polymers

DISSERTATION

zur Erlangung des akademischen Grades

Doktor der technischen Wissenschaften

eingereicht von

Andreas Reh, M.Sc.

Matrikelnummer 1228520

an der
Fakultät für Informatik der Technischen Universität Wien

Betreuung: Ao.Univ.Prof. Dipl.-Ing. Dr.techn. Eduard Gröller

Diese Dissertation haben begutachtet:

(Ao.Univ.Prof. Dipl.-Ing.
Dr.techn. Eduard Gröller)

(Prof. Dipl.-Ing. Dr.techn.
Markus Hadwiger)

(Prof. Klaus Müller, Ph.D.)

Wien, 31.01.2015

(Andreas Reh, M.Sc.)

Visualization of Porosity in Carbon Fiber Reinforced Polymers

DISSERTATION

submitted in partial fulfillment of the requirements for the degree of

Doktor der technischen Wissenschaften

by

Andreas Reh, M.Sc.

Registration Number 1228520

to the Faculty of Informatics
at the Vienna University of Technology

Advisor: Ao.Univ.Prof. Dipl.-Ing. Dr.techn. Eduard Gröller

Diese Dissertation haben begutachtet:

(Ao.Univ.Prof. Dipl.-Ing.
Dr.techn. Eduard Gröller)

(Prof. Dipl.-Ing. Dr.techn.
Markus Hadwiger)

(Prof. Klaus Müller, Ph.D.)

Vienna, 31.01.2015

(Andreas Reh, M.Sc.)

*If you cannot stand the heat,
get out of the kitchen.*

HARRY S. TRUMAN

Erklärung zur Verfassung der Arbeit

Andreas Reh, M.Sc.
Haidbachstraße 45, 4061 Pasching

Hiermit erkläre ich, dass ich diese Arbeit selbständig verfasst habe, dass ich die verwendeten Quellen und Hilfsmittel vollständig angegeben habe und dass ich die Stellen der Arbeit - einschließlich Tabellen, Karten und Abbildungen -, die anderen Werken oder dem Internet im Wortlaut oder dem Sinn nach entnommen sind, auf jeden Fall unter Angabe der Quelle als Entlehnung kenntlich gemacht habe.

(Ort, Datum)

(Unterschrift Verfasser)

Acknowledgements

This thesis is the result from a collaborative work of the Institute of Computer Graphics and Algorithms, Vienna University of Technology, and the Upper Austrian University of Applied Sciences - Wels Campus from December 2010 until December 2014.

I want to thank my supervisors Eduard Gröller and Christoph Heinzl for their great guidance and support during the last years. I would also like to thank the CT-group of the University of Applied Sciences Upper Austria, Wels Campus, especially Johann Kastner, Bernhard Plank, Christian Gusenbauer, Johannes Weissenböck, Artem Amirkhanov, Aleksandr Amirkhanov, Dietmar Salaberger, Michael Reiter, Sascha Senck and Elena Sell as well as Günther Mayr from the active thermography group for their inspirations and contributions to this thesis and to a productive and enjoyable working environment. Thanks to the vis-group of the Institute of Computer Graphics and Algorithms, Vienna University of Technology, for their suggestions and valuable advice when preparing conference talks. Further I thank Jakov Šekelja from FACC for the preparation of CFRP samples and evaluation feedback, Michael Schöbel for providing the AISiC datasets and the Institute for Carbon Composites, Technische Universität München (University of Technology, Munich) for their input regarding 4D-XCT tasks. Last but not least, I want to dedicate this thesis to my parents who enabled my academic studies with their support.

This work has been funded by the program "Regionale Wettbewerbsfähigkeit OÖ 2010-2013", which was financed by the European Regional Development Fund and the Government of Upper Austria. Furthermore the presented work was partly financed by the K-Project ZPT of the Austrian Research Promotion Agency (FFG) and the doctoral program "Förderung des wissenschaftlichen Nachwuchses an der Fachhochschule OÖ" of the University of Applied Sciences Upper Austria financed by the Government of Upper Austria.

Abstract

Industrial research is continuously increasing efforts in designing new-tailored light-weight materials in order to meet the high demands regarding efficiency, environment, safety as well as comfort. Especially in the aeronautics industry a high demand for advanced composite materials is observable. The new generations of aircrafts are made of more than 50 % of these novel composite materials. Carbon fiber reinforced polymers (CFRPs) are currently considered as the most promising candidate since this material is outperforming the majority of conventional materials. As a result of the manufacturing process this material tends to have pores inside. Pores in the material are typically inclusions of air. As they have an impact on the mechanical properties of the component, their determination and evaluation is an important task in quality control and a particular challenge for non-destructive testing (NDT) practitioners. Besides the characterization of individual pores, their spatial distribution in the tested component is a relevant factor. For example, a high concentration of pores in certain regions leads to different material characteristics as compared to a homogenous distribution of the pores.

This work is based on 3D X-ray Computed Tomography (XCT) to gain new insight into CFRP components. Based on domain experts' questions, specific tasks were derived. Besides the quantitative porosity determination, the main visualization tasks are: giving a fast porosity overview, exploring the individual pores, and tracking features over time based on XCT time-series. In this thesis, three novel visual analysis tools are presented to solve these tasks.

To enhance the evaluation workflow for non-destructive testing (NDT) practitioners, a visualization pipeline for the interactive exploration and visual analysis of CFRP specimens is developed. After the calculation of local pore properties, i.e., volume, surface, extents and shape factors, a drill-down approach is employed to explore pores in a CFRP specimen. Therefore **Porosity Maps (PM)** are presented to allow for a fast porosity overview and selecting a region of interest. Pores in this region may be filtered and visualized with a parallel-coordinates selection.

Furthermore a novel visualization technique which allows for a fast porosity overview and exploration of pores by focusing more on their shapes is proposed. In this method, all objects (pores) are clustered into a **Mean Object (MObject)**. To explore this MObject, the visualization of mean object sets (MObject Sets) in a radial and a parallel alignment is introduced. By selecting a specific property such as the volume or shape factor and the desired number of classes, a MObject is split up into sub-classes. With this approach, intended classifications and visualizations of MObjects may be explored by the user. These representative MObjects may be exported as volumetric datasets to serve as input for successive calculations and simulations.

For an overview of the pore properties in the dataset local MObjects are calculated in a grid and combined with a color-coded homogeneity visualization. Both approaches were evaluated with real-world CFRP specimens.

To go one step further, time as a fourth dimension is added to analyze a process over time, e.g., how the features evolve and formate over time. Therefore features in a series of XCT scans are tracked with the **Fuzzy Feature Tracking** approach and are then visualized together with the extracted events in multiple linked-views, each emphasizing individual aspects of the 4D time-series data. Spatial feature information, global temporal overview, and global temporal evolution of how the features are tracked and connected over the whole time-series are covered with the visual-analysis system. The results and advantages of the Fuzzy Feature Tracking tool are demonstrated using various real-world applications, such as AlSiC alloys under thermal load or wood shrinkage analyses.

Kurzfassung

In der Luft- und Raumfahrtindustrie ist eine besonders hohe Nachfrage an Verbundwerkstoffen ersichtlich, da moderne Flugzeuge zu mehr als 50 % aus diesen Materialien gefertigt werden. Besonders kohlefaserverstärkte Kunststoffe (CFK) nehmen aufgrund ihrer Materialeigenschaften einen immer wichtigeren Stellenwert ein. Ihre besonders hohe Festigkeit in Relation zu ihrem niedrigen Gewicht machen sie zu dem aktuell vielversprechendsten Material für die Zukunft im Leichtbau. Aufgrund von Artefakten beim Herstellungsprozess tendieren diese Materialien dazu, porös zu sein. Da die kleinen Lufteinschlüsse einen sehr großen Einfluss auf die Materialeigenschaften wie die Druckfestigkeit, die interlaminae Scherfestigkeit oder das Elastizitätsmodul haben, ist es ein wichtiger Schritt in der Qualitätssicherung von CFK-Komponenten, die Porosität quantitativ zu ermitteln sowie auch die Verteilung und die Formfaktoren der einzelnen Poren zu analysieren. Eine inhomogene Verteilung der Poren im Bauteil wie z.B. in einer bestimmten Lage führt zu anderen Materialeigenschaften wie eine homogene Verteilung.

In dieser Arbeit wurde die Röntgencomputertomographie (CT) als drei-dimensionales und zerstörungsfreies Verfahren angewendet, um Poren in CFK zu analysieren. Basierend auf praxisrelevanten Fragestellungen von Endanwendern, wie z.B. Materialwissenschaftlern oder Statikern im Bereich der zerstörungsfreien Prüfung und Qualitätssicherung, wurden spezifische Aufgaben abgeleitet und lösungsorientierte Visualisierungsmethoden implementiert.

Neben einer exakten Porositätsermittlung sowie der Berechnung von lokalen Poreneigenschaften, wie Volumen, Dimensionen und Formfaktoren, wurden neue Visualisierungskonzepte entwickelt. Um eine schnelle Beurteilung von CFK-Komponenten zu ermöglichen, wurden **Porosity Maps (PM)** vorgestellt. Für die visuelle Analyse einzelner Poren wurde auf das Konzept der parallelen Koordinaten zurückgegriffen. In einem mehrstufigen Analyseverfahren können kritische Bereiche in den Porosity Maps interaktiv ausgewählt werden und in weiterer Folge die darin enthaltenen Poren mithilfe der parallelen Koordinaten gefiltert werden, um sie in einer 3D Darstellung zu visualisieren.

Weiters wurden Visualisierungskonzepte entwickelt, die sich bei der Darstellung der Homogenität sowie der Analyse der einzelnen Poren auf deren Formfaktoren fokussieren. Das Visualisierungskonzept von **Mean Objects (MObjects)** löst diese Anforderung. Dabei werden alle Einzelporen in einem CT-Datensatz basierend auf ihrem Mittelpunkt zentriert, aufsummiert und normalisiert. Der resultierende wahrscheinlichkeitbasierte Datensatz kann mit Transferfunktionen visualisiert werden. Um diese Durchschnittsporen weiter analysieren zu können, wurden interaktive Visualisierungen entwickelt. Dabei kann eine Durchschnittspore basierend auf einer berech-

neten Poreneigenschaft in weitere Durchschnittsporen aufgeteilt werden, um so die Analyse zu verfeinern. Als Ergebnis können die gefundenen repräsentativen Durchschnittsporen exportiert werden, um z.B. in weiterführende Simulationen einfließen zu können. Darüber hinaus kann die Homogenität der berechneten Poreneigenschaften über die gesamte CFK-Komponente visualisiert werden. In einer Homogenitätsvisualisierung können unter anderem lokale Abweichungen von durchschnittlichen Poreneigenschaften zur jeweiligen globalen durchschnittlichen Poreneigenschaft angezeigt werden. Beide Methoden wurden anhand von CFK-Proben demonstriert und verifiziert.

In weiterer Folge wurde zu den drei-dimensionalen Daten die Zeit als vierte Dimension hinzugefügt, um einen Prozess analysieren zu können. Ein mögliches Beispiel ist, wie innere Strukturen entstehen und sich über die Zeit entwickeln. Dazu werden Strukturen in einer zeitlichen Messreihe mit dem neu entwickelten **Fuzzy Feature Tracking** Konzept beobachtet und visualisiert. Räumliche Informationen werden ebenso wie eine zeitliche Übersicht und die zeitliche Entwicklung der Strukturen von einer Messung zur nächsten in den Visualisierungen dargestellt. Die Methoden wurden an realen Anwendungen wie der thermischen Belastung von AlSiC Legierungen oder einem Austrocknungsprozess von Holz demonstriert.

Contents

| | |
|--|-----------|
| List of Figures | xv |
| List of Tables | xx |
| 1 Introduction and Overview | 1 |
| 1.1 Carbon Fiber Reinforced Polymers | 2 |
| 1.2 Porosity Determination | 5 |
| 1.2.1 Acid Digestion | 5 |
| 1.2.2 Materialography | 5 |
| 1.2.3 Ultrasonic Testing | 5 |
| 1.2.4 Active Thermography | 5 |
| 1.2.5 3D X-Ray Computed Tomography | 7 |
| 1.3 Visualization Tasks | 9 |
| 1.4 Contributions of this Thesis | 11 |
| 2 Pre-processing | 13 |
| 2.1 Data Enhancement | 13 |
| 2.2 Segmentation of Pores | 13 |
| 2.3 Calculation of Pore Properties | 14 |
| 3 Porosity Maps - Visual Analysis of Porosity in Carbon Fiber Reinforced Polymers | 17 |
| 3.1 Tasks and Contributions | 18 |
| 3.2 Related Work | 19 |
| 3.3 Visualization Pipeline | 20 |
| 3.3.1 Data Acquisition | 21 |
| 3.3.2 Pre-processing | 22 |
| 3.4 Visual Analysis of Porosity | 22 |
| 3.4.1 Porosity Maps | 22 |
| 3.4.2 Interactive Exploration and Visualization | 24 |
| 3.4.3 Best-Viewpoint Calculation | 26 |
| 3.5 Results and Evaluation | 28 |
| 3.5.1 Quantitative Porosity Determination | 29 |
| 3.5.2 Segmentation Verification | 29 |
| 3.5.3 Visual Analysis of Porosity | 30 |

| | | |
|----------|---|-----------|
| 3.5.4 | Domain Experts Feedback | 31 |
| 3.5.5 | Evaluation Questionnaire | 35 |
| 3.6 | Summary | 35 |
| 4 | MObjects - Interactive Exploration of Defects in Industrial XCT Data | 37 |
| 4.1 | Tasks and Contributions | 39 |
| 4.2 | Related Work | 41 |
| 4.2.1 | Parameter-Space Analysis | 41 |
| 4.2.2 | Clustering | 42 |
| 4.2.3 | Hierarchical Visualization | 42 |
| 4.2.4 | Uncertainty Visualization | 42 |
| 4.2.5 | Comparative Visualization | 43 |
| 4.2.6 | Visualization of Multivariate Data | 43 |
| 4.3 | Visualization and Exploration Pipeline | 43 |
| 4.3.1 | Data Acquisition | 45 |
| 4.3.2 | Pre-processing | 45 |
| 4.4 | Visualization | 45 |
| 4.4.1 | MObject Visualization | 46 |
| 4.4.1.1 | Uncertainty Cloud | 46 |
| 4.4.1.2 | Transfer-Function Design | 46 |
| 4.4.2 | Local MObjects Visualization | 47 |
| 4.4.3 | MObject Set Visualization | 49 |
| 4.4.3.1 | Radial MObject Set Visualization (Beginners Mode) | 50 |
| 4.4.3.2 | Parallel MObject Set Visualization (Expert Mode) | 51 |
| 4.4.3.3 | Scaling through Visual Linking | 52 |
| 4.5 | Results and Evaluation | 52 |
| 4.5.1 | Local MObjects Visualization | 53 |
| 4.5.2 | Radial MObject Set Visualization | 58 |
| 4.5.3 | Parallel MObject Set Visualization | 59 |
| 4.5.4 | Evaluation Questionnaire | 60 |
| 4.6 | Summary | 63 |
| 5 | Fuzzy Feature Tracking - Visual Analysis of Industrial 4D-XCT Data | 65 |
| 5.1 | Tasks and Contributions | 67 |
| 5.2 | Related Work | 69 |
| 5.2.1 | Fuzzy Feature Tracking | 70 |
| 5.2.2 | Fuzzy Tracking Graph Visualization | 70 |
| 5.2.3 | Uncertainty Visualization | 71 |
| 5.3 | Visual-Analysis Pipeline | 71 |
| 5.3.1 | Data Acquisition | 73 |
| 5.3.2 | Pre-processing | 73 |
| 5.4 | Fuzzy Feature Tracking | 73 |
| 5.5 | Visual Analysis of 4D-XCT Data | 77 |
| 5.5.1 | Volume Player | 78 |

| | | |
|----------|--|------------|
| 5.5.2 | 3D Data View | 79 |
| 5.5.3 | Event Explorer | 79 |
| 5.5.4 | Fuzzy Tracking Graph | 80 |
| 5.6 | Results and Evaluation | 81 |
| 5.6.1 | Wood-Shrinkage Analysis | 81 |
| 5.6.1.1 | Case Study | 82 |
| 5.6.1.2 | Domain Experts Feedback | 82 |
| 5.6.2 | AlSiC Alloys under Thermal Load | 82 |
| 5.6.2.1 | Case Study | 84 |
| 5.6.2.2 | Domain Experts Feedback | 84 |
| 5.6.3 | Design Lessons Learned | 84 |
| 5.7 | Summary | 86 |
| 6 | Conclusion | 87 |
| 6.1 | Summary of the Contributions | 87 |
| 6.2 | Revisiting the Research Questions | 88 |
| 6.3 | Outlook | 89 |
| 6.4 | Reflections | 90 |
| A | Porosity-Maps Evaluation-Questionnaire | 93 |
| A.1 | Previous Work | 94 |
| A.2 | Porosity Overview | 95 |
| A.3 | Comparison of Active Thermography, Porosity Maps, and Ultrasonic Testing | 96 |
| B | MObjects Evaluation-Questionnaire | 99 |
| B.1 | Previous Work | 100 |
| B.2 | MObject Visualization (T1) | 101 |
| B.3 | Local MObject Visualization (T2) | 102 |
| B.4 | MObjects Exploration (T3) | 109 |
| | Bibliography | 113 |
| | Curriculum Vitae | 121 |

List of Figures

| | | |
|-----|--|----|
| 1.1 | Used materials in the Boeing 787 Dreamliner [34]. | 2 |
| 1.2 | 3D renderings of a carbon fiber reinforced polymer (CFRP) specimen. (3) CFRP combines (1) carbon fiber bundles and (2) epoxy resin. | 3 |
| 1.3 | CFRP production process: (1) Molding of carbon fiber plies and (2) curing in an autoclave (Image courtesy of FACC AG). | 4 |
| 1.4 | Destructive and non-destructive testing methods for porosity determination: (1) Acid digestion. (2) Materialography. (3) Ultrasonic testing. (4) Active thermography. (5) 3D X-ray Computed Tomography (GE Phoenix xray nanotom XCT system at the University of Applied Sciences Upper Austria - Wels Campus). | 6 |
| 1.5 | Functional principle of 3D X-ray Computed Tomography: (1) Specimen. (2) Rotary Plate. (3) X-ray source. (4) Detector. | 8 |
| 1.6 | Cross-sectional image of a CFRP specimen scanned with 3D X-ray Computed Tomography: (1) Epoxy resin (matrix). (2) Fiber bundles in z direction. (3) Fiber bundles in x direction. (4) Small pores inside the fiber bundles. (5) Big pores in the matrix. | 9 |
| 1.7 | Classification of how the tasks were addressed in the contributions of this thesis. | 12 |
| 3.1 | Pipeline for the visual analysis of porosity in CFRP specimens. | 20 |
| 3.2 | XCT xy cross-sectional images of specimens PrePreg 1 (1), PrePreg 2 (2), PrePreg 3 (3) contain pores in black. The gray areas indicate the epoxy resin and the fiber bundles. | 21 |
| 3.3 | (A) 3D view with highlighted selected pores. (B, C and D) Porosity maps with region of interest selection. (E) Quantitative information view showing the global properties volume, number of pores and porosity separately for specimen, region of interest (ROI) and parallel-coordinates selection. (F) Parallel-coordinates view for individual pore selection. | 23 |
| 3.4 | (1) Illustration of the porosity-map calculation-step. (2) Specimen Maximum Color Mapping (SMCM) and (3) View Maximum Color Mapping (VMCM) of a small region in specimen PrePreg 1 in the xz view. The porosity-map values correspond to the number of pore voxels. | 24 |

| | | |
|------|--|----|
| 3.5 | Visual analysis of porosity in a sample specimen. An interactive exploration with a drill-down approach is shown in three stages: (1) Visualization of all pores and fast evaluation of the specimen based on porosity maps, where the values are encoded as the number of pore voxels. (2) Highlighted visualization of pores in a region of interest. (3) Accentuation of specific pores in the region of interest. (A) Porosity-maps interaction with a cuboid region of interest. (B) Further filtering of pores based on their local properties using parallel coordinates. | 25 |
| 3.6 | Best-viewpoint calculation: (A) For each position $P_{\alpha,\beta}$ on the sphere the viewpoint is evaluated. (B) Varying of the viewpoint in steps of 10° in α and β . (1, 2 and 3) Histogram-based best-viewpoint calculation showing three different viewpoints: Histograms are divided into the three classes of (1) critical, (2) borderline and (3) not critical pixels. | 27 |
| 3.7 | (1) Viewpoint of a CFRP dataset. Best-viewpoint widgets for (1): (2) Color mapping on a sphere and (3) cylinder sticks. The color mapping ranges from green, indicating a good viewpoint, to red visualizing unfavorable viewpoints. | 28 |
| 3.8 | Simulated dataset to verify the quantitative evaluation: (1) 3D rendering of the virtual specimen with pores given as cylinders and cuboids. (2) Cross-sectional image of the virtual specimen in an xy view. | 30 |
| 3.9 | (1, 2 and 3) PrePreg 1 specimen after porosity determination. In (1) a 3D view as well as in (2) an xz view and in (3) an xz porosity-map view is given. The porosity map values are encoded as the number of pore voxels. (4 and 5) Porosity evaluation of a region of interest in specimen PrePreg 1. Different pore classifications are shown. (4) The biggest pore in the region is selected and highlighted. (5) Only the long and thin micro pores in the fiber bundles are highlighted. | 32 |
| 3.10 | Visualization of different pore classes: (1) Parallel-coordinates view. (2) Big pores. (3) Smaller nodular and disc-shaped pores. (4) Long and thin micro pores. (5) Combined visualization of (2, 3 and 4). | 33 |
| 3.11 | Comparison of active-thermography images (1, 3 and 5) to porosity maps (2, 4 and 6) of the specimens PrePreg 4-6. (1 and 2) PrePreg 4 shows a porosity of 1.81 %. (3 and 4) PrePreg 5 shows a porosity of 3.53 %. (5 and 6) PrePreg 6 shows a porosity of 7.20 %. The porosity-map values are encoded as the number of pore voxels. Based on the thermal-diffusivity model high values in the active-thermography images depict a high porosity, which is encoded as the observation time in seconds. | 34 |
| 4.1 | Illustration of the MObject calculation showing pores of a CFRP dataset. (1) First the individual pores are spatially aligned according to their centers. (2) Second the MObject is calculated by aggregating the pore voxels. | 38 |
| 4.2 | From a set of individual objects a MObject is calculated. MObjects are visualized by transfer functions based on the probability of each voxel of belonging to the MObject (1 and 2). The MObject cut-through (C) shows areas with high probability (H) in the center. Medium (M) and low (L) probabilities represent the uncertainty cloud (U) showing outliers of individual objects. | 39 |

| | | |
|------|---|----|
| 4.3 | Pipeline for the visualization and interactive exploration of MObjects in a dataset. After the stages Data Acquisition (1) and Pre-processing (2) the user can decide between the visualization of the global MObject (3) or a local MObjects visualization (4). Through interactive selection (5) one is able to start the exploration with a local MObject. Otherwise the global MObject is the input for the exploration. The child MObjects are calculated in the MObject Set Calculation (6) stage for further visualization in the MObject Set Visualization (7) stage. The interaction techniques Visual Linking (8) and Interactive Selection (9) of MObjects are provided. Interactive selection is done by selecting a MObject (A) in a MObject Set (B) to calculate a new MObject Set (C) out of the selected MObject (A). | 44 |
| 4.4 | (1) MObject showing a small uncertainty cloud using a low uncertainty filter $\sigma = 0.15$. (2) A high uncertainty filter $\sigma = 0.9$ leads to an uncertainty cloud showing the MObject's core and outliers. | 47 |
| 4.5 | Based on the partitioning (1) of the volume into cells, local MObjects (2) and a color-coded homogeneity visualization (3) is shown to the user. The color-coding illustrates the deviation of the average cell properties from the global average property. Red indicates the highest positive deviation, whereas blue shows the highest negative deviation. | 48 |
| 4.6 | Illustration of the MObject Set calculation showing pores of a CFRP dataset. All individual pores of the parent MObject (1) are divided into two clusters A (2) and B (3). The resulting child MObjects (4 and 5) make up a new MObject Set (6). . . . | 50 |
| 4.7 | The radial MObject Set visualization shows all possible combinations between the properties (1) and (2). | 51 |
| 4.8 | Parallel MObject Set visualization for a step by step exploration. MObject Sets (1), (3) and (5) are calculated and visualized after interactive selections (2) and (4). . . | 51 |
| 4.9 | Illustration of the visual-linking approach. After selecting a MObject (1) in a MObject Set (A), visual linking shows the selected child MObject inside the parent MObject (2) of the parent MObject Set (B). | 52 |
| 4.10 | (1) Local MObjects visualization using a high uncertainty filter $\sigma = 0.9$. (2 and 3) Enlarged visualization of two MObjects. | 54 |
| 4.11 | (1) Visualization of the CFRP dataset. (2) Homogeneity visualization of the deviation from the average pore volume in a 4 x 3 grid showing the CFRP dataset in the background. | 55 |
| 4.12 | Homogeneity visualization of the deviation from the average pore. (1) Deviation of the extent in x direction and (2) deviation of the extent in y direction in a 4 x 3 grid showing the CFRP dataset in the background. | 56 |
| 4.13 | Homogeneity visualization of the deviation from the average pore. (1) Deviation of the extent in z direction and (2) deviation of the shape factor in a 4 x 3 grid showing the CFRP dataset in the background. | 57 |
| 4.14 | Radial MObject Set visualization of a CFRP dataset showing combinations of the properties (1) shape factor and (2) pore volume. | 58 |
| 4.15 | Parallel MObject Set visualization of a CFRP dataset showing the selected path without visual linking. | 59 |

| | | |
|------|---|----|
| 4.16 | Parallel MObject Set visualization of a CFRP dataset showing the selected path with visual linking. | 60 |
| 4.17 | Representative mean pores of a CFRP dataset showing the visual-linking visualization (top row) and the MObjects (bottom row). (1 and 2) Nodular and disc-shaped pores. (3 and 4) Long and thin micro pores in x and z direction. | 61 |
| 5.1 | Voids in SiC particle reinforced aluminum (AlSiC). (A and B) Cross-sectional images of two adjacent time-steps of the cooling down process from (A) 400 °C to (B) 300 °C. (C) Overlay of (A) and (B) showing a zoom-in indicating that void 2 has to be assigned either to void 1 or to void 3. | 66 |
| 5.2 | Pipeline for the visual analysis of 4D-XCT time-series. After the stages data acquisition (1) volume registration (2) is applied. Furthermore pre-processing (3) steps enhance the data. The acquired and enhanced time-series consists of time-steps (4) which are the basis for the Fuzzy Feature Tracking (5). For visualizing the time-steps and the Fuzzy Feature Tracking result, a 3D Data View (6) showing 3D renderings, an Event Explorer (7) consisting of scatter plots and a Fuzzy Tracking Graph (8) are used. Interactive selection (9) of an event in the Event Explorer leads to an update of the 3D Data View and the Fuzzy Tracking Graph. | 72 |
| 5.3 | Fuzzy Feature Tracking to find probable corresponding features for A in B . (1) Radial search at the centroid position of a_i in B . (2) Volume overlap calculation for each probable feature in B based on bounding boxes. (3) Volume ratio calculation for each probable feature in B . (4) Tracking Uncertainty calculation for each correspondence from a_1 to the probable features b_1, b_2 and b_3 in B | 74 |
| 5.4 | 4D-XCT visual-analysis tool consisting of four linked views: (A) Volume Player. (B) 3D Data View. (C) Event Explorer. (D) Fuzzy Tracking Graph. (1) A selection in the Event Explorer leads to an update (2 and 3) of the 3D Data View and the Fuzzy Tracking Graph. | 77 |
| 5.5 | Volume Player. | 78 |
| 5.6 | Five volume blending steps between the two time-steps $t(30 \text{ min})$ and $t(60 \text{ min})$ of the wood-shrinkage analysis. | 78 |
| 5.7 | 3D Data View. | 79 |
| 5.8 | Event Explorer. | 79 |
| 5.9 | Fuzzy Tracking Graph. | 80 |
| 5.10 | Calculation and visualization of the Fuzzy Tracking Graph: After an (1) event selection in the Event Explorer, (2) a tracking graph is built and the (3) edge crossings are minimized. Then (4) event types and Tracking Uncertainty are encoded. | 81 |
| 5.11 | Results of the wood-shrinkage time-series: Event Explorer of time-step $t(60 \text{ min})$ with two selections (1 and 3) of large merge events. Selections lead to updates (2 and 4) of the Fuzzy Tracking Graph. (5) Visual clutter in the Fuzzy Tracking Graph. (6) Annual growth ring in time-step $t(60 \text{ min})$ | 83 |

| | | |
|------|---|-----|
| 5.12 | Results of the AISiC time-series: (A) 3D Data View of a void during a heating and cooling cycle ($30^{\circ}\text{C} \rightarrow 200^{\circ}\text{C} \rightarrow 300^{\circ}\text{C} \rightarrow 400^{\circ}\text{C} \rightarrow 300^{\circ}\text{C} \rightarrow 190^{\circ}\text{C} \rightarrow 50^{\circ}\text{C}$). (B) Fuzzy Tracking Graph showing two areas (1 and 4) with encoded Tracking Uncertainty. (2 and 3) Highlighting of an interesting split (2) and merge (3) event for the sequence ($300^{\circ}\text{C} \rightarrow 400^{\circ}\text{C} \rightarrow 300^{\circ}\text{C}$). | 85 |
| A.1 | (1) PrePreg component after porosity determination in 3D iso view (2) in 3D xz view (3) and porosity map xz view. | 95 |
| A.2 | Comparison of active thermography images (1-3), porosity maps (4-6), and ultrasonic images (7-9). Based on the thermal diffusivity model high values in the active thermography images depict a high porosity, which is encoded as the observation time in seconds. | 96 |
| B.1 | 3D renderings of individual objects in (a) isometric view, (b) xy view. (c and d) 3D rendering of MObject visualization generated from the input of image (a) using two different transfer function settings. | 101 |
| B.2 | Visualization of segmented pores in a CFRP dataset. | 102 |
| B.3 | Local MObjects visualization of the CFRP dataset from Figure B.2. | 104 |
| B.4 | Color-coded visualization of the deviation from the average pore (a) volume, (b) shape factor, (c) extent in x direction, (d) extent in y direction, and (e) extent in z direction. | 106 |
| B.5 | Visualization of (a) segmented pores (b) local MObjects, and (c) the color-coded cell visualization. | 108 |
| B.6 | MObject Set visualization showing the selected path and the visual linking approach of the rendered MObjects. | 110 |
| B.7 | (a) Rendering of individual objects (pores) of a CFRP dataset. (b) Mean object (MObject) visualization of the individual objects from (a). | 111 |
| B.8 | Rendering of mean objects (MObjects) of a CFRP dataset. | 112 |

List of Tables

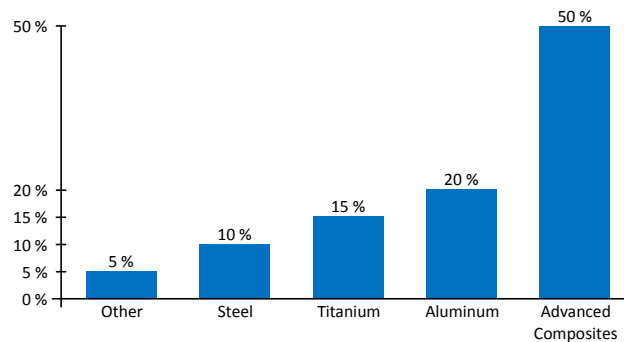
| | | |
|-----|---|----|
| 1.1 | Specifications of the GE Phoenix xray nanotom XCT system. | 7 |
| 3.1 | XCT-based porosity results for specimens PrePreg 1-3 compared to the reference methods ultrasonic testing (US) using the pulse-echo technique and acid digestion (AD). The used data type is unsigned short. CPU: Intel® Xeon® X5680. | 29 |
| 3.2 | Porosity results of the verification on a virtual XCT dataset. The dataset size is 392 x 415 x 445 voxels. | 30 |
| 4.1 | Summary of the Evaluation Questionnaire | 63 |

Introduction and Overview

During the last decades, a clear trend formed in industry of constantly driving industrial research towards new tailored materials as well as cost-effective, function-oriented, highly integrated and light-weight components. The driving forces behind this trend are the high requirements regarding efficiency, environment, safety as well as comfort. Especially in the aeronautics and automotive industry there is a high demand for advanced composite materials which meet the challenging demands. To achieve this goal, carbon fiber reinforced polymers (CFRPs) are currently considered as the most promising candidate, due to their increased stiffness and strength-to-weight ratio. The new generations of aircrafts, such as the Airbus A350 XWB, Boeing 787 Dreamliner or Bombardier C Series, are made of at least or more than 50 % of these novel composite materials.

Composites in the Airframe

When planing a new design of an airplane engineers have to determine the right material for each specific part. Aluminum which was highly used in older generations of airplanes is capable of handling compression loads very well whereas it is sensitive to tension loads. For composites it is inverse. They perform excellent at handling with tension but are not as efficient in handling compressions [34]. Figure 1.1 shows an overview of the used materials of a Boeing 787 Dreamliner. The airframe and primary structures are made of composites (50 %). Conventional materials such as aluminum (20 %), titanium (15 %), steel (10 %) as well as other materials are also used. As a result, this approach offers an average weight saving of 20 % compared to conventional aluminum designs.



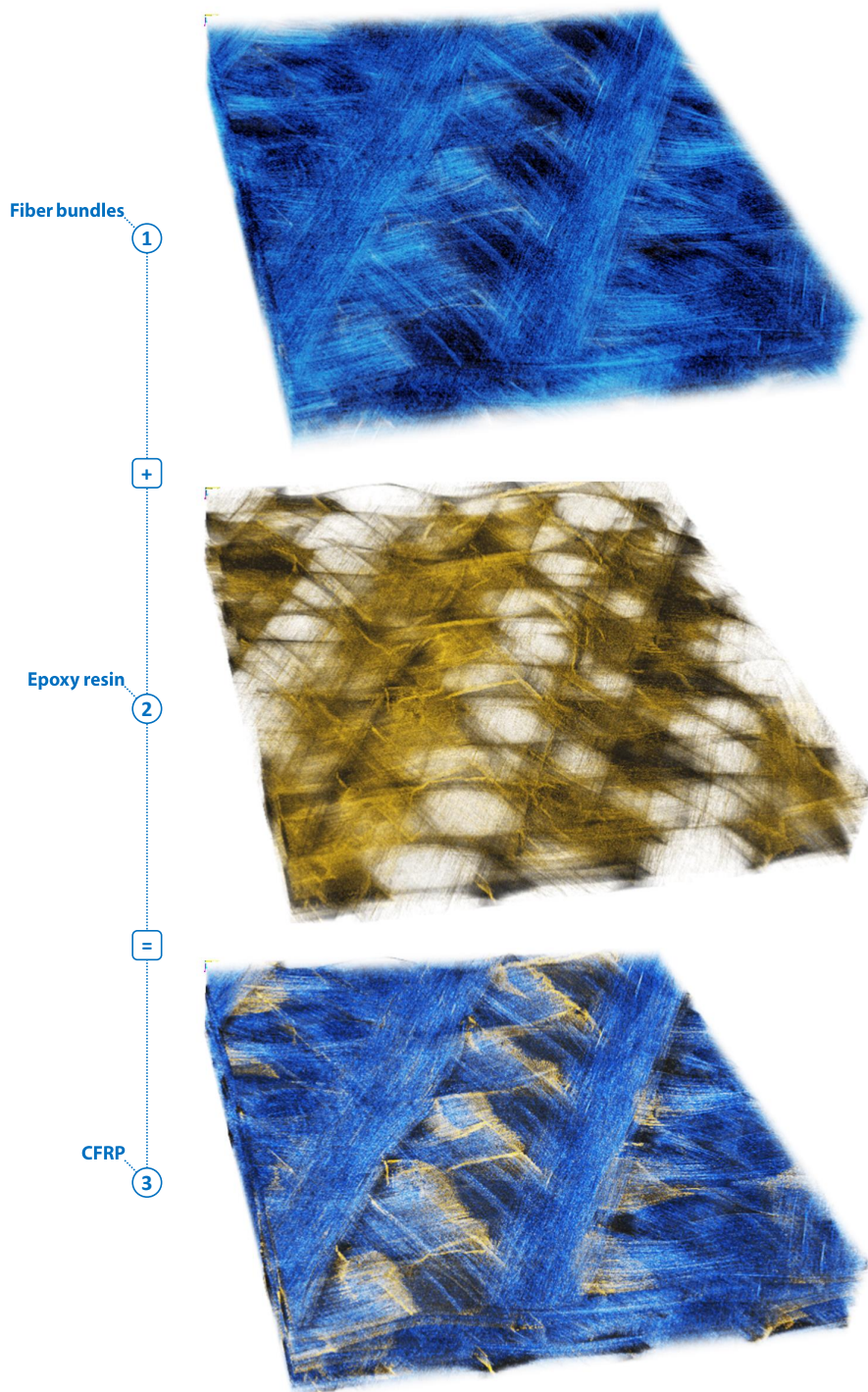
❖ Figure 1.1 — Used materials in the Boeing 787 Dreamliner [34].

1.1 Carbon Fiber Reinforced Polymers

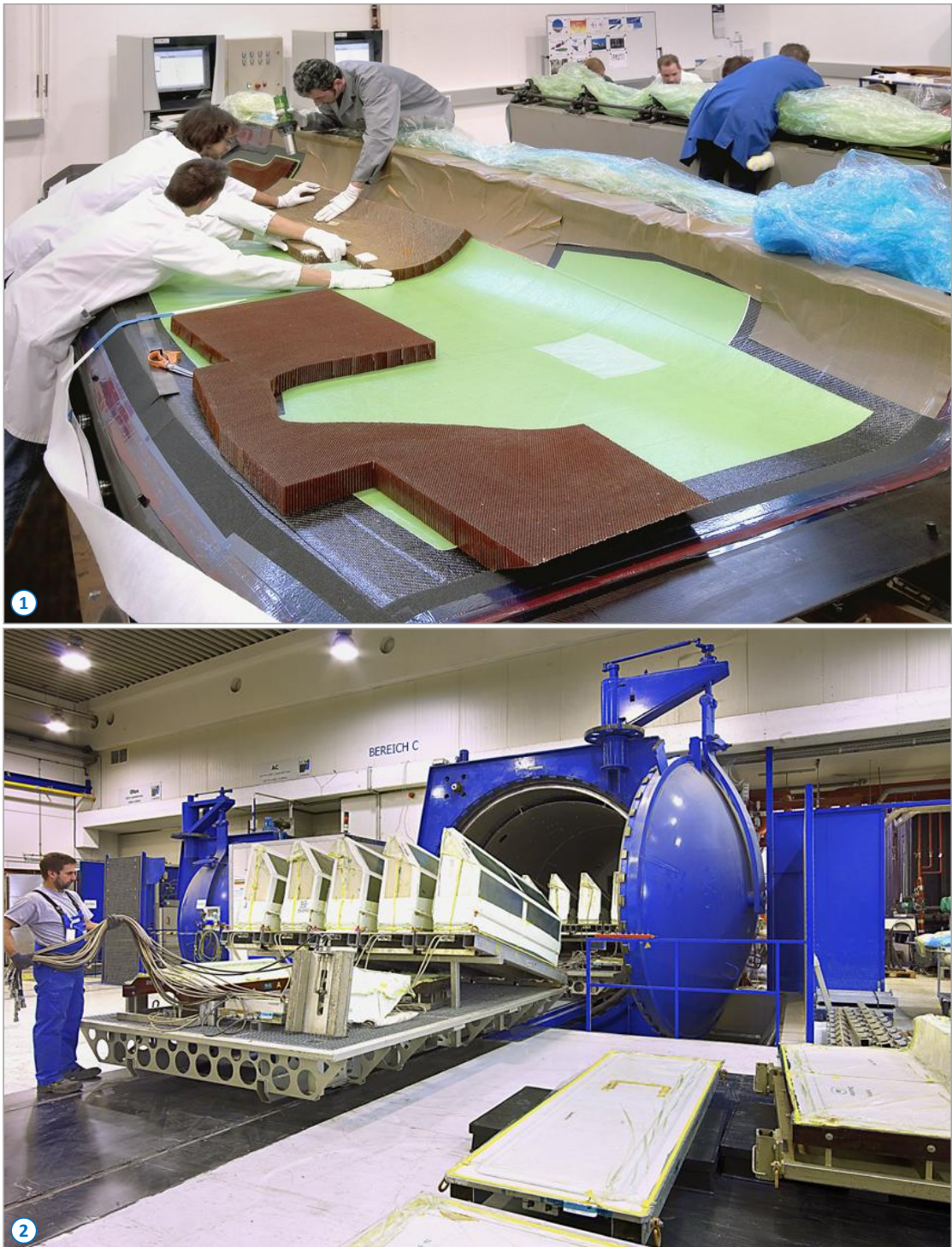
As shown in Figure 1.2, (3) CFRP consists of (1) carbon fiber bundles (blue), e.g., braided in a twill-weave pattern, and (2) epoxy resin (yellow) in between these bundles. This combination results in a material system fulfilling the above mentioned demands. Different manufacturing methods for producing CFRP components exist. Fiber plies are either layered together with epoxy resin (wet lay-up) or with preimpregnated (PrePreg) fiber plies consisting of carbon fibers and epoxy resin (dry lay-up). With the molding approach fiber plies are layered into a mold in the shape of the final component. Then the mold is heated or air-cured. With vacuum bagging a mold is also used and placed in a vacuum bag. The specimens which were used in this thesis are made of PrePreg fiber plies. Figure 1.3 shows the two main stages of the production process. With epoxy resin pre-impregnated carbon fiber plies are cut out and layered into a mold in the shape of the final product (1). To get the final component, the epoxy resin has to cure in an autoclave under high pressure and heat (2). As a result of manufacturing artifacts CFRPs tend to have pores inside. Pores are small inclusions of air. Porosity is defined as the volume of pores compared to the volume of the component including fiber bundles, resin and pores.

Influencing Characteristics of Porosity

Porosity has a large impact on the mechanical properties of a specimen such as compressive and interlaminar shear strength as well as the elasticity modulus of the material. The shear strength decreases by 7 % per 1 % of porosity [13]. Thus it is an important task in quality control to quantify and study the porosity of such materials [41]. In high-safety applications 'zero-tolerance rules' may be required (no pores), or the level of void content has to be below a given threshold. Less demanding applications can have more relaxed standards, allowing void contents of a few percent [63]. Besides quantitative porosity, the distribution and shape of pores are important properties for CFRP analysis. As ultrasonic testing, which is the current state-of-the-art method for non-destructive porosity determination in aeronautics, is increasingly facing its limits, the accurate determination of porosity in CFRPs is a highly active field of research.



❖ Figure 1.2 — 3D renderings of a carbon fiber reinforced polymer (CFRP) specimen. (3) CFRP combines (1) carbon fiber bundles and (2) epoxy resin.



❖ Figure 1.3 — CFRP production process: (1) Molding of carbon fiber plies and (2) curing in an autoclave (Image courtesy of FACC AG).

1.2 Porosity Determination

The methods for porosity determination can be divided into the two groups of destructive and non-destructive testing. Acid digestion and materialography in combination with microscopic analysis belong to the group of destructive testing methods [13]. Ultrasonic testing, active thermography and 3D X-ray Computed Tomography (XCT) are non-destructive testing methods [53]. Figure 1.4 shows an overview of these methods.

1.2.1 Acid Digestion

Acid digestion is a destructive reference method based on gravimetry (see Figure 1.4 (1)). Volume and mass of the specimen, epoxy resin and fiber content have to be measured accurately. Because the specimen is destroyed during the determination, no porosity overview and no calculation of local pore properties are available.

1.2.2 Materialography

In *materialography*, another destructive method, slices of the specimen are grinded and analyzed with microscopic 2D image processing methods (see Figure 1.4 (2)). Porosity is calculated statistically based on a minimal set of 30 slice images. Quantitative porosity can only be determined with reduced accuracy because of grinding artifacts. Due to the estimation being based on a limited number of slices for the whole specimen, a porosity overview as well as the calculation of local pore properties is complex and time-consuming.

1.2.3 Ultrasonic Testing

The currently used state-of-the-art method for non-destructive porosity determination in aeronautics is *ultrasonic testing* (see Figure 1.4 (3)). The porosity level is estimated from ultrasonic velocity and attenuation. Pore distribution, size and shape factor have a strong influence on the ultrasonic attenuation [48]. The resulting measurement errors have to be considered in quality control. They may lead to a wrong interpretation of porosity and subsequently to a rework or in the worst case to a rejection of possibly useable components. Ultrasonic testing provides standardized means of porosity estimation but an imprecise overview of porosity in the specimen. Due to the low resolution, the evaluation of specific pores is not possible.

1.2.4 Active Thermography

Another NDT method for the determination of porosity is *active thermography* (see Figure 1.4 (4)), more specifically pulsed thermography. Generating heat with flashes of light, the propagation of surface temperatures in pulsed thermography depends on the diffusivity of the sample and its geometry. Quantitative porosity is calculated by means of a heat conduction model and the linear relation to the diffusivity [53]. Compared to ultrasonic testing, active thermography



❖ **Figure 1.4** — Destructive and non-destructive testing methods for porosity determination: (1) Acid digestion. (2) Materialography. (3) Ultrasonic testing. (4) Active thermography. (5) 3D X-ray Computed Tomography (GE Phoenix|xray nanotom XCT system at the University of Applied Sciences Upper Austria - Wels Campus).

❖ Table 1.1 — Specifications of the GE Phoenix|xray nanotom XCT system.

| | |
|---|-----------------------------------|
| X-ray source | 180 kV nanofocus tube |
| Minimum focal spot diameter | < 1 μm |
| Detector | 2300 * 2300 pixel 12 bit detector |
| Minimum voxel size | 0.5 μm |
| Sample weight | < 2 kg |
| Sample diameter | < 68 mm |
| Sample diameter with scan range enlargement | < 210 mm |
| Sample length | < 150 mm |
| Maximum penetration length (polymers) | 50 mm |
| Maximum penetration length (aluminum) | 30 mm |
| Maximum penetration length (steel) | 4 mm |

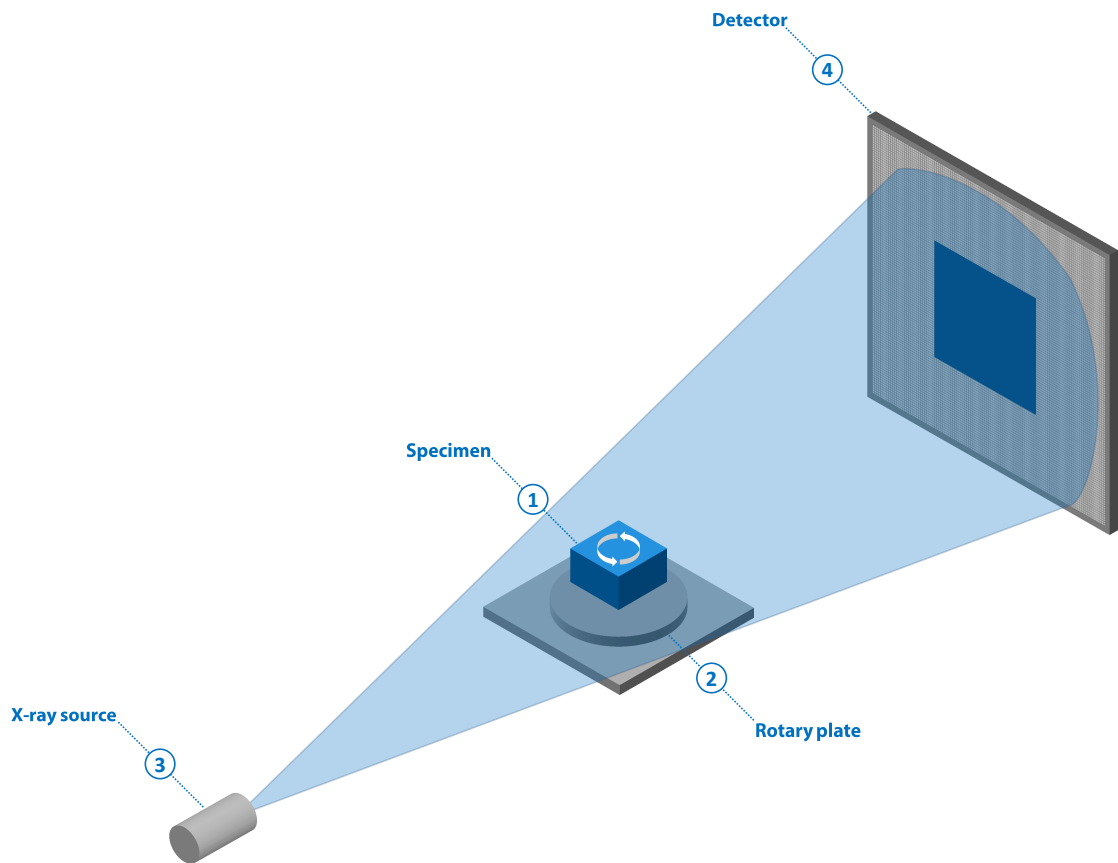
provides an improved porosity estimation. It gives a more detailed but still imprecise overview of porosity in the specimen compared to ultrasonic testing, but yet no specific evaluation of individual pores.

1.2.5 3D X-Ray Computed Tomography

In recent years *3D X-ray Computed Tomography (XCT)* provides a new possibility for NDT of CFRP components (see Figure 1.4 (5)). A specimen is placed on a rotary plate between an X-ray source and a detector. A series of 2D projection images for many angular positions is taken and the corresponding 3D volumetric dataset is reconstructed. One of the main problems regarding porosity determination using XCT is the partial volume effect [30] and the resulting discretization error of the scanned structures. Another critical problem of all methods is the missing ground truth of quantitative porosity. The accuracy of porosity determination using the reference methods ultrasonic testing and acid digestion [1] is about $\pm 1\%$.

3D X-ray Computed Tomography (XCT) non-destructively generates a 3D volumetric representation of the specimen from a series of 2D X-ray attenuation images. Figure 1.5 shows the functional principle of XCT data acquisition in detail: The specimen (1) is placed on a rotary plate (2) between X-ray source (3) and detector (4). 2D projection images recording the information on X-ray attenuation of the specimen at the detector are acquired at each angular position of the rotary plate. After acquiring the 2D projection images for the complete series of angular positions, a 3D volumetric dataset is reconstructed. This dataset is also called raw dataset. XCT allows NDT practitioners to bring new insights into material systems and has become a highly attractive method in various engineering disciplines for both metrology and non-destructive testing tasks.

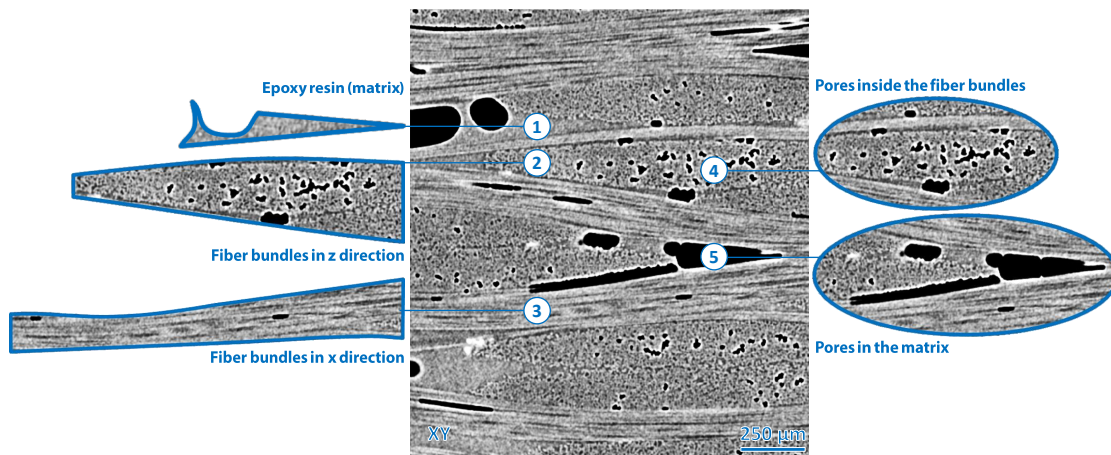
In this work, the XCT scans were performed on a GE Phoenix|xray Nanotom 180 NF device at the University of Applied Sciences Upper Austria - Wels Campus (see Figure 1.4 (5)). The specifications of the device are listed in Table 1.1. The reconstruction algorithm of the device



❖ Figure 1.5 — Functional principle of 3D X-ray Computed Tomography: (1) Specimen. (2) Rotary Plate. (3) X-ray source. (4) Detector.

included a correction for beam hardening. This avoids over-segmentation in the middle of the specimen due to gray value modifications caused by the beam-hardening effect during the measurement.

As described in Section 1.1, CFRPs consist of carbon fiber bundles and epoxy resin. After measuring a specimen with XCT, the basis for further pre-processing and visualization stages is a 3D volumetric dataset, where each voxel has a certain gray value. Figure 1.6 shows a cross-sectional image of a CFRP specimen scanned with XCT. The gray areas indicate the epoxy resin (1), also called the matrix, as well as the fiber bundles in z (2) and x (3) direction. Black areas show small inclusions of air, the so called pores. Small micro pores (4) occur inside the fiber bundles whereas bigger pores (5) mostly originate in the matrix. These pores are a result of manufacturing artifacts and they have a strong impact on the mechanical properties of a specimen such as compressive and interlaminar shear strength as well as the elasticity modulus of the material.



❖ **Figure 1.6** — Cross-sectional image of a CFRP specimen scanned with 3D X-ray Computed Tomography: (1) Epoxy resin (matrix). (2) Fiber bundles in z direction. (3) Fiber bundles in x direction. (4) Small pores inside the fiber bundles. (5) Big pores in the matrix.

1.3 Visualization Tasks

During my collaborations with domain experts from industry and academics, a detailed list of domain-specific requirements was set up. Specifically, NDT practitioners from the University of Applied Sciences Upper Austria, Wels Campus, CFRP specialists from FACC, a company manufacturing aircraft components, and material scientists from the Institute for Carbon Composites, Technische Universität München (University of Technology, Munich) were involved. The experts' requests converged to the following general questions:

Question 1: *What is the quantitative porosity?*

Porosity has a strong impact on the mechanical properties of a component. Regarding quality control, quantitative porosity is the most important value to determine if a component meets the specifications or if it needs to be reworked or in the worst case rejected.

Question 2: *How are the pores distributed?*

In terms of material properties, the distribution of pores is a factor of high importance. Are the pores distributed uniformly or do pores appear in clusters? For example, porosity in a specific layer may be more critical than a homogenous distribution of pores as this may lead to a delamination of the affected layers.

Question 3: *What are the shapes of the pores?*

Are pores nodular, disc-shaped, or elongated? Besides the related property volume, also the extents of the pores in x, y and z direction are interesting.

Question 4: *How does a feature evolve over time?*

When analyzing a process over time, e.g., a fatigue test of a CFRP component, it is of high interest how the pores or cracks evolve and formate over time. Further questions arise: How are the features created, continuing, splitting, merging, or dissipating in the course of time and which features are involved in a split or merge event?

The whole process was iterative involving a close collaboration with the experts over the last four years in terms of developing and evaluating the tools. To address the questions from above, the following main visualization tasks for the analyses of CFRP components were derived:

Task 1: *Quantitative Porosity*

The quantitative porosity of a CFRP component has to be determined and compared to existing reference methods such as ultrasonic testing or active thermography. For this a scalar value is sufficient.

Task 2: *Porosity Overview*

As the pore distribution influences the local mechanical properties of the component, a fast overview of the porosity is needed. Besides the porosity an overview of pore properties, e.g., the volume or the extents of the pores, in certain regions have to be visualized. A combined visual representation of all features or objects of interest inside a CFRP dataset can show the average shape factor amongst other properties.

Task 3: *Exploration of Pores*

Pores have to be evaluated individually. After the calculation of individual pore properties, e.g., volume, extents, and shape factors, pores may be filtered according to their properties. For example, pores may be classified by their shape factors. Big and nodular pores only appear between fiber bundles whereas thin micro pores originate between the individual fibers.

Task 4: *Feature Tracking*

As pre-processing stage, all occurring events, e.g., creation, continuation, split, merge and dissipation, from one time-step to another one have to be determined. Regarding visualization, the spatial information including the extracted features for each time-step, the temporal overview of the events and corresponding feature properties as well as the temporal overview of the events and their connections have to be visualized.

1.4 Contributions of this Thesis

Considering the domain experts' questions (Question 1 - Question 4) and the derived tasks (Task 1 - Task 4) from Section 1.3, three visual-analysis tools with the following contributions were investigated. The contributions are based on research papers and described in the Chapters 3, 4 and 5. Figure 1.7 shows how each contribution covers the above tasks.

Contribution 1 - Porosity Maps

Porosity Maps - Visual Analysis of Porosity in Carbon Fiber Reinforced Polymers [60] presents a visual analysis system for CFRP specimens (see Chapter 3). Porosity Maps (PM) are introduced, to allow for a fast porosity evaluation of the specimen. Furthermore a drill-down approach to explore pores in two stages is employed. A selection in the PMs is followed by a filtering of individual pores with parallel coordinates according to their local properties.

Contribution 2 - MObjects

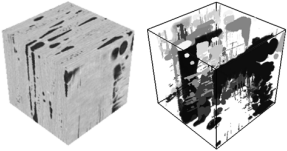
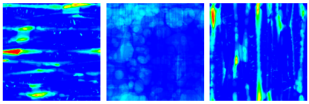
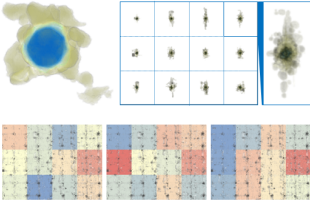
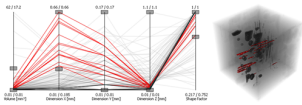
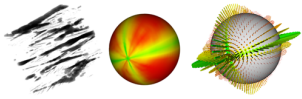
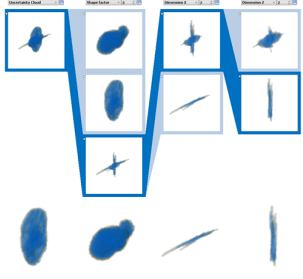
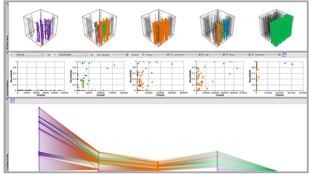
MObjects - Interactive Exploration of Defects in Industrial XCT Data [59] aims at the exploration of a high number of individual pores, i.e., generally all kinds of defects, in a dataset (see Chapter 4). All objects, e.g., pores, are aggregated into a mean object (MObject) which shows an overview of the pore shapes. For a fast overview of the pore properties in a dataset, a local MObjects visualization in combination with a comparative homogeneity visualization of cells is presented. Exploration of pores is done by splitting up a MObject into sub-classes of MObjects.

Contribution 3 - Fuzzy Feature Tracking

Fuzzy Feature Tracking - Visual Analysis of Industrial 4D-XCT Data [58] deals with monitoring a process over time by using a series of XCT scans (see Chapter 5). An integrated visual-analysis tool with multiple linked-views to evaluate series of XCT data is introduced. Each visualization emphasizes individual aspects of the 4D time-series data, such as the spatial feature information (3D Data View), the global temporal overview (Event Explorer) and a global temporal evolution of how the features are tracked and connected over the whole time-series (Fuzzy Tracking Graph).

Evaluation

Contributions 1 and 2 were rated with evaluation questionnaires to research the practical relevance. The questionnaires are provided as Appendices (see Appendix A and B). Contribution 3 presents two real-world applications from different domains. This incorporates two case studies demonstrating the advantages of the tool including feedback from the domain experts.

| | Contribution 1 Porosity Maps | Contribution 2 MObjects | Contribution 3 Fuzzy Feature Tracking |
|---------------------------------|--|--|--|
| Task 1 Quantitative Porosity | <p>Pore Segmentation, Property Calculation</p>  | | |
| Task 2 Porosity Overview | <p>Porosity Maps</p>  | <p>Global MObject, Local MObjects, Homogeneity Visualization</p>  | |
| Task 3 Exploration of Pores | <p>Parallel Coordinates</p>  <p>Best-Viewpoint Widget</p>  | <p>MObject Sets</p>  | |
| Task 4 Feature Tracking | | | <p>Fuzzy Feature Tracking, 3D Data View, Event Explorer, Fuzzy Tracking Graph, Volume Player</p>  |

❖ Figure 1.7 — Classification of how the tasks were addressed in the contributions of this thesis.

Pre-processing

This chapter introduces the pre-processing stages which are applied on the XCT data of CFRP specimens. After enhancing the data (see Section 2.1) individual pores have to be segmented with a suitable segmentation technique (see Section 2.2). Based on the segmented pores global specimen properties as well as individual pore properties are calculated (see Section 2.3). These properties are the main input for the visual-analysis tools which were developed in this thesis.

2.1 Data Enhancement

The enhancement of XCT data is essential for the segmentation of pores if ambient noise is present in the scanned datasets. I recommend anisotropic diffusion as described by Perona and Malik [56] as it allows smoothing of homogenous regions without blurring edges. Anisotropic diffusion leads to improved results for a subsequent analysis of industrial XCT data [37]. The data which was used in this thesis has low noise. Thus only five iterations with a conductance of one and a time step of 0.0625 seconds was used for smoothing the data and preserving the edges.

2.2 Segmentation of Pores

Segmentation is a common image processing task with a wide range of applications and many approaches are found in the literature. Detailed surveys have been published on GPU-based segmentation by Hadwiger et al. [33] and on threshold techniques by Sezgin and Sankur [67]. Adams and Bischof [2] group the segmentation methods into four main approaches, threshold techniques, boundary-based methods, region-based methods, and hybrid techniques.

Threshold techniques assign an object membership based on a density threshold, where no neighborhood information is taken into account. Based on a threshold value, all voxels below this threshold are set to zero and all voxels above are set to one. The problem of thresholding is to find the optimal value to classify the voxels into foreground voxels (pores) and background voxels (resin and fibers). Otsu [55] proposed an automatic threshold-selection method for bimodal histograms by maximizing the separability of the resulting classes in gray levels. Thereby the histogram is divided into two classes minimizing the intra-class variance and maximizing the inter-class variance.

Boundary-based methods detect object borders with an edge detection filter and connect the identified edges to form a closed region. A well-established edge detection filter is the Canny edge detector [22]. Region-growing methods start from one or multiple regions and grow these regions as long as a homogeneity criterion is valid [2, 83]. The start regions, also called seeds, are manually specified by the user or automatically by an algorithm. A region-based segmentation approach is the watershed transform, where the image is considered as a height field. Beucher [12] applied it to image segmentation. Homogenous regions, also called catchment basins, are constructed by a flooding process. This process leads to over-segmentation. Felkel et al. [26] overcome this problem by placing markers manually. Al-Raoush et al. [5] applied the watershed transform to segment touching or overlapping particles and to calculate the distribution of the local void ratio from 3D images.

Since region growing methods and the watershed transform are time- and memory-consuming, Otsu's thresholding technique [55] was applied for the data which was used in this thesis. In Section 3.5.1 it will be shown that the results are satisfying compared to the described reference methods acid digestion and ultrasonic testing. As these reference methods have a range of inaccuracy of about $\pm 1\%$, the evaluation of the segmentation result is difficult. Thus a virtual specimen with pores given as geometric primitives like cylinders and cuboids was created in Section 3.5.2. Then a simulated XCT scan of the virtual specimen was generated. Otsu's thresholding method was applied and compared to the known ground truth. However, for further developments and specific analyses tasks the segmentation step could be replaced easily in the pipelines of the visual-analysis tools presented in the Chapters 3, 4 and 5.

2.3 Calculation of Pore Properties

After segmentation a connected-components filter, using 26-connectivity, labels objects in the binary image, which is essential for calculating the pore properties. Based on this labeled dataset, global specimen properties and local pore properties are calculated.

Global Specimen Properties

- **Specimen volume:** V_S

The volume V_S of the specimen is the sum of all background (epoxy resin and fibers) and pore voxels, but without surrounding air voxels.

- **Specimen porosity:** P_S

The specimen porosity P_S is calculated as follows:

$$P_S = \frac{V_P}{V_S} \quad (2.1)$$

where V_P is the volume of all pores.

Local Pore Properties

- **Volume:** V_i

The volume V_i of a pore i is the sum of all voxels with the same label, which was assigned by the connected-components filter.

- **Extent:** $extent_{x_i}, extent_{y_i}, extent_{z_i}$

To calculate the extent of a pore along the x, y and z coordinate axes the calculation is performed on the discretized pore. For the extent along the x axis the two voxels with minimal and maximal x coordinate values are determined respectively. The extents $extent_{x_i}, extent_{y_i}, extent_{z_i}$ are then the differences between the maximal and minimal coordinates along the x, y and z axes of pore i :

$$\begin{aligned} extent_{x_i} &= max_{x_i} - min_{x_i} + 1, \\ extent_{y_i} &= max_{y_i} - min_{y_i} + 1, \\ extent_{z_i} &= max_{z_i} - min_{z_i} + 1 \end{aligned} \quad (2.2)$$

where max_{d_i} is the maximum index and min_{d_i} is the minimum index of the pore i in the dataset in direction d .

- **Centroid:** $centroid_{x_i}, centroid_{y_i}, centroid_{z_i}$

The centroid of a pore i is calculated from the extents:

$$\begin{aligned} centroid_{x_i} &= min_{x_i} + extent_{x_i}/2, \\ centroid_{y_i} &= min_{y_i} + extent_{y_i}/2, \\ centroid_{z_i} &= min_{z_i} + extent_{z_i}/2. \end{aligned} \quad (2.3)$$

- **Shape factor:** F_i

The shape factor F_i of a pore i is defined as the ratio between the pore surface S_i and the pore volume V_i :

$$F_i = \frac{S_i}{V_i} \quad (2.4)$$

where the calculation of S_i is based on the faces of the pore surface voxels.

- **Directional shape factors:** $F_{(x/z)_i}$, $F_{(y/z)_i}$, $F_{(x/y)_i}$

Mayr et al. [53] define the shape factors of typical ellipsoidal pores for each direction in space as follows:

$$F_{(x/z)_i} = \frac{\text{extent}_{x_i}}{\text{extent}_{z_i}} \quad (2.5)$$

$$F_{(y/z)_i} = \frac{\text{extent}_{y_i}}{\text{extent}_{z_i}} \quad (2.6)$$

$$F_{(x/y)_i} = \frac{\text{extent}_{x_i}}{\text{extent}_{y_i}} \quad (2.7)$$

Porosity Maps - Visual Analysis of Porosity in Carbon Fiber Reinforced Polymers

This chapter is based on the following publication:

A. Reh, B. Plank, J. Kastner, E. Gröller, and C. Heinzl. Porosity Maps - Interactive Exploration and Visual Analysis of Porosity in Carbon Fiber Reinforced Polymers. *Computer Graphics Forum*, 31(3), pages 1185-1194, June 2012 (Full paper reviewed).

Related publications:

J. Kastner, B. Plank, A. Reh, D. Salaberger, C. Heinzl. Advanced X-ray tomographic methods for quantitative characterisation of carbon fibre reinforced polymers. *4th International Symposium on NDT in Aerospace*, Augsburg, Germany, October 2012 (Extended abstract reviewed, pp. 9).

A. Reh, B. Plank, J. Kastner, E. Gröller, and C. Heinzl. Advanced Visualization Methods for Porosity in Carbon Fiber Reinforced Polymers. *1st International Conference on Tomography of Materials and Structures (ICTMS 2013)*, Ghent, Belgium, July 2013 (Extended abstract reviewed, pp. 4).

J. Weissenböck, A. Amirkhanov, W. Li, A. Reh, A. Amirkhanov, J. Kastner, E. Gröller, C. Heinzl. FiberScout: An Interactive Tool for Exploring and Analyzing Fiber Reinforced Polymers. In *Proceedings of IEEE Pacific Visualization Symposium 2014 (PacificVis 2014)*, pages 153-160. March 2014 (Full paper reviewed).

Carbon fiber reinforced polymers (CFRPs) are currently considered as the most promising candidate in the aeronautics industry since this material is outperforming the majority of conventional

materials. Besides the quantitative porosity in a CFRP specimen, the distribution and shape factors of pores are important properties for CFRP analysis. For example porosity in a specific layer may be more critical than a homogenous distribution of pores. Together with a company partner from the aeronautics industry and material scientists dealing with composites the following questions were identified:

Q1: *What is the quantitative porosity?*

Q2: *Are the pores distributed uniformly or do clusters of pores occur?*

Q3: *What is the volume, extent, and shape factor of a pore?*

Q4: *Where are pores with certain properties located in the specimen?*

Q5: *What is the best viewpoint for analyzing 3D renderings of pores?*

3.1 Tasks and Contributions

Based on the domain experts' questions and the main tasks [Task 1: Quantitative Porosity](#), [Task 2: Porosity Overview](#) and [Task 3: Exploration of Pores](#) (see Section 1.3), the following sub-tasks for porosity determination and analysis are identified:

T1: *Quantitative Porosity*

The NDT practitioner wants to evaluate a CFRP specimen regarding its quantitative porosity and to compare the results with other reference methods. Therefore a scalar value is sufficient in this case.

T2: *Porosity Overview*

For a detailed evaluation of the specimen, a fast overview of the porosity is needed, as the pore distribution influences the local mechanical properties of the component.

T3: *Exploration of Pores*

To evaluate individual pores, the calculation of local properties is important. In particular the shape factor has a strong influence on mechanical properties and also on the results of reference measurements acquired by ultrasonic testing or active thermography. For example, only big and nodular pores between fiber bundles or thin micro pores between the individual fibers should be analyzed based on the resulting pore classification.

T4: Best Viewpoint

When evaluating a volume with segmented pores, a good viewpoint is needed. Depending on the analysis task it should avoid or prefer occlusions and enable the analysis of the majority of pores from the considered viewpoint. Due to overlapping pores in the view direction, the expressivity of a 3D view strongly depends on the viewpoint.

To answer the domain experts' questions and to solve the derived tasks a visual-analysis tool with the following contributions is introduced:

Quantitative Porosity Determination

The porosity analysis of CFRPs is achieved in the pre-processing step of the porosity determination. The local pore properties like volume, extent, and shape factor are calculated automatically and enable a classification of the pores.

Homogeneity Visualization using Porosity Maps

Porosity maps allow for fast porosity evaluation of the specimen and for a comparison to corresponding ultrasonic and active-thermography images. NDT practitioners are able to easily analyze the homogeneity of porosity in the specimen with these maps.

Interactive Exploration of Pores using Porosity Maps and Parallel Coordinates

Interactive exploration of a CFRP specimen is done in a two stages drill-down approach. A region of interest is selected in the porosity maps. Refinement of the selection using parallel coordinates leads to a visualization for an effective porosity analysis.

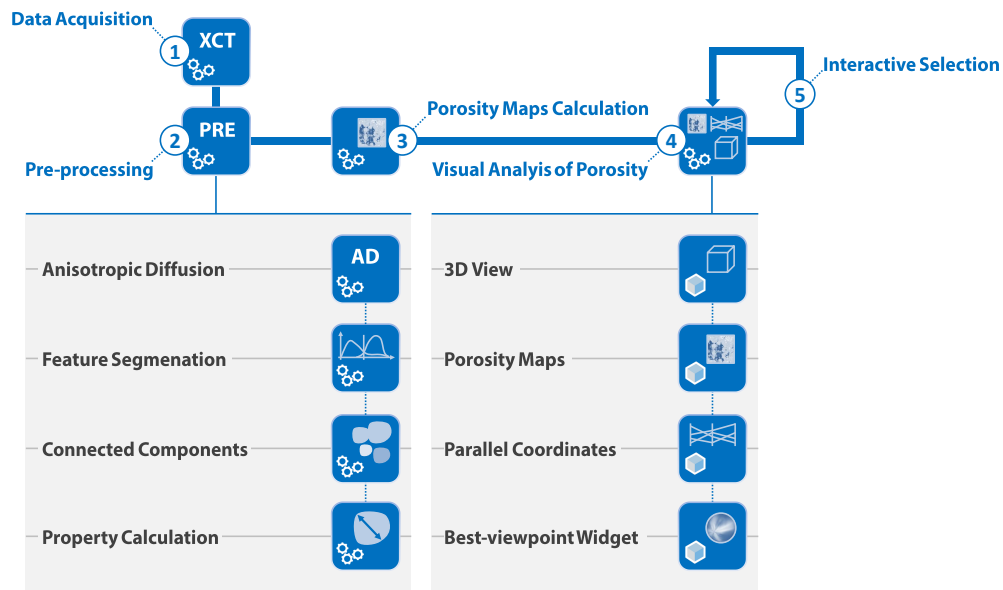
Best Viewpoint Widget

Porosity maps are calculated as specific projections along the coordinate axes. These may not be the ideal projection directions. Therefore an optimal projection-direction search (best viewpoint) is proposed which maximizes the pore overlap in the result image.

3.2 Related Work

Related work in the application domain and in the field of segmentation has already been described in Sections 1.1 and 2.2. This section will focus on methods related to the tasks T1 - T4:

The porosity topic is not limited to material science alone. Seismic engineers use porosity mapping based on geostatistical methods to find oil reservoirs [25]. Britz et al. [18] use micro-CT to quantify and visualize cortical bone microstructures. Due to the availability of several local pore properties, a visualization technique is needed to display multivariate data. Inselberg [39] introduced parallel coordinates, a plot consisting of n parallel axes, depicting an n -dimensional

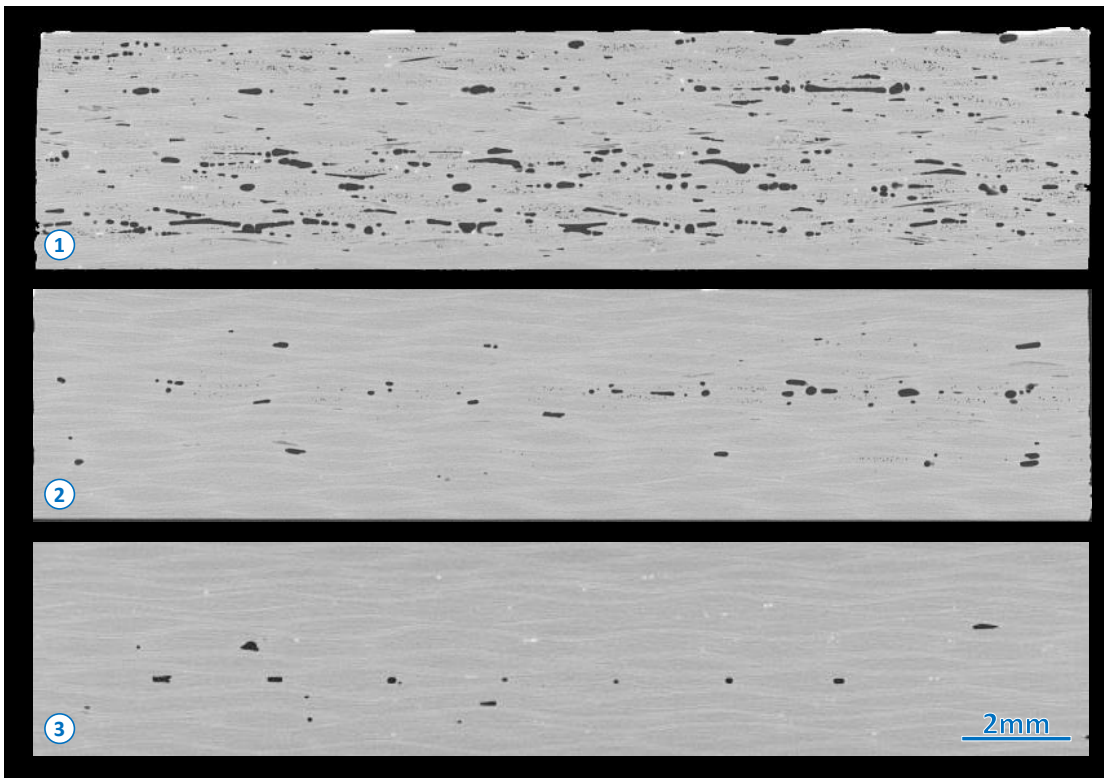


❖ Figure 3.1 — Pipeline for the visual analysis of porosity in CFRP specimens.

point set. For example, Blaas et al. [14] used parallel coordinates for interactive exploration of large multi-timepoint data sets. In this work parallel coordinates are applied by assigning each local pore property to a parallel axis. Pore properties are visualized by polylines crossing an axis at the corresponding positions. Parallel coordinates are applied in a wide range of applications. Hadwiger et al. [32] discussed interactive exploration and feature detection of industrial XCT data, including real-world applications. Because of the big number of pores in a CFRP specimen, a drill-down approach is essential for exploring the data. Interactive drill downs using enlarged detail views of the data are employed by Lex et al. [46] to explore biomolecular data. Yuan et al. [82] introduce a visual-analytics system including data drill-down for the exploration of seismic data together with satellite-based observational data. For better exploration, multiple linked-views are essential. E.g., SimVis [24] uses multiple linked-views to explore large sets of data. Regarding best-viewpoint selection, Bordoloi and Shen [15] presented an entropy-based view selection for volume rendering. Many metrics for image-entropy calculation have been proposed. Typically they are used for image registration of medical datasets [52, 74]. As proposed by Kohlmann et al. [44] deformed viewing spheres may be used for navigation in medical datasets. For a better user-oriented adaptability of the metric, a histogram-based approach is employed in this work.

3.3 Visualization Pipeline

Figure 3.1 illustrates the visualization pipeline for quantitative porosity determination and interactive exploration of pores. After the data-acquisition stage (1), pre-processing (2) steps are



❖ **Figure 3.2** — XCT xy cross-sectional images of specimens PrePreg 1 (1), PrePreg 2 (2), PrePreg 3 (3) contain pores in black. The gray areas indicate the epoxy resin and the fiber bundles.

applied including the calculation of pore properties which are required for the interactive exploration and visual analysis of porosity. Furthermore porosity maps (3) are calculated for the three axis-aligned directions. For the visual analysis of porosity (4) a 3D view, porosity maps, parallel coordinates and a best-viewpoint widget are used. With interactive selection (5) in the porosity maps and the parallel coordinates, a drill-down of the data is enabled.

3.3.1 Data Acquisition

In this chapter, samples of preimpregnated fibers (PrePreg) consisting of carbon fibers and 40 weight percent epoxy resin were used to evaluate the quantitative porosity determination. Plates with a porosity between 0 % and 10 % were manufactured by varying the vacuum pressure during the heating phase. For further investigations six specimens were cut out of these plates. They are denoted as PrePreg 1-3 with a size of $17 \times 20 \times 4.5 \text{ mm}^3$ each and PrePreg 4-6 with a size of $17 \times 20 \times 2 \text{ mm}^3$ each. Figure 3.2 depicts XCT xy cross-sectional images from PrePreg 1-3 with different levels of porosity. The black holes correspond to pores and the gray areas indicate the epoxy resin and fiber bundles. Single carbon fibers can not be seen, because the voxel size of the measurements is $10 \text{ }\mu\text{m}$ and the fiber diameter is about $8 \text{ }\mu\text{m}$. All XCT scans

were performed on a GE Phoenix|xray nanotom XCT system with a 180 kV nano focus tube. The reconstruction algorithm of the device included a correction for beam hardening. This avoids over-segmentation in the middle of the specimen due to gray-value modifications caused by beam hardening during the measurement.

3.3.2 Pre-processing

For enhancing the data quality anisotropic diffusion is applied (see Section 2.1). Pores are segmented with Otsu's thresholding method (see Section 2.2). After labeling the individual pores with a connected-components filter using 26-connectivity neighborhoods the individual properties **volume**, **extent** and **shape factor** are calculated for each individual pore (see Section 2.3).

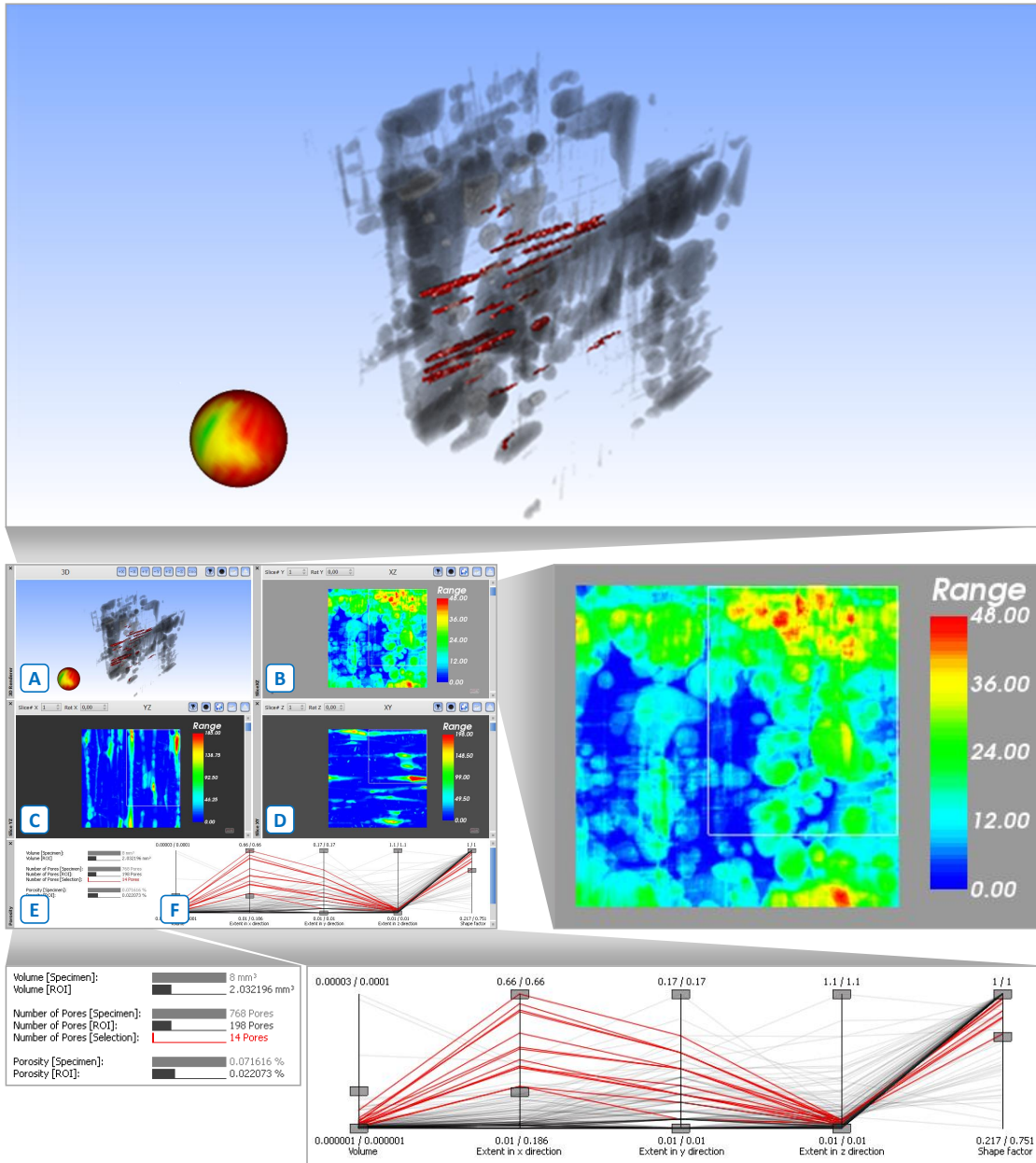
3.4 Visual Analysis of Porosity

The visual analysis of porosity includes the quantitative and qualitative porosity determination for CFRP specimens to solve T1 to T4. Figure 3.3 shows the visual-analysis framework. The CFRP volume is shown in a 3D view (A) and three orthogonal porosity map views (B, C and D), described in Section 3.4.1. The porosity tab shows a quantitative information view (E) and a parallel-coordinates view for pore filtering (F).

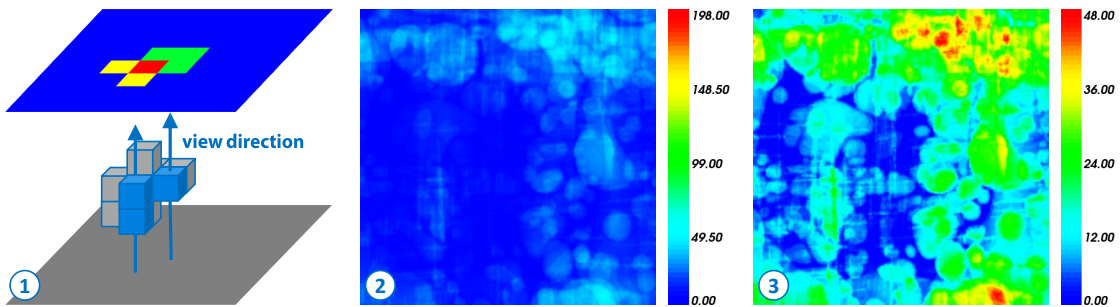
3.4.1 Porosity Maps

Material properties strongly depend on the distribution of the pores in the CFRP specimen, e.g., a homogenous distribution of pores is less critical than a high porosity in a certain layer. Thus the pore homogeneity is a relevant factor when analyzing a CFRP specimen. A porosity overview is needed to allow the user a fast evaluation of the specimen. This overview should show regions with low and high porosity in the specimen. For visualizing the porosity overview, the concept of porosity maps (PMs) is introduced. PMs are calculated for the three axis-aligned directions. Two reasons exist, why axis-aligned PMs are calculated and no other projection directions are used. First, typically axis-aligned cross-sectional images are used when evaluating XCT data. Second, reference methods, such as ultrasonic testing and active thermography, are applied orthogonal to the surface of the component which has to be measured. Thus the result images of these methods also show axis-aligned images. So PMs enable a comparability to the reference results. To calculate an individual pixel of a PM, all pore voxels along a ray orthogonal to the slice direction are summed up. This is shown in Figure 3.4 (1). Finally the PM values are mapped to colors according to one of the following modes:

- **Specimen Maximum Color Mapping (SMCM):** In this mode the maximum of all three calculated PMs is used for the particular PM color-mapping (see Figure 3.4 (2)). This mode allows the user to compare the three axis-aligned views (xy, xz and yz). If analyzing flat plate-like specimens or specimens with a low porosity in one direction evaluation problems may occur. This problem can be seen in Figure 3.5 (1)). In the y direction (xz



❖ **Figure 3.3** — (A) 3D view with highlighted selected pores. (B, C and D) Porosity maps with region of interest selection. (E) Quantitative information view showing the global properties volume, number of pores and porosity separately for specimen, region of interest (ROI) and parallel-coordinates selection. (F) Parallel-coordinates view for individual pore selection.



❖ Figure 3.4 — (1) Illustration of the porosity-map calculation-step. (2) Specimen Maximum Color Mapping (SMCM) and (3) View Maximum Color Mapping (VMCM) of a small region in specimen PrePreg 1 in the xz view. The porosity-map values correspond to the number of pore voxels.

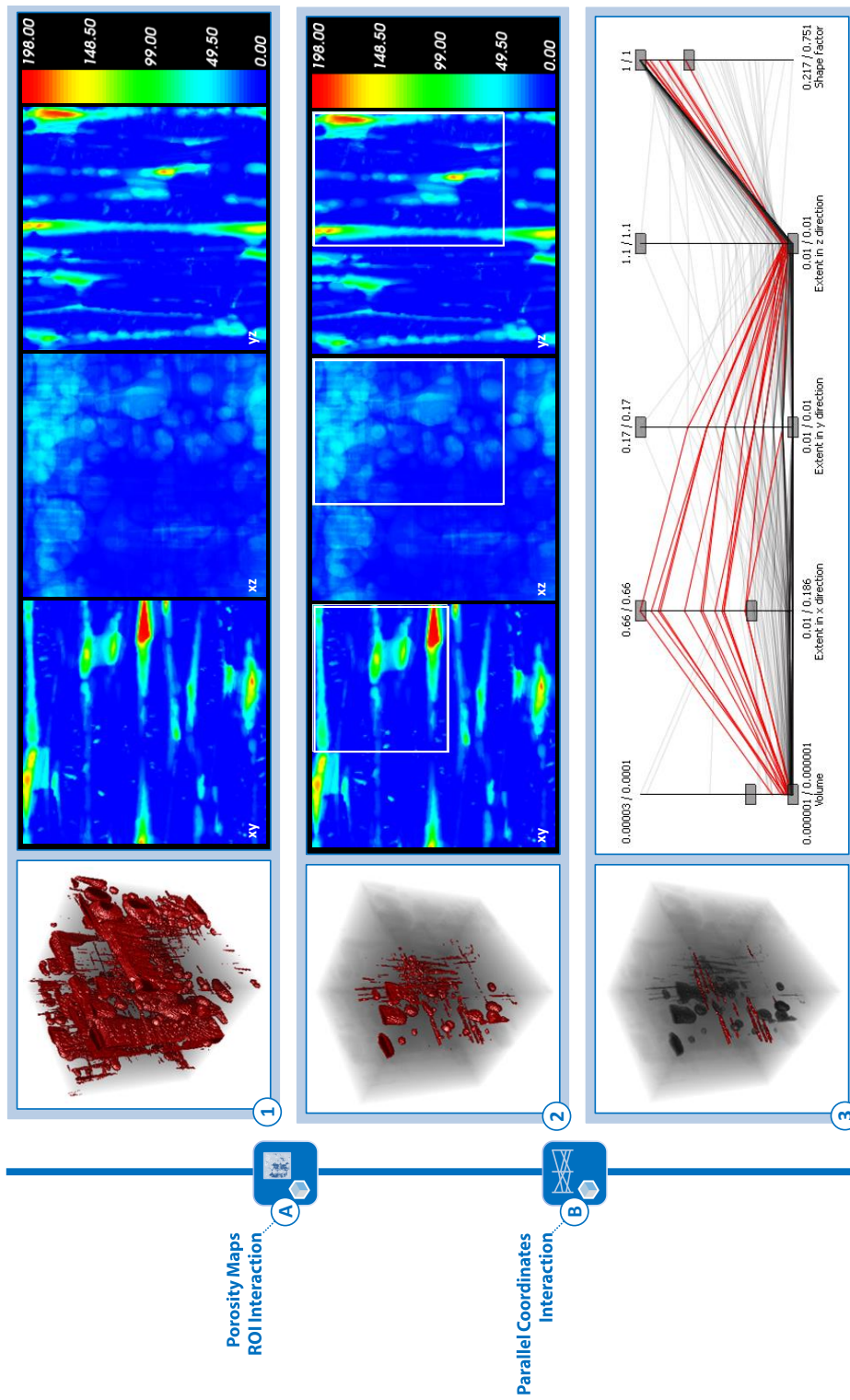
view) only low porosity is present compared to the x (yz view) and z direction (xy view). Therefore the contrast in the xz view is low which makes it difficult to evaluate this view.

- **View Maximum Color Mapping (VMCM):** The maximum of each PM is used for its own color mapping (see Figure 3.4 (3)). Thus the before described analysis problem of the SMCM mode is solved. As a drawback the comparability between the views is not ensured.

Which mode is chosen by the NDT practitioner strongly depends on the component dimensions. Summing up the advantages and disadvantages of the proposed modes, it can be said: If the SMCM mode is selected, colors are consistent in all views. The comparability is ensured, but the mode leads to problems with flat components. If the VMCM mode is used, the best contrast in the separate views is achieved but a comparison is not possible. Although rainbow color maps show a lack of perceptual ordering and an uncontrolled luminance variation [16], they were used in this chapter. The reason can be found in the comparability to other reference methods of the domain experts where rainbow color maps are also used. Of course other color maps [35] may be applied to the data.

3.4.2 Interactive Exploration and Visualization

During interactive exploration, the current selection is shown in the 3D view. The pores are mapped to color and opacity by a transfer function. Different colors and opacity values for pores inside and outside of the defined region of interest (ROI) as well as selected and unselected pores in the parallel-coordinates view enable a detailed analysis for the user. A quantitative information view and a parallel-coordinates view for interaction complete the visual-analysis setup. The axes of the parallel-coordinates view show the five calculated local pore properties, i.e., volume, extent in x, y and z direction and shape factor (Figure 3.3 (F)). The quantitative information view, shown in Figure 3.3 (E), displays the quantitative porosity to the user, and is helpful when exploring the specimen. It depicts quantitative porosity information for the



❖ **Figure 3.5** — Visual analysis of porosity in a sample specimen. An interactive exploration with a drill-down approach is shown in three stages: (1) Visualization of all pores and fast evaluation of the specimen based on porosity maps, where the values are encoded as the number of pore voxels. (2) Highlighted visualization of pores in a region of interest. (3) Accentuation of specific pores in the region of interest. (A) Porosity-maps interaction with a cuboid region of interest. (B) Further filtering of pores based on their local properties using parallel coordinates.

specimen, for the region of interest and for the parallel-coordinates selection by numerical values as well as by bar charts.

Figure 3.5 shows an example of the drill-down approach during interactive exploration in three stages. Initially no filtering is applied, so all pores are highlighted (see Figure 3.5 (1)). A detailed porosity overview of the specimen is provided. Based on the porosity maps, the user can interactively specify a ROI in the volume (see Figure 3.5 (A)). In the second stage (Figure 3.5 (2)) all pores outside the defined ROI are faded out. Simultaneously the parallel-coordinates view is updated, so that only pores inside the ROI are shown. In the third stage (see Figure 3.5 (3)) only selected pores inside the ROI are highlighted. The user can filter pores in the parallel-coordinates view regarding their local properties on the basis of lower and upper bounds (see Figure 3.5 (B)). For example, only long and thin needle-like pores are filtered in a region with high porosity (see Figure 3.5 (3)).

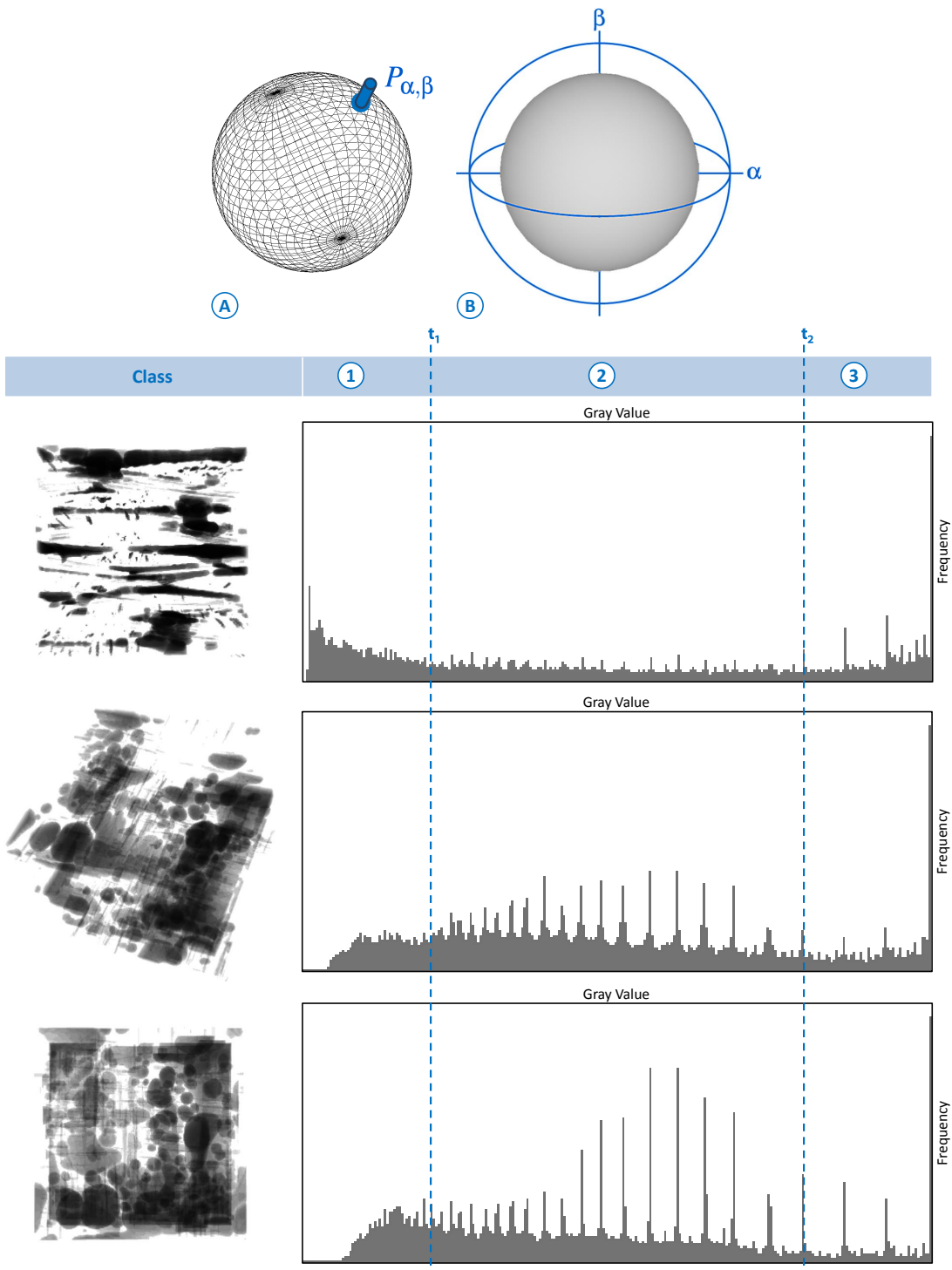
3.4.3 Best-Viewpoint Calculation

The goal of the best-viewpoint calculation is to rate the quality of viewpoints. In the application domain of CFRP characterization, a good viewpoint maximizes the pore overlap in the result image so that the fiber structure is better visible. The main idea is to calculate porosity maps for different viewpoints and to evaluate them. For the PMs only axis-aligned directions have been considered so far. To increase expressivity of the result images these constraints are now relaxed. PMs are investigated after calculating them from arbitrary directions (i.e., viewpoints). For a fast porosity-map calculation, the opacity of the pores is adjusted in relation to the maximum length of the volume. Overlapping pores cause darker areas in the image. All possible viewpoints are given as a parameterized sphere surrounding the specimen. The direction for the PM calculation is then defined by connecting the viewpoint on the sphere to the sphere center. A discrete set of viewpoints $P_{\alpha,\beta}$ (see Figure 3.6 (A)) is evaluated by varying the spherical parameters α, β in 10° steps (see Figure 3.6 (B)).

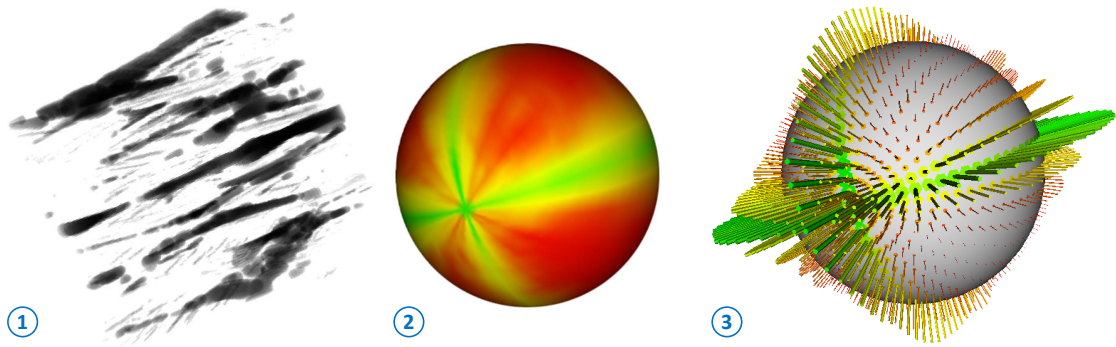
As dark regions in the 3D rendering are the result of overlapping pores and less or non overlapping pores cause bright regions, a histogram-based approach was implemented. For each viewpoint the histogram of the corresponding PM is rated. The histogram is divided into $n = 3$ classes of (1) critical, (2) borderline and (3) not critical pixels using the thresholds t_1 and t_2 . Using more classes indeed leads to a finer partition of the histogram but also to a more complex parameterization of the proposed approach.

As critical pixels in black and dark gray are the result of overlapping pores, they make an important contribution to a good viewpoint. Borderline pixels in gray show single pores or pores with less overlapping. Their contribution to a good viewpoint is low. Whereas light gray and white pixels are not critical for a good viewpoint. Based on their contribution to a good viewpoint each class is weighted with user-defined weights ω_1, ω_2 and ω_3 . The quality value $Q_{\alpha,\beta}$ for a viewpoint $P_{\alpha,\beta}$ is then calculated as follows:

$$Q_{\alpha,\beta} = \sum_{i=1}^n \sigma_i \omega_i \quad (3.1)$$



❖ **Figure 3.6** — Best-viewpoint calculation: (A) For each position $P_{\alpha, \beta}$ on the sphere the viewpoint is evaluated. (B) Varying of the viewpoint in steps of 10° in α and β . (1, 2 and 3) Histogram-based best-viewpoint calculation showing three different viewpoints: Histograms are divided into the three classes of (1) critical, (2) borderline and (3) not critical pixels.



❖ Figure 3.7 — (1) Viewpoint of a CFRP dataset. Best-viewpoint widgets for (1): (2) Color mapping on a sphere and (3) cylinder sticks. The color mapping ranges from green, indicating a good viewpoint, to red visualizing unfavorable viewpoints.

where σ_i is the sum of pixels in class i . The weights are introduced to allow the user to evaluate viewpoints with different definitions of the viewpoint quality. For example, a viewpoint showing less overlapping pores can be rated as a good viewpoint.

Figure 3.6 shows the best-viewpoint calculation using three viewpoints of a subvolume of the specimen PrePreg 1. The thresholds $t_1 = 50$ and $t_2 = 200$ were used to divide the histograms which are based on 8 bit images. The classes of critical, borderline and not critical pixels were weighted with $\omega_1 = 0.9$, $\omega_2 = 0.1$ and $\omega_3 = 0.0$.

After calculating $Q_{\alpha,\beta}$ for all viewpoints, the values are visualized on a sphere where two methods are proposed. Figure 3.7 shows the best-viewpoint widgets for one exemplary viewpoint (1). In the first approach, quality values $Q_{\alpha,\beta}$ are mapped to colors on a sphere (see Figure 3.7 (2)). With this method, quality values are interpolated in-between the calculated viewpoints. The second method attaches colored cylindrical sticks to a gray sphere. The length of the sticks also encodes the quality values $Q_{\alpha,\beta}$ (see Figure 3.7 (3)). Using this method, the quality values are only visualized for the rated viewpoints. But instead the quality values of viewpoints on the visible border of the sphere can be seen by the user before rotating the sphere in a certain direction. For both methods a color mapping is applied, where views showing the twill-weave pattern of frequently overlapping pores are rated better (in green) than views showing a homogenous image with more pores being visible (in red). In the implementation a rotation of the sphere is linked to the corresponding rotation of the specimen.

3.5 Results and Evaluation

For the practical evaluation of the quantitative porosity determination the results for the three specimens PrePreg 1-3 were compared with the results from the reference methods ultrasonic testing and acid digestion in Section 3.5.1. Furthermore the porosity determination is verified

❖ **Table 3.1** — XCT-based porosity results for specimens PrePreg 1-3 compared to the reference methods ultrasonic testing (US) using the pulse-echo technique and acid digestion (AD). The used data type is unsigned short. CPU: Intel® Xeon® X5680.

| Dataset | PrePreg 1 | PrePreg 2 | PrePreg 3 |
|----------------------|-------------------|-------------------|-------------------|
| Dataset size [voxel] | 1982 x 458 x 1673 | 2001 x 452 x 1686 | 1993 x 441 x 1701 |
| t [min] | 13.02 | 12.98 | 12.94 |
| No. of pores | 115165 | 15772 | 4167 |
| Porosity (XCT) | 4.57 % | 0.81 % | 0.39 % |
| Porosity (US) | 5.06 % | 0.91 % | 0.54 % |
| Porosity (AD) | 3.89 % | 0.53 % | 0.00 % |

using a virtual dataset from a simulated XCT scan (see Section 3.5.2). To show the applicability and the key benefits of the visual-analysis approach, the exploration of pore classifications on specimen PrePreg 1 as well as the comparison of porosity maps and active thermography images based on the specimens PrePreg 4-6 (see Section 3.5.3) is presented. In Section 3.5.4 feedback from CFRP, ultrasonic testing and active-thermography experts is summarized who assessed the results of the approach. User feedback about porosity maps concludes the evaluation in Section 3.5.5.

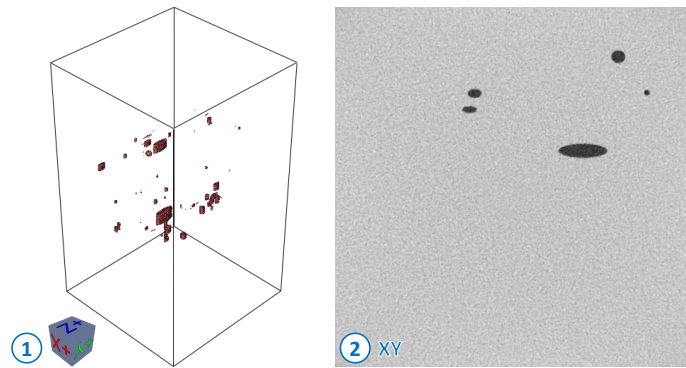
3.5.1 Quantitative Porosity Determination

The quantitative porosity was determined for the three specimens PrePreg 1-3 using ultrasonic testing, active thermography and XCT. The results are shown in Table 3.1. Pre-processing times including the anisotropic-diffusion filter, Otsu’s thresholding, the connected-components labeling and the porosity determination depend on the dataset size and the number of pores. The comparison to the reference methods ultrasonic testing and acid digestion shows that the XCT-based results are in the range of inaccuracy (about ± 1 %) of ultrasonic testing and acid digestion. The 0.00 % value for porosity in PrePreg 3 measured with acid digestion shows the method’s inaccuracy. It may be explained by calculations using imprecisely known mass densities of fibers and resin.

3.5.2 Segmentation Verification

The problem of evaluating the quantitative results has already been mentioned in Section 2.2. As the reference methods acid digestion and ultrasonic testing have a range of inaccuracy of about ± 1 %, no ground truth is available to compare the results.

For a further quantitative evaluation of the accuracy of the proposed method a small volume was cut out of the PrePreg 3 dataset and reproduced as a virtual specimen with pores given as geometric primitives like cylinders and cuboids. 73 axis-aligned pores were created in the dataset with volumes ranging from 2.8×10^{-5} to 3.94×10^{-2} mm³. Figure 3.8 shows a 3D rendering (1) of the virtual specimen and a cross-sectional image in an xy view (2). After a



❖ **Figure 3.8** — Simulated dataset to verify the quantitative evaluation: (1) 3D rendering of the virtual specimen with pores given as cylinders and cuboids. (2) Cross-sectional image of the virtual specimen in an xy view.

❖ **Table 3.2** — Porosity results of the verification on a virtual XCT dataset. The dataset size is 392 x 415 x 445 voxels.

| Dataset | Porosity |
|---|----------|
| Virtual dataset (ground truth) | 0.210 % |
| Virtual dataset (presented porosity pipeline) | 0.198 % |

simulated XCT scan generated from the data by the SimCT tool [61] the porosity result of the simulated dataset with a porosity of 0.198 % was compared to the porosity value of the virtual specimen, where the known porosity (ground truth) is exactly 0.210 % (see Table 3.2). It can be assumed that the deviation of 0.012 % is due to partial volume effects. The result shows that the segmentation gives satisfying results for the simulated data.

3.5.3 Visual Analysis of Porosity

In this section the interactive exploration and visual analysis of a small subvolume of specimen PrePreg 1 is presented. Furthermore porosity maps of the specimens PrePreg 4-6 are compared to the corresponding active thermography images. Porosity maps show the pore distribution in the whole specimen and hence they are a new way of finding regions with a high porosity. Specimen PrePreg 1 is shown after the porosity determination in a 3D view (see Figure 3.9 (1)) as well as in an xz view (see Figure 3.9 (2)). Due to the high number of pores the evaluation of the specimen is a difficult task for the NDT practitioner. The corresponding xz porosity map is shown in Figure 3.9 (3). It visualizes areas with low (blue) and high (red) porosity. Aligned pores will produce high values in the PM whereas a jittered arrangement of the pores will lead to lower values. Based on the porosity map, a ROI with the highest porosity was cut out. The use of parallel coordinates allows the user to filter pores with specific pore properties. In Figure 3.9 (4) the biggest pore in the region is highlighted. Figure 3.9 (5) shows long and thin micro pores

in the fiber bundles. Selected pores are highlighted in red. Not-selected pores are given in black, whereas white and gray illustrate the typical twill-weave pattern of the fiber bundles in the component.

With this approach only one selection can be shown. Thus the visualization of individual pores was further refined by identifying and visualizing classes of pores [76]. To do so, pores can be classified in accordance to specific property ranges, e.g., only big pores may be selected in the parallel coordinates view. The selected pores make up a new class. The tool allows the user to render each class individually or all classes together in one 3D view.

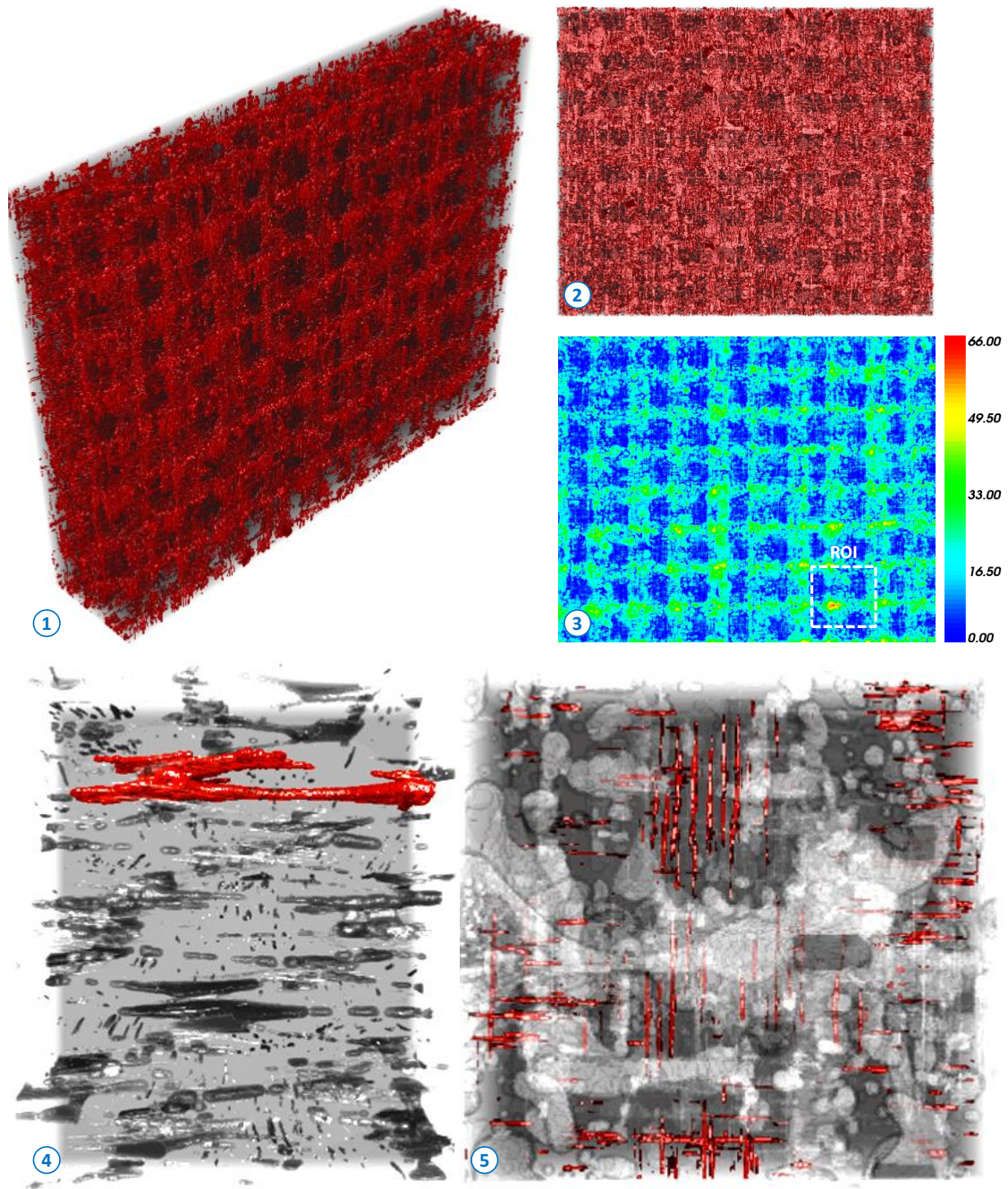
Figure 3.10 shows the selection and visualization of three pore classifications. Using the parallel coordinates visualization (1) three classifications are created. Big pores ($volume \geq 0.03$) are shown in red (2). Smaller nodular and disc-shaped pores ($volume < 0.03$ and $shapefactor < 0.75$) are highlighted in yellow (3). Blue indicates the long and thin micro pores in the fiber bundles (4) ($volume < 0.03$ and $shapefactor \geq 0.75$). If rendering only one class it can be seen, that big pores (2) are present in the whole dataset, except in the upper left corner. Smaller nodular and disc-shaped pores (3) and long and thin micro pores in the fiber bundles (4) are more or less homogeneously distributed in the dataset. The rendering of all classes together (5) shows that the porosity is slightly increasing from left to right in the dataset.

Comparison to Active-Thermography Images

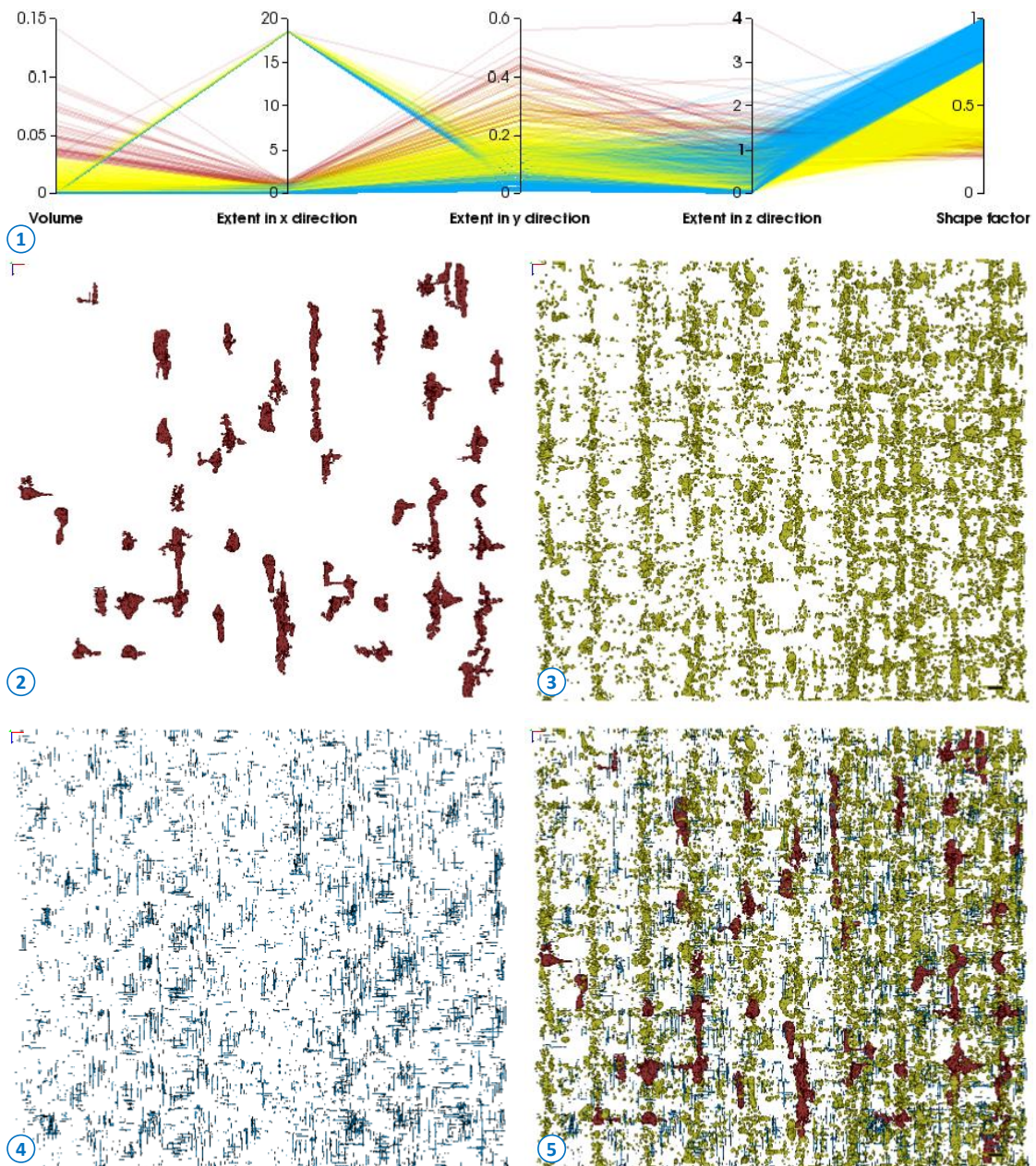
Active-thermography images show the temperature distribution that is influenced by the pores. Figure 3.11 compares such active-thermography images (1, 3 and 5) to porosity maps (2, 4 and 6) generated from XCT data. The XCT results show significantly more details. The maximum porosity can be identified more easily as the method uses 3D voxel information based on segmented pores. The structure of the pore network along the twill-weave pattern of the fibers is visible due to the better resolution of the XCT measurement (10 μm) compared to active thermography (about 150 μm). Further the thermal diffusivity blurs the images.

3.5.4 Domain Experts Feedback

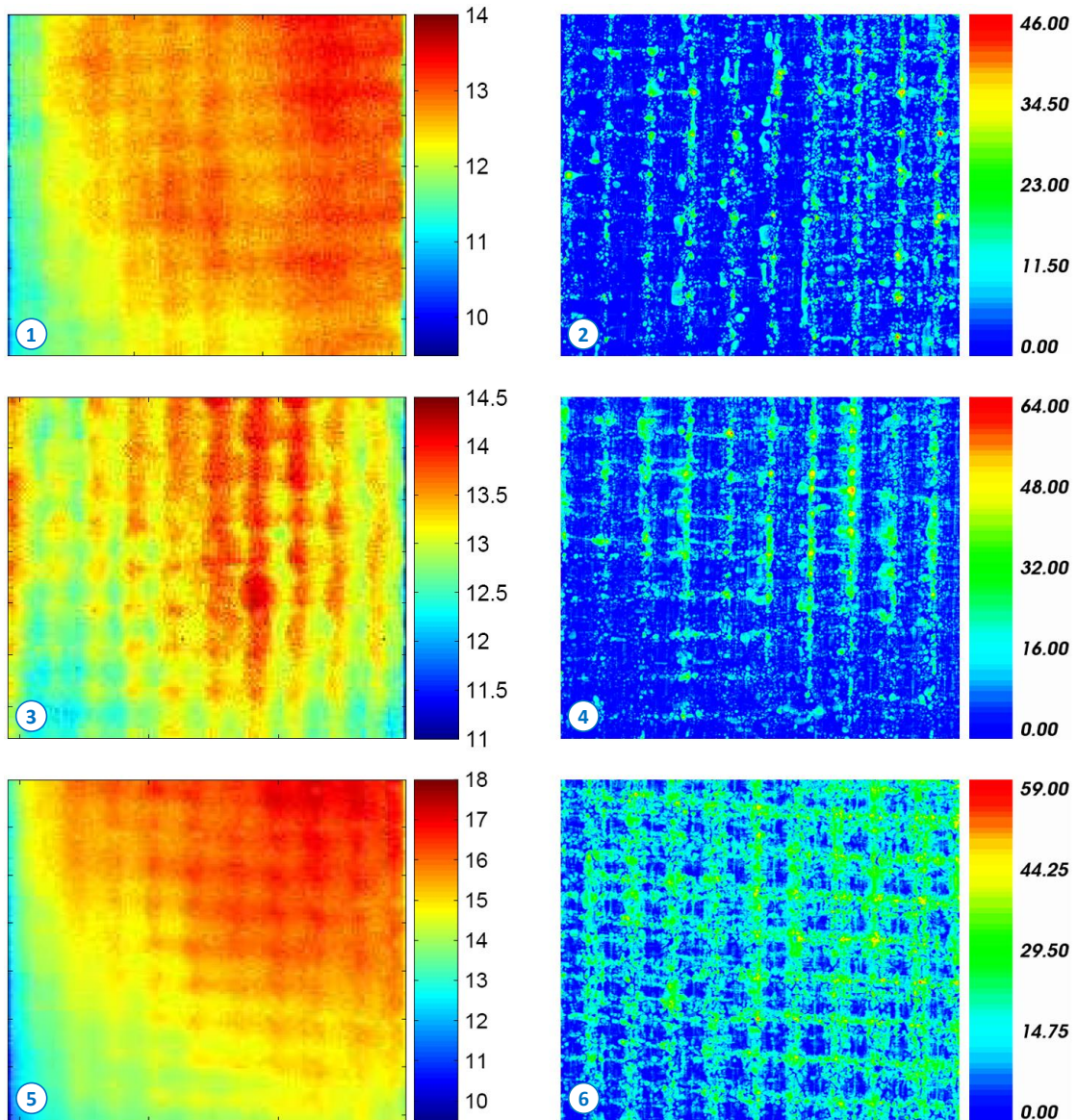
The results generated by the proposed porosity pipeline for XCT data were shown to a domain expert of a company manufacturing aircraft components. In his opinion porosity maps (PMs) are an enrichment providing previously unknown quality and detail in the porosity analysis of CFRP components. The new insight into CFRP components which can be gained with this approach allows the NDT practitioners to modify common techniques as ultrasonic testing, which is the standard non-destructive testing method in the aeronautic industry. PMs facilitate a fast comparison to the corresponding ultrasonic-attenuation images. As a further result, a better exploration of the data allows the CFRP manufacturers to draw conclusions about the manufacturing process. Active-thermography domain-experts mentioned that the visual-analysis approach increases their understanding of CFRP components. New findings about the pore distribution can be used to enhance their techniques.



❖ Figure 3.9 — (1, 2 and 3) PrePreg 1 specimen after porosity determination. In (1) a 3D view as well as in (2) an xz view and in (3) an xz porosity-map view is given. The porosity map values are encoded as the number of pore voxels. (4 and 5) Porosity evaluation of a region of interest in specimen PrePreg 1. Different pore classifications are shown. (4) The biggest pore in the region is selected and highlighted. (5) Only the long and thin micro pores in the fiber bundles are highlighted.



♦ Figure 3.10 — Visualization of different pore classes: (1) Parallel-coordinates view. (2) Big pores. (3) Smaller nodular and disc-shaped pores. (4) Long and thin micro pores. (5) Combined visualization of (2, 3 and 4).



❖ **Figure 3.11** — Comparison of active-thermography images (1, 3 and 5) to porosity maps (2, 4 and 6) of the specimens PrePreg 4-6. (1 and 2) PrePreg 4 shows a porosity of 1.81 %. (3 and 4) PrePreg 5 shows a porosity of 3.53 %. (5 and 6) PrePreg 6 shows a porosity of 7.20 %. The porosity-map values are encoded as the number of pore voxels. Based on the thermal-diffusivity model high values in the active-thermography images depict a high porosity, which is encoded as the observation time in seconds.

3.5.5 Evaluation Questionnaire

For further evaluation of the PM approach, a questionnaire was filled out by eleven engineering students. The questionnaire consisted of three tasks (see Appendix A). In the first task, areas with high porosity in images of the specimen PrePreg 1 after porosity determination should be marked. Images from Figure 3.9 (1-3) showing segmented pores in the 3D view, the xz view and the corresponding xz PM (without the marked region of interest) were used. The results showed, that the localization of interesting areas with high porosity is easier using PMs than with the 3D views of segmented pores. The second and third task concerned the comparison of images from active thermography, ultrasonic testing and PMs as well as the identification of related images from the different methods. Three specimens were evaluated. All students preferred PMs for finding areas with high porosity, followed by active-thermography images. But they were not able to assign the result images of the different methods to the specimens.

3.6 Summary

In this chapter, an approach for the interactive exploration and visual analysis of CFRP specimens was presented. The goal is to enhance the evaluation of such components. The solution includes porosity determination and the calculation of local pore properties for pore classification and their visualization. The accuracy of the quantitative porosity determination was shown using real-world CFRP specimens. The results were compared to the reference methods ultrasonic testing and acid digestion. Furthermore porosity maps were compared with active-thermography images and demonstrated that porosity maps show significantly more details. The introduced pipeline integrates ROI and parallel-coordinates interaction in a two-stage drill-down approach. The best-viewpoint widget allows the user to see on a sphere the quality-varying viewing-directions of the corresponding porosity maps. It could be shown, that the combination of porosity maps and interactive exploration is a promising tool for NDT practitioners.

MObjects - Interactive Exploration of Defects in Industrial XCT Data

This chapter is based on the following publication:

A. Reh, C. Gusenbauer, J. Kastner, E. Gröller, and C. Heinzl. MObjects — A Novel Method for the Visualization and Interactive Exploration of Defects in Industrial XCT Data. *IEEE Transactions on Visualization and Computer Graphics (TVCG)*, 19(12), pages 2906-2915, December 2013 (Full paper reviewed).

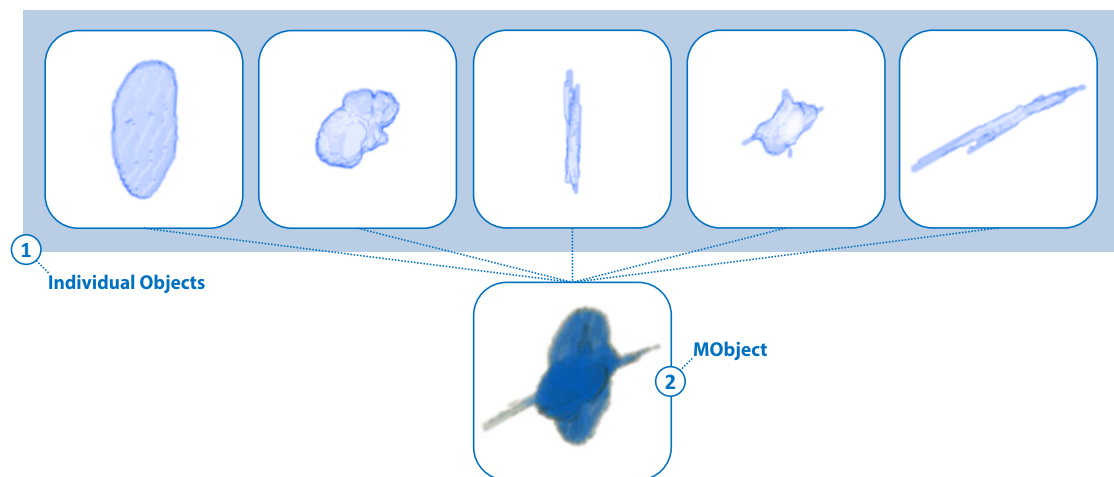
Related publications:

J. Weissenböck, A. Reh, D. Salaberger, C. Heinzl, J. Kastner. Advanced Visualization and Exploration Techniques for Fiber Reinforced Polymers. 11th European Conference on Non-Destructive Testing (ECNDT 2014), Prague, Czech Republic, October 2014 (Extended abstract reviewed, pp. 9).

B. Plank, G. Mayr, A. Reh, D. Kiefel, R. Stössel, J. Kastner. Evaluation and Visualisation of Shape Factors in Dependence of the Void Content within CFRP by Means of X-ray Computed Tomography. 11th European Conference on Non-Destructive Testing (ECNDT 2014), Prague, Czech Republic, October 2014 (Extended abstract reviewed, pp. 9).

C. Heinzl, J. Weissenböck, A. Reh, J. Kastner, T. Dierig, T. Günther, R. Stössel. Software tools for robust extraction, analysis and visualization of porosities in XCT scans of fiber-reinforced polymers. 6th Symposium for NDT in Aerospace, Madrid, Spain, November 2014 (Extended abstract reviewed, pp. 8).

In the previous chapter a drill-down approach to explore pores in a CFRP dataset was introduced. The main focus was the determination of the quantitative porosity and the comparison with existing reference methods like ultrasonic testing, active thermography, and acid digestion. A fast porosity overview with the porosity-maps visualization and an individual pore visualization



❖ **Figure 4.1** — Illustration of the MObject calculation showing pores of a CFRP dataset. (1) First the individual pores are spatially aligned according to their centers. (2) Second the MObject is calculated by aggregating the pore voxels.

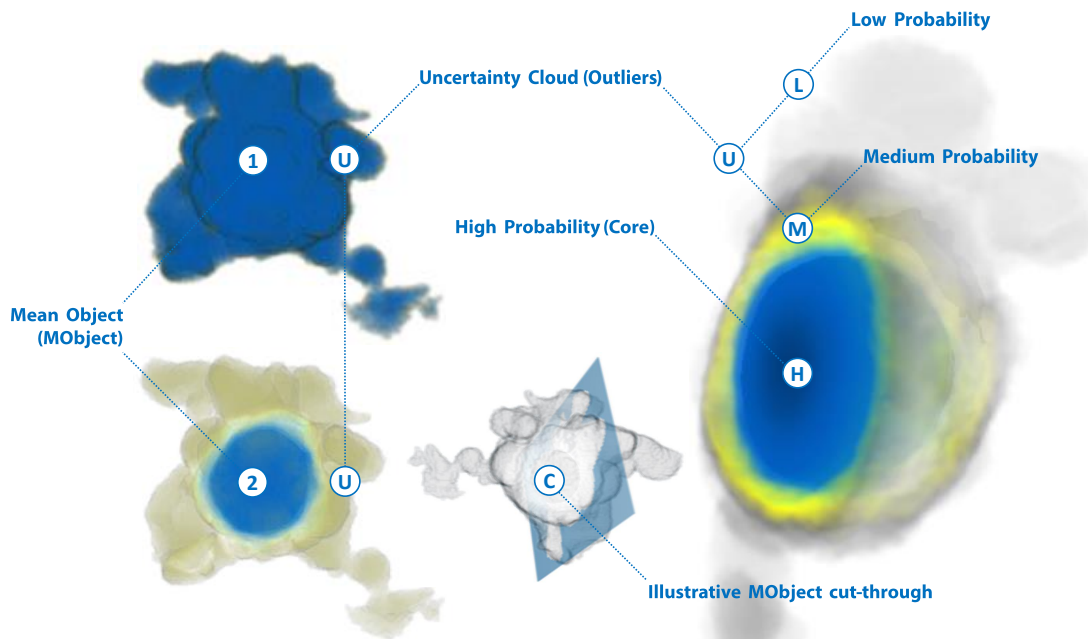
with parallel coordinates was presented and showed satisfying results. After evaluating further specimens during my work I found out that analyzing the pores individually is insufficient in certain evaluation scenarios, e.g., if the mean characteristics of the pores are needed. Due to the high spatial resolution, industrial XCT allows the user to detect a high number of pores (*individual objects*) inside. At first glance these pores have similar shapes and it is a difficult task to evaluate the data by identifying representative structures of interest in the dataset. Furthermore occlusions of pores may lead to evaluation problems using an individual pore visualization. In addition the following questions were identified together with the domain experts:

Q1: *Are the pores nodular, disc-shaped, or elongated?*

Q2: *What is the mean shape of all pores?*

Q3: *How are the pores distributed with respect to their properties?*

As a solution to the above described problem and to answer the domain experts' questions *mean objects (MObjects)* are introduced. With this method the main tasks [Task 2: Porosity Overview](#) and [Task 3: Exploration of Pores](#) (see Section 1.3) are addressed by focusing more on the shapes of the pores. Therefore the pores in the 3D dataset are examined individually (see Figure 4.1 (1)). To compute the MObject, the pores are spatially aligned according to their centers. The value of each voxel in the MObject is the sum of individual pores that overlap it (see Figure 4.1 (2)). By normalizing the MObject values to one, each voxel holds the *probability* of belonging to the MObject. Figure 4.2 illustrates the novel visualization approach with an illustrative MObject



❖ **Figure 4.2** — From a set of individual objects a MObject is calculated. MObjects are visualized by transfer functions based on the probability of each voxel of belonging to the MObject (1 and 2). The MObject cut-through (C) shows areas with high probability (H) in the center. Medium (M) and low (L) probabilities represent the uncertainty cloud (U) showing outliers of individual objects.

cut-through (C). A MObject is visualized by transfer functions based on the probability of each voxel in the MObject dataset (1 and 2). Areas with a high probability (H) represent the MObject *core* in the center. The surrounding medium and low probabilities (M and L) represent an *uncertainty cloud* (U) and correspond to *outliers* of individual objects. The calculated MObject of the whole dataset is then explored by a decomposition using interactive selection. The resulting set of MObjects is called *MObject Set*. With the help of the MObject Sets it is now possible to find *representative MObjects* in the dataset. For the specific application of CFRP analysis representative MObjects are structures of interest in the dataset. For example, *representative mean pores* in a CFRP component are nodular and disc-shaped pores within the epoxy resin as well as long and thin micro pores in the fiber bundles. Although the approach can be used for all kinds of defects in material sciences, e.g., pores, inclusions, particles, fibers, and even cracks, the focus of this chapter can be found in the evaluation of pores.

4.1 Tasks and Contributions

The previously introduced problem descriptions and their demands regarding material sciences lead to the following detailed tasks for the visualization and exploration of MObjects. The tasks are denoted as T1 - T3 for this chapter.

T1: MObjects Visualization

A non-destructive testing (NDT) practitioner analyses visual representations of features or objects of interest inside a CFRP dataset regarding their individual properties, e.g., volume, extent, or shape factors. Due to the high number of pores the calculation and visualization of MObjects is the most important task.

T2: Local MObjects Visualization

Besides individual pore properties, the spatial distribution of the pores is an important property of the investigated specimen. Non-destructive testing practitioners need a fast overview of the pore homogeneity. To achieve this goal, the dataset is divided into cells. For each cell a local MObject is calculated and visualized.

T3: MObjects Exploration

Ultrasonic testing practitioners and active thermography experts are searching for MObjects as representatives of the structures of interest in the dataset. The MObjects are needed to improve the ultrasonic calibration-curve and the simulations of the thermal-diffusivity model. Therefore the MObject of a CFRP dataset is explored interactively.

To accomplish tasks T1 - T3 MObjects of the segmented pores are calculated and visualized. For the interactive exploration of MObjects novel visual-analysis methods are introduced. Thus the contributions of this chapter are:

MObjects Calculation and Visualization

MObjects are calculated by aggregating a set of individual pores. As the calculation produces probabilities for each voxel, an uncertainty cloud using transfer functions is visualized.

Homogeneity Visualization using Local MObjects

For a fast homogeneity overview of the specimen the dataset is divided into regular sub-volumes. For each of these volumes a local MObject is calculated. The homogeneity visualization is extended with a color-coding of the sub-volumes regarding their individual properties.

Interactive Exploration of MObjects

For the interactive exploration and visualization of pores in a CFRP dataset, two methods are introduced. In a *beginners mode* the MObjects are arranged in a radial design. All possible combinations of the user-defined properties are calculated and visualized. In the *expert mode*, the MObjects are arranged in parallel. They are constructed interactively from one level to the next in order to allow the user an in-depth exploration of the dataset. The resulting representative MObjects can be exported as volumetric datasets to serve as input for ultrasonic calibrations and active-thermography simulations. Each voxel holds the probability of the MObject membership.

4.2 Related Work

In the following sections the related work for the MObjects visualization and exploration pipeline is reviewed. Segmentation of pores has already been discussed in Section 2.2. A general overview of parameter-space analysis is given in Section 4.2.1. As clustering of pores is relevant for this chapter, this topic is shortly reviewed in Section 4.2.2. For the calculation and visualization of MObjects I focus on the previous work of hierarchical and uncertainty visualization in Section 4.2.3 and 4.2.4. Further I refer to comparative visualization in Section 4.2.5 with respect to the visualization of pore homogeneity. Finally the visualization of multivariate data for the exploration of MObjects is surveyed in Section 4.2.6.

4.2.1 Parameter-Space Analysis

The resulting set of segmented pores together with their properties like the volume, extent, and shape factors make up a new parameter space, which has to be explored (T3). A broad range of methods and applications for parameter-space analysis exists:

Design galleries by Marks et al. [51] present an interface with an automatically generated selection of different graphics or animations. These can be produced by varying the input parameters, e.g., opacity and color transfer-functions for volume rendering. Ma [49] introduces Image Graphs, where the nodes in the graphs show result images. Each edge depicts the change of the rendering parameters between its connected nodes. Changes in the rendering parameters propagate through the graph. Bruckner and Möller [19] developed a system to assist graphics artists in generating special effects, e.g., smoke or explosions. Their visual-exploration approach of the parameter spaces allows the user to find the appropriate parameters for the desired results. Torsney-Weir et al. [71] introduced Tuner, a system for parameter finding in image segmentation. Tuner systematically explores the parameter space in two stages. After sampling the parameter space, a statistical model for the estimation of the segmentation algorithm's response is applied. Based on this information the user can navigate through the parameter space to find areas with high response values.

Amirkhanov et al. [8] presented a tool for the visual optimality and stability analysis of 3DCT specimen placements. For parameter-space analysis a stability widget based on penetration-length calculation, radon-space analysis as well as placement-stability analysis is used. Another approach by Bruckner et al. [20] is realized in the BrainGazer software. The system is used for the exploration and analysis of neural circuits. Visual queries based on semantic and spatial relationships are applied to a database of fruit-fly brains. Berger et al. [11] presented an interactive approach to analyze a sampled parameter space. Fritz et al. [28] presented a visual approach to analyze graphite particles in ductile iron and fibers in steel fibers reinforced sprayed concrete. Other interesting papers concerning this chapter are available as well [9, 73, 80].

4.2.2 Clustering

By calculating MObjects, similar individual objects are identified and grouped with respect to one of their properties. Therefore a cluster algorithm is used. Xu [81] published a detailed survey on clustering algorithms. In this work the user can decide on the number of clusters since he has knowledge from previous analyses how to find representative MObjects. As the clustering algorithm is easily replaceable, simple k-means is taken for clustering individual objects. Clustering itself is considered to be out of scope for this chapter and is not discussed in more detail.

4.2.3 Hierarchical Visualization

The calculation of MObjects is based on the composition and decomposition of mean and individual objects. Thus hierarchical visualizations for the interactive exploration of the MObjects (T3) are reviewed. A combination of hierarchy visualization and scientific visualization was presented by Balabanian et al. [10]. Their method integrates visualizations for hierarchically organized volumetric datasets. A graph shows the hierarchy and the nodes display the corresponding 3D volumetric data. Brambilla et al. [17] introduced a hierarchical splitting scheme for the analysis of integral surfaces. At each hierarchy level the cuts are chosen according to a surface complexity metric. Ip et al. [40] partition the histogram of a volumetric dataset into an exploration hierarchy using a normalized-cut multilevel segmentation approach. Inspired by these techniques, the MObject Set visualization is introduced. After a decomposition of the dataset's MObject, the user is able to explore the data in a graph, where the nodes show 3D representations of the MObjects.

4.2.4 Uncertainty Visualization

A MObject is calculated by aggregating individual objects of one cluster. Thereby each voxel holds the probability of belonging to the newly generated MObject. These probabilities as well as the regions with elevated uncertainty are visualized (T1). Kniss et al. [42] present an approach for the interactive exploration of uncertainty including a risk and decision analysis. They render the results of the risk analysis into a unified probabilistic data space. As MObjects are aggregated from all considered individual objects, the approach by Kniss et al. [42] is not suitable for the visualization. Point-based probabilistic surfaces were introduced by Grigoryan and Rheingans [31]. They visualize surfaces with uncertainties using points as display primitives. Although their approach is useful for visualizing uncertainty on surfaces, we can not apply it to the data at hand. Fout and Ma [27] present fuzzy volume rendering. By computing the posteriori uncertainty they provide a verifiable volume rendering. Heinzl et al. [38] compute a probability volume of multi-material components using a statistical analysis. Similarly I provide insight into the MObjects' data to show the core and the outliers. Transfer functions are also used to emphasize a user-defined border of probability. They are suitable for visualizing the a priori-based uncertainty of an MObject.

4.2.5 Comparative Visualization

The issue of visualizing the pore homogeneity in the dataset (T2) can be resolved with comparative visualization. Malik et al. [50] refer to a wide range of comparative visualization approaches. Additionally they propose a base tile pattern for a multi-image view for comparative visualization, which is an extension of the checkerboard-pattern [69] approach and attribute blocks [54]. Malik et al. compare 2D slices of volumetric datasets with different measurement parameters. Ahrens et al. [3] visualize differences between scientific simulations. Schmidt et al. [64, 65] present a novel approach to visualize differences and similarities in large sets of images [64] and a comparative visual-analysis technique for 3D meshes [65]. These methods are not applicable to the segmented pores data. Thus the dataset is divided into cells and local MObjects are calculated for each cell. Furthermore a homogeneity visualization is added, where the cells are color-coded based on the deviation of the local average from the global average.

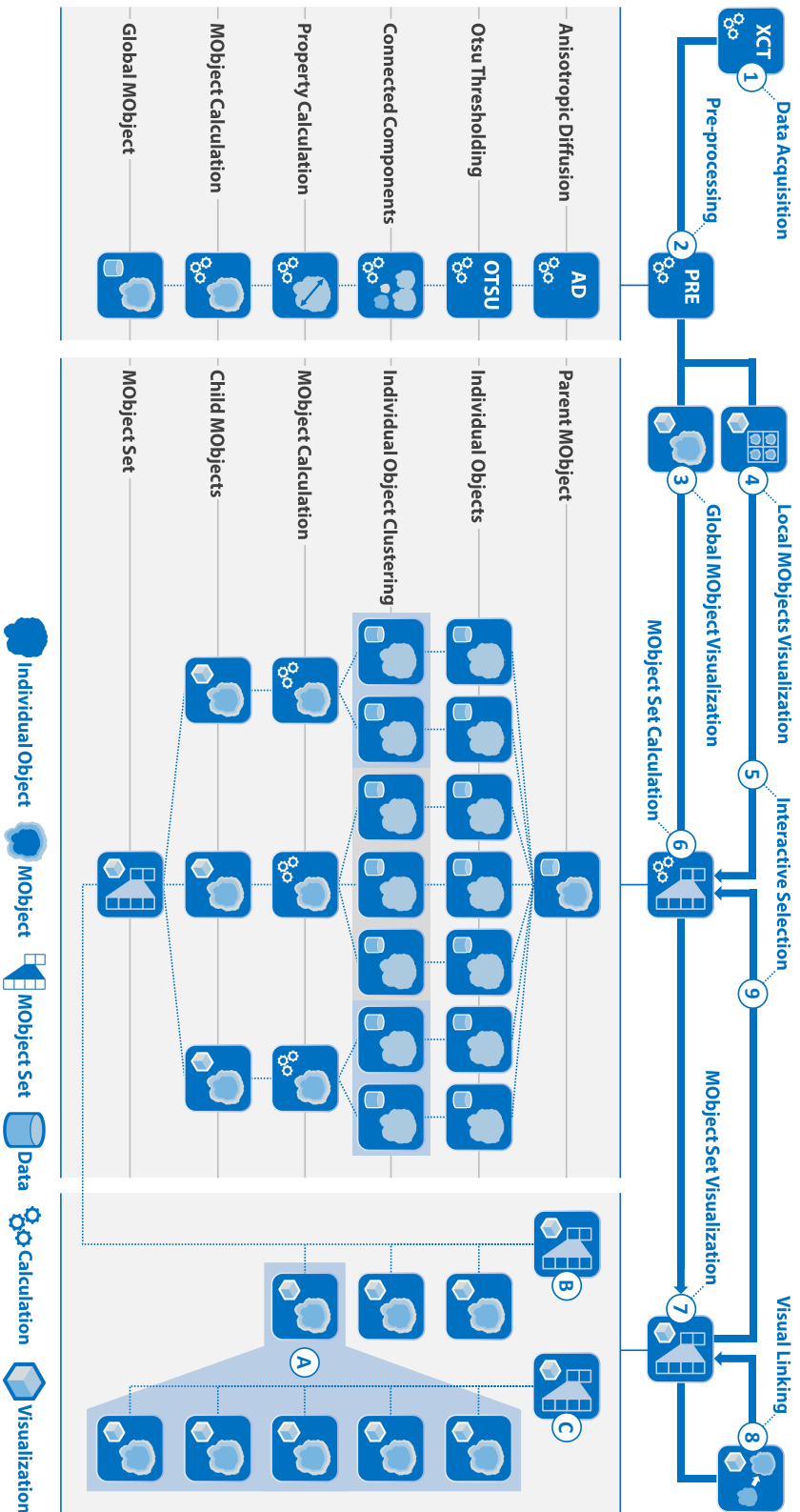
4.2.6 Visualization of Multivariate Data

Parallel coordinates introduced by Inselberg [39] are a common visualization approach for displaying and filtering multivariate data. Kosara et al. [45] extended parallel coordinates and presented parallel sets for dealing with categorical data. Instead of individual data points, they show data frequencies between the axes and visualize the relations between categories. StratomeX by Lex et al. [47] was inspired by parallel sets, where datasets of genomic data are represented as columns and subtypes as bricks in the columns.

The MObject Set visualization in parallel alignment was inspired by these techniques (T3). Parallel coordinates can serve as classifiers for the selection of individual pores and parallel sets share the idea of clustered objects. Due to the usage of categories, both approaches are not applicable to volumetric datasets. They do not visualize the spatial relationship between as well as the appearance of the objects.

4.3 Visualization and Exploration Pipeline

In this chapter representative structures of interest in an XCT dataset, e.g., pores in a CFRP component, have to be identified. Therefore a pipeline for the visualization and interactive exploration of MObjects is proposed. The pipeline is illustrated in Figure 4.3. In the data acquisition stage (1) 3D X-ray Computed Tomography (XCT) data is generated (see Section 4.3.1). On the resulting volumetric dataset pre-processing steps (2), described in Section 4.3.2, are performed to calculate the resulting global MObject of the dataset. This MObject is considered as mean pore and represents the aggregation of all pores in the component. For further visualization of the MObject two methods are proposed. In the first approach, the global MObjects visualization (3), the global MObject serves as input for further exploration. For a fast overview of the dataset a local MObjects visualization (4) is suggested. The dataset is divided into cells and for each cell a local MObject is calculated and shown in combination with a color-coded homogeneity visualization. Through interactive selection (5) the subsequent exploration starts with



❖ **Figure 4.3** — Pipeline for the visualization and interactive exploration of MObjects in a dataset. After the stages Data Acquisition (1) and Pre-processing (2) the user can decide between the visualization of the global MObject (3) or a local MObjects visualization (4). Through interactive selection (5) one is able to start the exploration with a local MObject. Otherwise the global MObject is the input for the exploration. The child MObjects are calculated in the MOBject Set Calculation (6) stage for further visualization in the MOBject Set Visualization (7) stage. The interaction techniques Visual Linking (8) and Interactive Selection (9) of MObjects are provided. Interactive selection is done by selecting a MObject (A) in a MOBject Set (B) to calculate a new MOBject Set (C) out of the selected MObject (A).

one of the local MObjects instead of the global one. All the individual objects in the MObject of interest are then clustered in the MObject Set calculation (6). The parent MObject is further subdivided into new child MObjects based on one of their calculated properties. For example, the parent MObject is classified into two child MObjects based on the shape factors of the pores. The first MObject only contains nodular pores, whereas the second one consists of long and thin pores. The user is then able to interact with the resulting MObject Set visualization (7). Through visual linking (8) or interactive selection (9) an iterative calculation and visualization of the MObject Sets will be triggered upon each major change in the classification. By selecting a MObject (A) in a MObject Set (B) a new MObject Set (C) consisting of new child MObjects can be calculated from the selected parent MObject (A).

4.3.1 Data Acquisition

In this chapter, carbon fiber reinforced polymer (CFRP) specimens were used made of pre-impregnated carbon fibers and epoxy resin. For the investigations plates with a size of 17 x 20 x 1 mm³ were used. The voxel size of the datasets was 10.5 μm. The XCT scans were performed on a GE Phoenix|xray nanotom XCT system with a 180 kV nano focus tube. A tube voltage of 60 kV, a measurement current of 320 μA, and 500 ms integration time at the detector were used as scan parameters. Over-segmentation in the middle of the specimens may occur due to gray-value modifications caused by beam hardening during the measurement. Therefore a beam-hardening correction was applied during the reconstruction.

4.3.2 Pre-processing

For pre-processing the data anisotropic diffusion for smoothing the data and Otsu's thresholding method for segmenting the pores was applied as described in Sections 2.1 and 2.2. The individual objects are then labeled by a connected-components filter using 26-connectivity neighborhoods. The labeled objects are the input to an individual property calculation stage which is the basis for the MObjects determination. To enable interactive exploration and classification of objects the properties [volume](#), [extent](#), [shape factor](#) and [directional shape factors](#) are calculated for each individual pore (see Section 2.3).

4.4 Visualization

Novel methods for the visualization and interactive exploration of MObjects which are based on a set of individual objects in a dataset are introduced. Besides the calculation and visualization of MObjects (see Section 4.4.1) a homogeneity visualization of the dataset is proposed. It uses local MObjects and a color-coding of the grid-based sub-volumes. The approach is based on the deviation of average individual properties, e.g., the average pore volume in a cell (see Section 4.4.2). To explore MObjects two visualization approaches are presented in Section 4.4.3 which use MObject Sets in radial and parallel arrangement. Furthermore interaction techniques for these two methods including visual linking are introduced.

4.4.1 MObject Visualization

For the visualization of a single MObject an uncertainty cloud surrounding the MObject core is introduced (see Section 4.4.1.1). Therefore transfer functions were used. They are described in more detail in Section 4.4.1.2. To calculate a MObject all individual objects are spatially aligned by their centers. The center position can be calculated from the extents $extent_{x_i}$, $extent_{y_i}$, $extent_{z_i}$ of the individual objects or the barycenter of each individual object can be used. Both methods showed similar results for pores in CFRP datasets as pores typically have nodular, disc, or long and elongated shapes. In order to avoid additional calculations, the extent-based approach was used. If transferring the MObjects idea to other application areas, the centroid calculation has to be reconsidered according to the specific requirements.

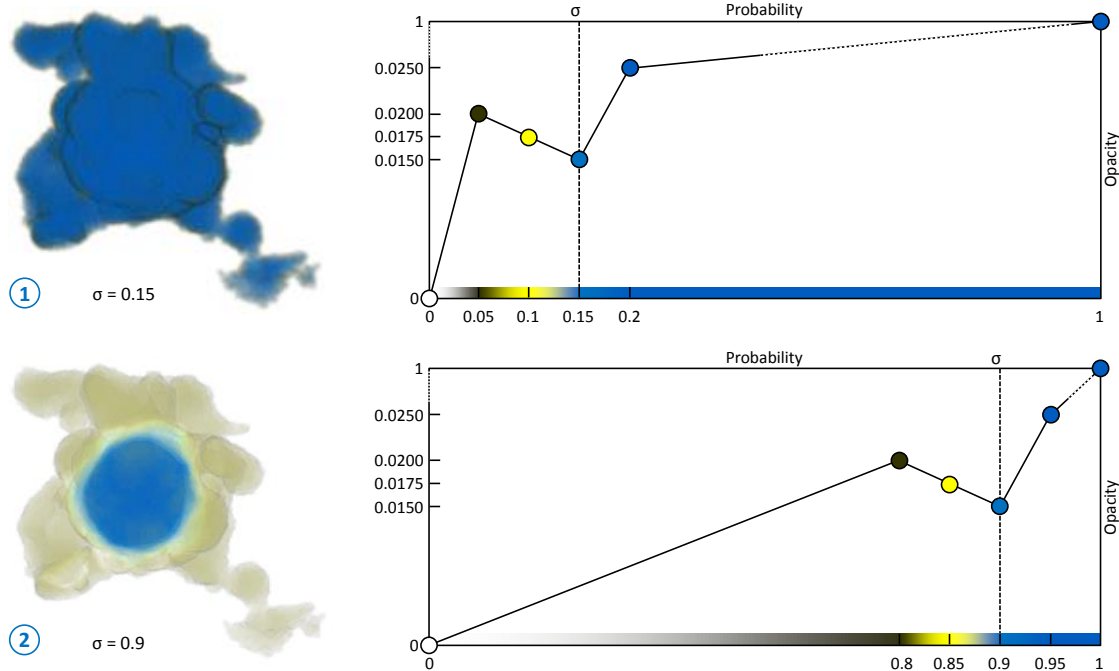
Although it is possible to rotate and register all individual objects in the calculation, they are aligned with their original orientation. This transformation without a rotation is important in the specific application area of CFRP analysis which is addressed in this thesis. Due to the layer structure of the material the MObject should clearly visualize the different orientations of the individual objects. To integrate an individual object into the MObject, each voxel of the individual object is examined separately. Therefore the distances Δx , Δy and Δz to the center are calculated for each voxel in the individual object dataset. After the distance calculation for one voxel, the corresponding voxel in the MObject with the same distances Δx , Δy and Δz to the center of the MObject is incremented. This step is done for each voxel of each individual object. To get the corresponding probabilities the resulting MObject values are normalized to one.

4.4.1.1 Uncertainty Cloud

A MObject is a volumetric dataset, where each voxel holds the probability of belonging to the MObject. This information has to be visualized accordingly. An uncertainty cloud surrounding the MObject's core is visualized. Uncertainty cloud and core are based on the stored probabilities. A high probability at a specific position means that nearly all of the individual objects which were summed up to the MObject, include this location. In Figure 4.2 the uncertainty cloud (**U**) is illustrated. The probability in the core of the MObject is typically high (**H**). As the contribution of outliers to the MObject is low, they have a medium (**M**) or low (**L**) probability of belonging to the MObject.

4.4.1.2 Transfer-Function Design

The uncertainty cloud is visualized using transfer functions. Colors for high probabilities (blue) to medium (yellow) and low probabilities (gray) are applied. Yellow-grey thus shows the outliers (see Figure 4.4). The step between high (blue) and medium (yellow) probabilities emphasizes for each MObject voxel if it belongs either to the core or the outliers of the MObject. For the interactive visualization and adaptability to different applications, the user steers this visualization by an uncertainty filter σ . Figure 4.4 shows how the gray-yellow-blue gradient is shifted

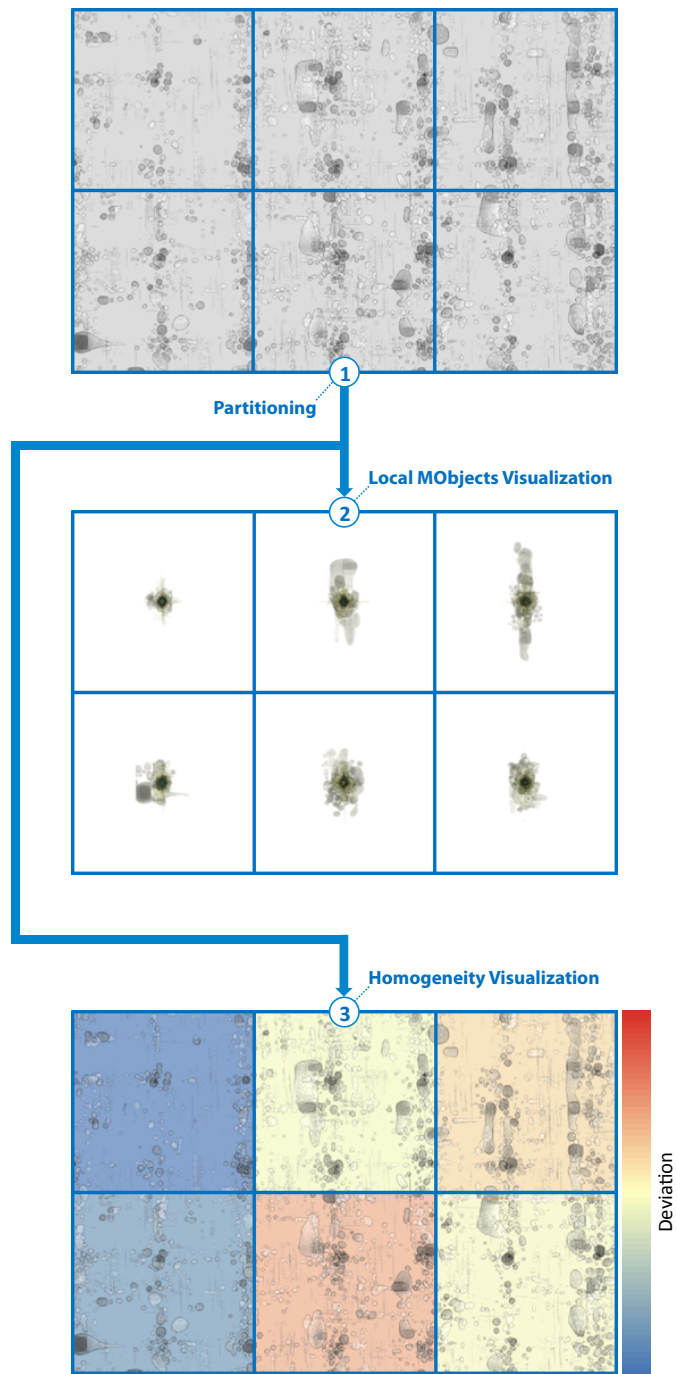


❖ Figure 4.4 — (1) MObject showing a small uncertainty cloud using a low uncertainty filter $\sigma = 0.15$. (2) A high uncertainty filter $\sigma = 0.9$ leads to an uncertainty cloud showing the MObject's core and outliers.

in the transfer function based on σ . Setting a low uncertainty filter, leads to a small uncertainty cloud and a visualization strongly representing the surface of the MObject (1). In the case of using a high uncertainty filter, one can clearly determine the core of the MObject and see the surrounding outliers (2). To emphasize the core, a lower opacity value at the position of σ is applied in the transfer function.

4.4.2 Local MObjects Visualization

Pore homogeneity is an important criterion in material sciences. This topic was already covered with porosity maps visualizing the porosity in a CFRP specimen [60] (see Chapter 3). As the homogeneity of the different pore properties is also helpful to find interesting regions for a further detailed analysis, this information has to be visualized in an easy to understand and intuitive way. Therefore a homogeneity visualization is proposed using local MObjects and a comparative homogeneity visualization with color-coded cells. Figure 4.5 describes the approach in more detail. First the volumetric dataset is partitioned into sub-volumes (1). I refer to them as cells. The cell size depends on the biggest pore extents in the dataset as the biggest pore should fit in a cell without overlapping. Based on this partitioning two visualizations to convey homogeneity to the user are implemented. In the first method local MObjects (2) are visualized. For



❖ Figure 4.5 — Based on the partitioning (1) of the volume into cells, local MObjects (2) and a color-coded homogeneity visualization (3) is shown to the user. The color-coding illustrates the deviation of the average cell properties from the global average property. Red indicates the highest positive deviation, whereas blue shows the highest negative deviation.

each cell a MObject is calculated and centered in the cell. All pores whose centers are inside the cell are considered. An overlapping pore is also assigned to the cell where the pore's center is located. The same transfer function is used for all local MObjects.

In the second approach the average pore properties and their deviations to the global average properties of the whole dataset are calculated. The user is able to guide this comparative homogeneity visualization by selecting a property. Each cell is colored according to its deviation from the selected global property (3). For color-coding the cells a diverging colormap [35] from blue over yellow to red is applied to show the negative and positive deviation of the average cell properties from the global average property of the specimen.

4.4.3 MObject Set Visualization

For the interactive exploration of MObjects in a dataset a visual representation is provided to the user. A parent MObject can be divided into a set of child MObjects which together make up a new MObject Set. All individual objects which belong to the parent MObject are clustered based on one of the calculated properties. For each cluster a new child MObject is calculated. The child MObjects together form a new MObject Set. The MObject Set may be explored interactively with a recursive selection and decomposition of the included child MObjects. Figure 4.6 illustrates this process using individual pores of a CFRP dataset. The parent MObject (1) is split up into the five contained individual objects. First, these individual objects are clustered according to their shape factors into two clusters A (2) and B (3). Second, all individual objects in a cluster are aggregated to new child MObjects (4 and 5). These child MObjects make up a new MObject Set (6). For the clustering two possibilities are provided to the user:

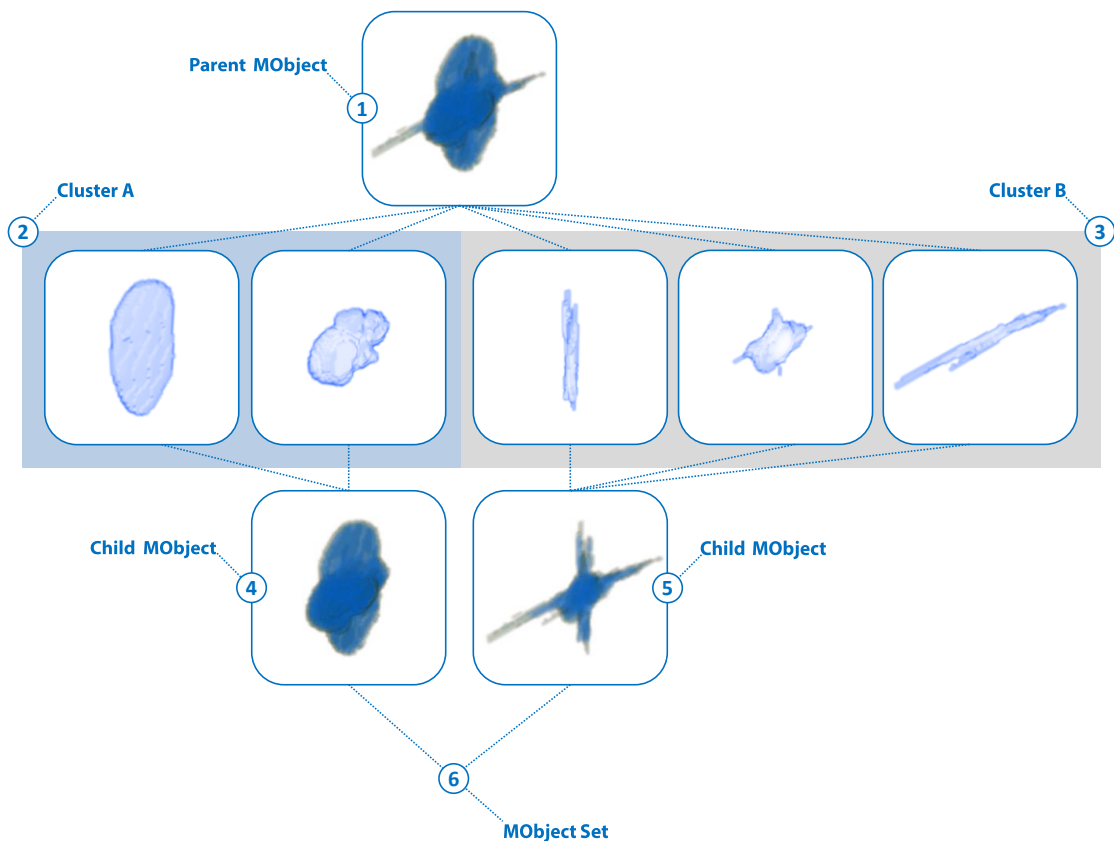
Automatic Clustering

The automatic clustering mode uses k-means clustering to assign the individual objects to classes. All the individual objects are classified into k clusters where each individual object belongs to the cluster with the closest mean. The user decides on the number k of clusters and which object property should be used for clustering.

User-defined Clustering

If the user wants to select the cluster centers by himself, it is possible to override the automatic clustering. One reason may be that specific domain-expert knowledge from previous analyses specifies the clustering for a certain property. In this case the user is able to modify the clustering done by the automatic approach employing a simple dialog.

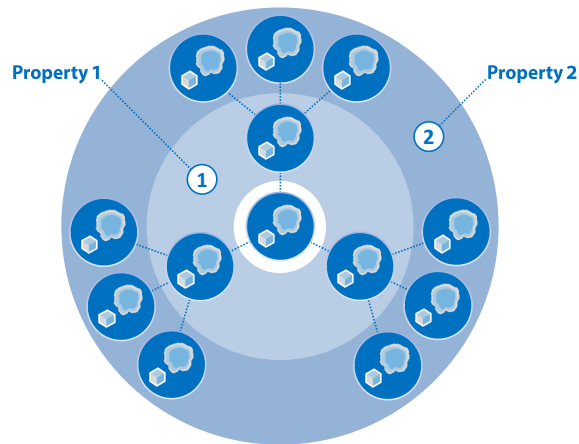
After clustering according to a certain property, a child MObject is calculated for each cluster out of all individual objects that belong to it. For the MObject Set visualization two modes are proposed. Section 4.4.3.1 describes the beginners mode where the radial MObject Set visualization is introduced. The expert mode with the parallel MObject Set visualization is described in Section 4.4.3.2.



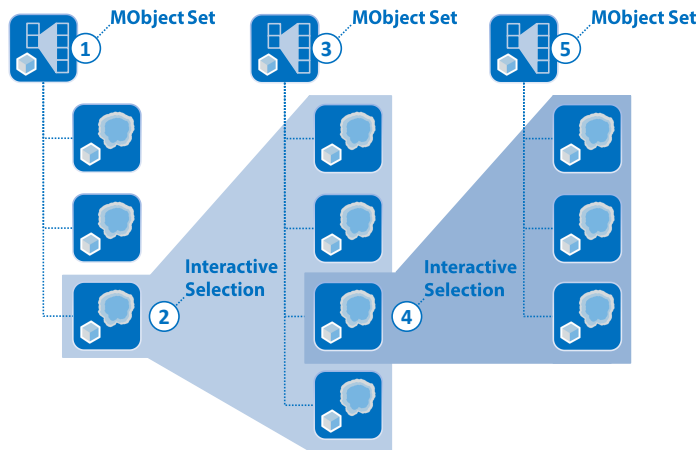
❖ Figure 4.6 — Illustration of the MObject Set calculation showing pores of a CFRP dataset. All individual pores of the parent MObject (1) are divided into two clusters A (2) and B (3). The resulting child MObjects (4 and 5) make up a new MObject Set (6).

4.4.3.1 Radial MObject Set Visualization (Beginners Mode)

For inexperienced users, setting the number of classes for clustering and specifying the sequence in which the properties shall be explored can be a challenging task. To give a better overview of the data and the resulting MObjects a beginners mode for an interactive exploration of MObjects is provided. Figure 4.7 illustrates the MObject Set visualization in a radial arrangement. In most evaluation scenarios two properties are sufficient (e.g., pore volume and shape factor). The user selects the number of classes and the desired properties for the MObject Set calculations. The radial design allows the user to render all possible combinations between the properties (1) and (2) and not only one at a time (see parallel MObject Set visualization in Section 4.4.3.2). Based on this visualization, parameters for the expert mode can be found more easily. The beginners mode further reduces the error rate of selecting undesired MObjects while exploring the data.



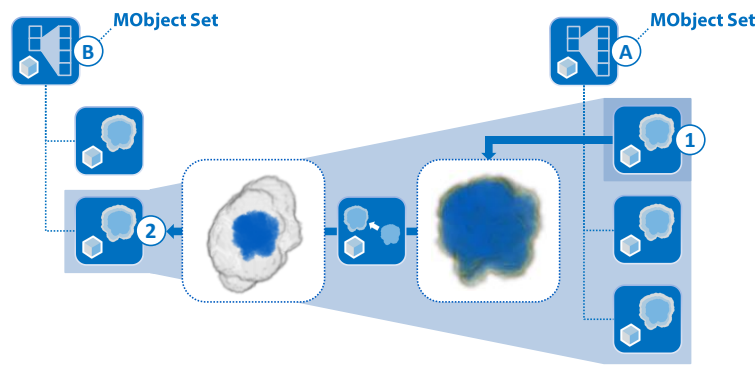
❖ Figure 4.7 — The radial MObject Set visualization shows all possible combinations between the properties (1) and (2).



❖ Figure 4.8 — Parallel MObject Set visualization for a step by step exploration. MObject Sets (1), (3) and (5) are calculated and visualized after interactive selections (2) and (4).

4.4.3.2 Parallel MObject Set Visualization (Expert Mode)

The before described radial MObject Set visualization (see Section 4.4.3.1) leads to a fixed classification of the individual objects. Experienced users want to cluster the pores based on their properties in a sequence that best fits their needs to extract the MObjects of interest. This sequence of properties may be different from case to case. To support this situation the parallel MObject Set visualization which is illustrated in Figure 4.8 is presented. MObject Sets are calculated and visualized after interactive selections. All individual objects of the dataset are clustered based on a property and a user-defined number of clusters, e.g., three shape factor classes. The resulting MObjects are shown in a MObject Set (1). Through interactive selection



❖ Figure 4.9 — Illustration of the visual-linking approach. After selecting a MObject (1) in a MObject Set (A), visual linking shows the selected child MObject inside the parent MObject (2) of the parent MObject Set (B).

of a MObject (2), the user is able to iteratively repeat the before described step of MObject Set calculation to explore the selected MObject. As a result a new child MObject Set (3) is calculated and visualized. As one would commonly use different properties as cluster criteria, it is possible to repeat the interactive selection step (4) to calculate another MObject Set (5) and finally explore the whole dataset to find the desired MObjects.

4.4.3.3 Scaling through Visual Linking

In the visualization all MObjects are rendered in individual frames of the same size. The MObjects are scaled to best fit their corresponding rendering frame. This leads to a diverging scaling of the MObjects. Thus visual linking is introduced. This approach connects all MObjects along the selection path so that it becomes obvious where a child MObject is located inside the parent MObject. Furthermore the scaling of a considered MObject in its hierarchical relationship is represented. To do so, the transfer function for all MObjects except the selected MObject in the visualization is changed in a way, that only the surfaces of the MObjects are shown in grey with a high opacity. The selected MObject is then shown in all MObjects along the selection path. Figure 4.9 illustrates this approach using a parallel MObject Set visualization with two MObject Sets (A) and (B). If selecting a child MObject (1) visual linking shows the selected MObject inside the parent MObject (2) of the parent MObject Set (B).

4.5 Results and Evaluation

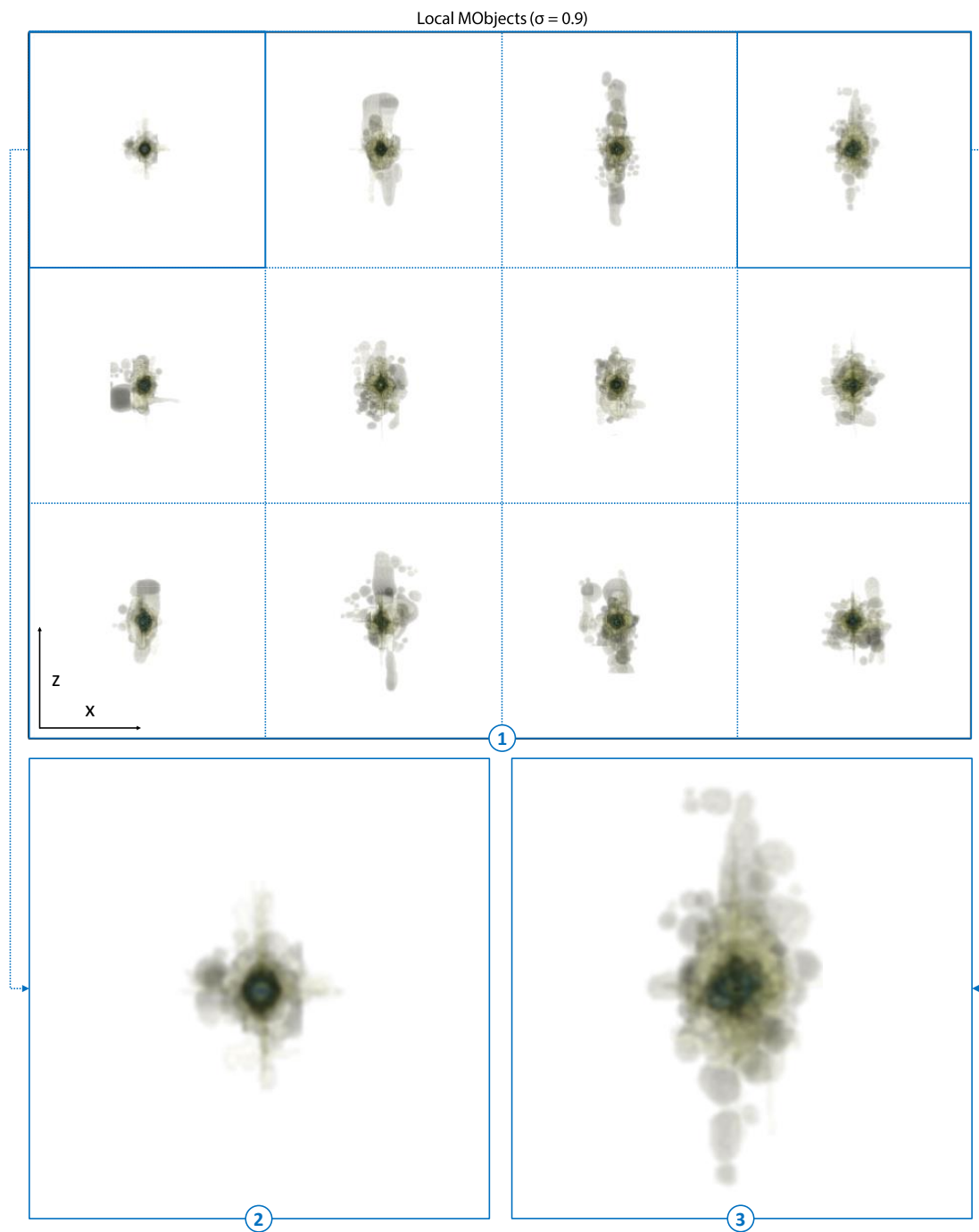
The initial design of the MObjects visualization is motivated by a high demand of material characterizations in the aeronautics industry. Especially carbon fiber reinforced polymers (CFRPs) show a great potential because of their increased stiffness and strength-to-weight ratio. As a result of the manufacturing process, CFRPs tend to have pores inside. They can occur as nodular

pores or crack-shaped delaminations in the epoxy resin or as long and thin micro pores inside the fiber bundles. In the following sections I show the local MObjects visualization including the color-coded homogeneity visualization (see Section 4.5.1) as well as the radial (see Section 4.5.2) and parallel (see Section 4.5.3) MObject Set visualization to explore a large number of individual pores. For the further evaluation user feedback from domain specialists was gathered through a questionnaire (see Section 4.5.4). The results show a CFRP dataset with a size of 1800 x 1600 x 100 voxels and a porosity of 1.94 %. The computational time including all pre-processing stages, the calculation of the global MObject and the local MObjects as well as the cell calculations for the color-coded homogeneity visualization was about 17 minutes on an Intel Xeon X5680 workstation with 48 GB RAM. Most of the time was spent for the pre-processing stages and the global MObject calculation. The MObject calculation and visualization stages are still non-optimized prototypes. As these prototypes are already suitable to test the acceptability of the presented approach using real-world components, the major focus was not the optimization at this stage of the development.

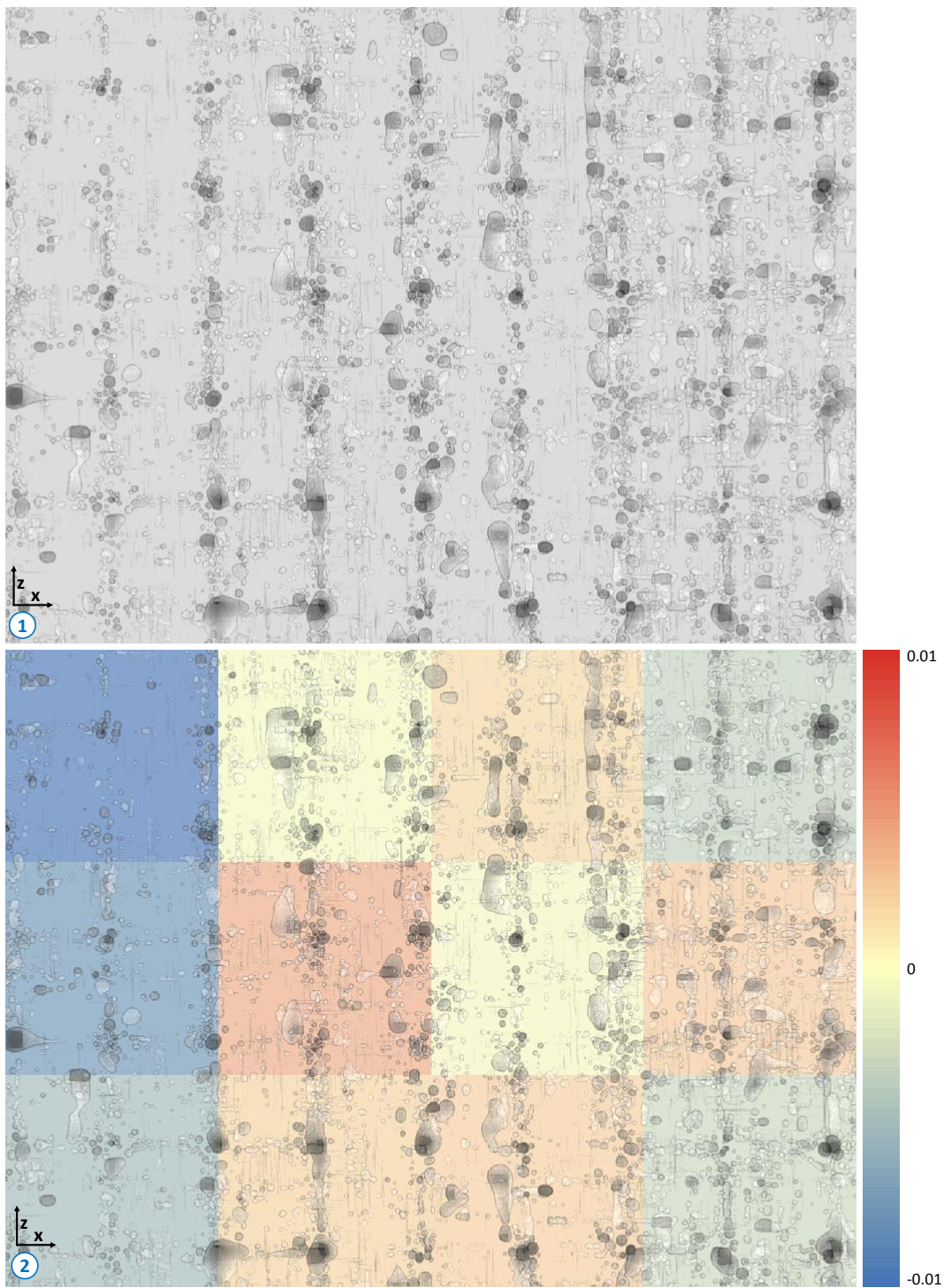
4.5.1 Local MObjects Visualization

In the local MObjects visualization the CFRP dataset is partitioned into a 4 x 3 grid of cells. The number of rows and columns in the grid is calculated automatically depending on the biggest pore extents in the dataset. With this grid, it is ensured that the MObjects fit into the cells without overlapping. For each cell a local MObject is calculated and shown to the user (see Figure 4.10 (1)). The MObjects can be visualized using different uncertainty filters, e.g., $\sigma = 0.9$. Figure 4.10 (2) and (3) shows two enlarged MObjects from (1). As the MObjects' cores look similar, there is a homogenous distribution of small individual pores over the dataset in x direction, whereas big individual pores can be seen as outliers in (3). These outliers lead to an inhomogeneous porosity distribution in the specimen. Based on the given partitioning the user can switch to the comparative homogeneity visualization with color-coded cells as shown in Figures 4.11, 4.12 and 4.13. Without coloring the cells (see Figure 4.11 (1)) it is hard to gain information about the pore homogeneity. By applying the color-coding, the user is able to see the homogeneity of one property. The visualization shows the deviation of the average pore volume (see Figure 4.11 (2)), the extent in x (see Figure 4.12 (1)), y (see Figure 4.12 (2)), and z direction (see Figure 4.13 (1)), as well as the shape factor (see Figure 4.13 (2)) from the corresponding average global property. Blue colors show a high negative deviation whereas red indicates a high positive deviation. In this example the homogeneity regarding the pore volume is particularly interesting. A trend can be seen, where in the left part of the specimen the average pore volume is significantly lower (see Figure 4.11 (2)). Related to active-thermography calculations, the homogeneity of the pore extent in x and z direction is of interest as typically thin plate-like specimens are measured in y direction.

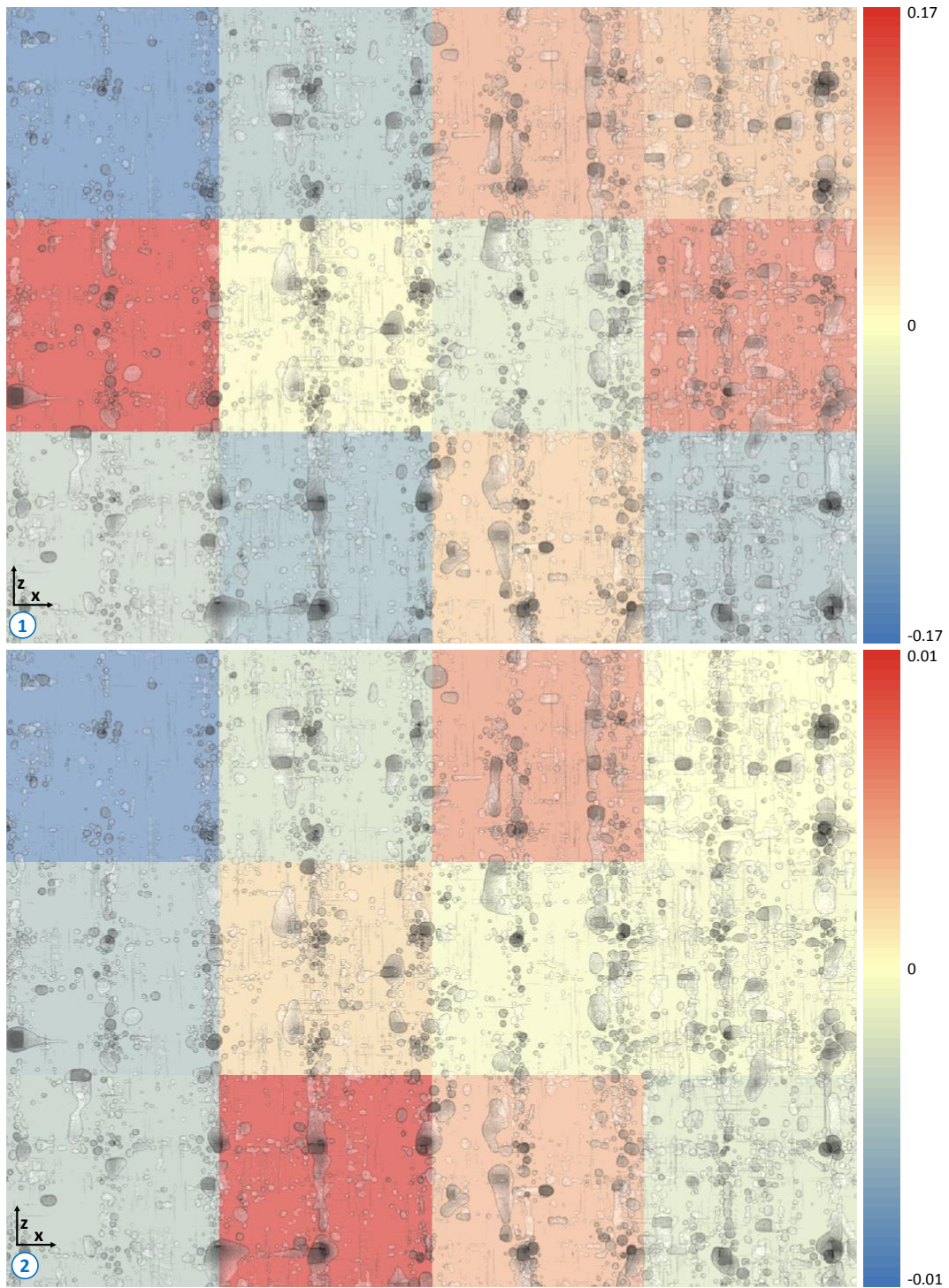
Especially the homogeneity of the extents in x direction (see Figure 4.12 (1)) shows cells with a high deviation with respect to the average. For the homogeneity of the extent in z direction (see Figure 4.13 (1)) lower values in the left part of the specimen are visualized similar to the pore volume deviation.



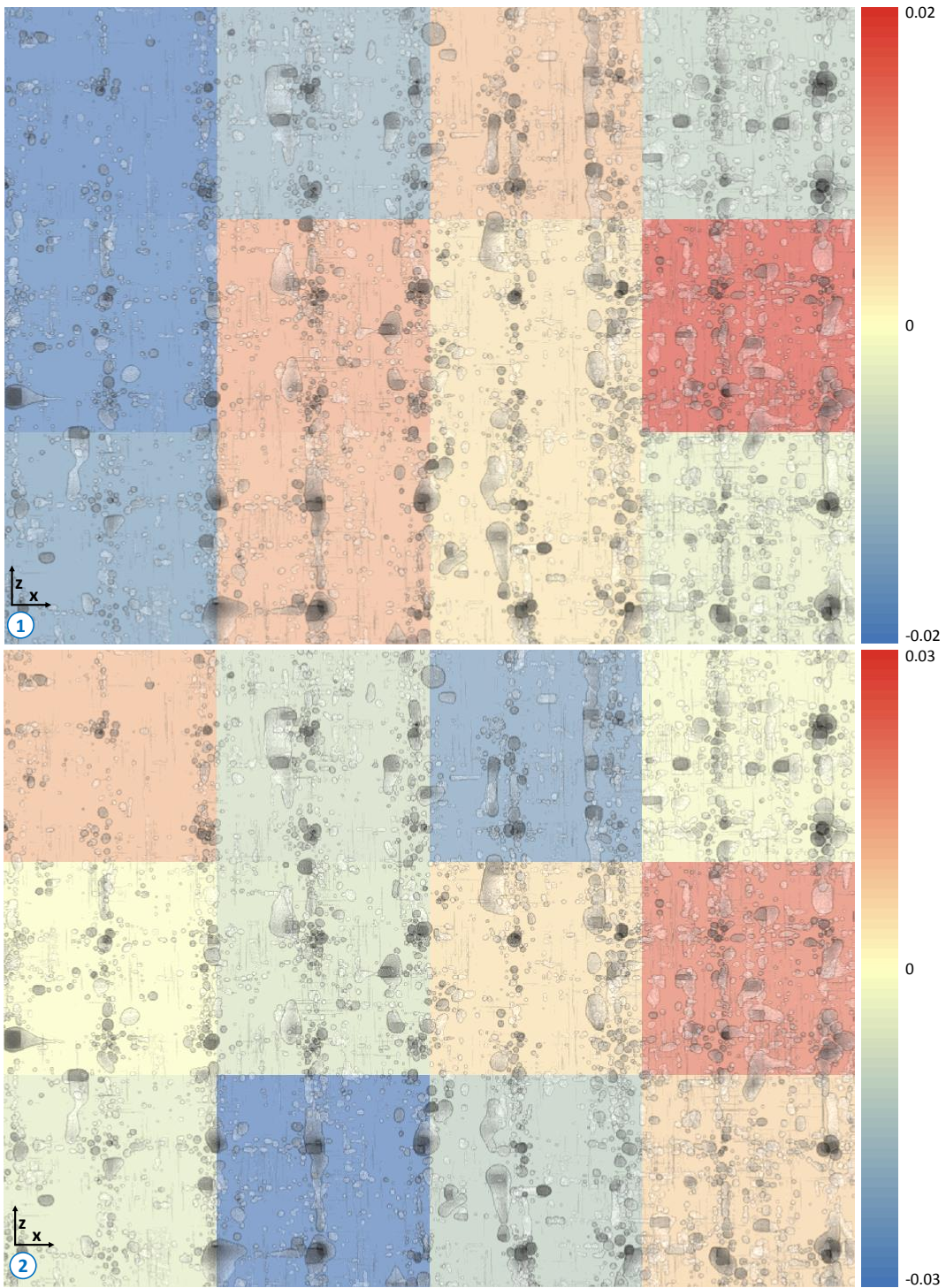
❖ Figure 4.10 — (1) Local MObjects visualization using a high uncertainty filter $\sigma = 0.9$. (2 and 3) Enlarged visualization of two MObjects.



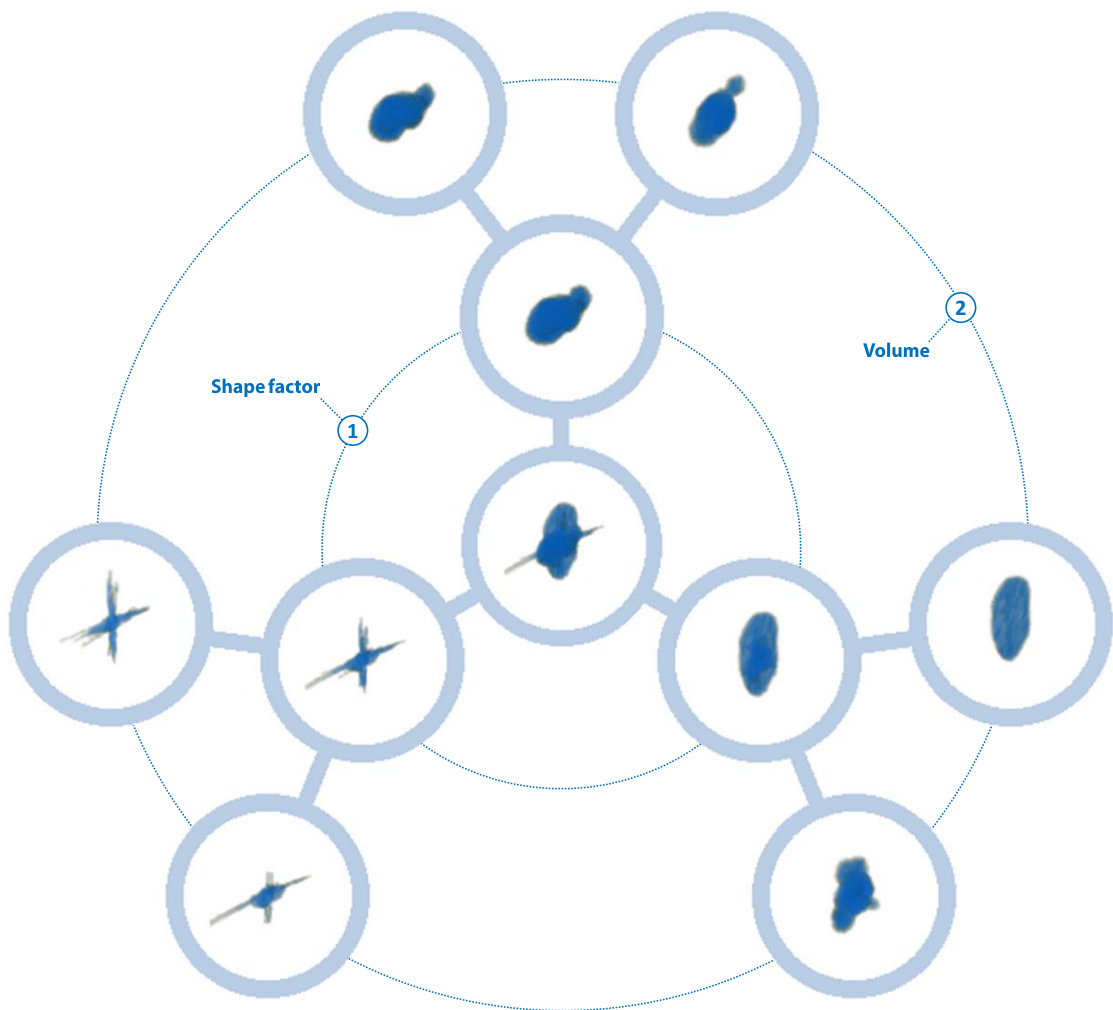
♦ Figure 4.11 — (1) Visualization of the CFRP dataset. (2) Homogeneity visualization of the deviation from the average pore volume in a 4 x 3 grid showing the CFRP dataset in the background.



❖ Figure 4.12 — Homogeneity visualization of the deviation from the average pore. (1) Deviation of the extent in x direction and (2) deviation of the extent in y direction in a 4 x 3 grid showing the CFRP dataset in the background.



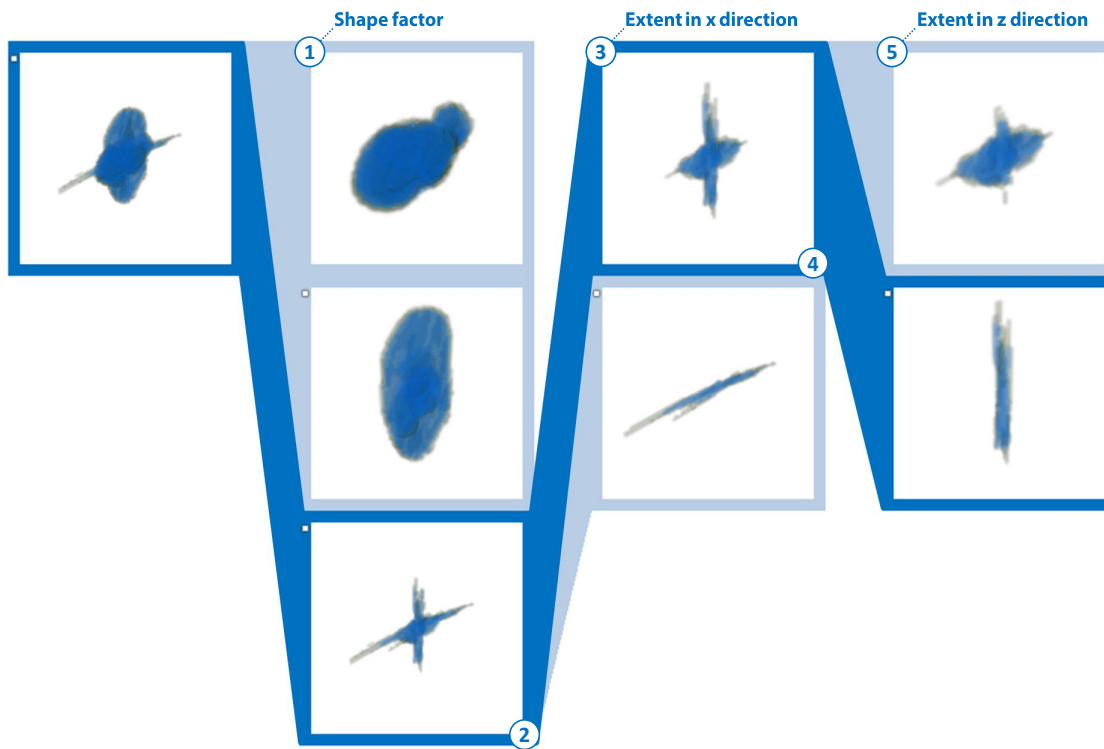
❖ **Figure 4.13** — Homogeneity visualization of the deviation from the average pore. (1) Deviation of the extent in z direction and (2) deviation of the shape factor in a 4 x 3 grid showing the CFRP dataset in the background.



❖ Figure 4.14 — Radial MObject Set visualization of a CFRP dataset showing combinations of the properties (1) shape factor and (2) pore volume.

4.5.2 Radial MObject Set Visualization

In the beginners mode the MObject Sets are arranged in a radial layout. The user can select the desired properties and the number of classes for the MObject Set calculations. The resulting visualization allows the user to see all possible combinations between the properties to get a better overview of the data and the resulting MObjects. Figure 4.14 shows the radial MObject Set visualization for a CFRP dataset. The MObject of the whole dataset is shown in the center of the radial arrangement. The inner circle shows the MObject classifications based on three shape-factor sub-classes (1). Each of these sub-classes is split up into two sub-classes according to pore volume (2). Hence all possible combinations of pore shape factor and volume are visualized in one view. Based on this information the user is able to draw conclusions about the individual



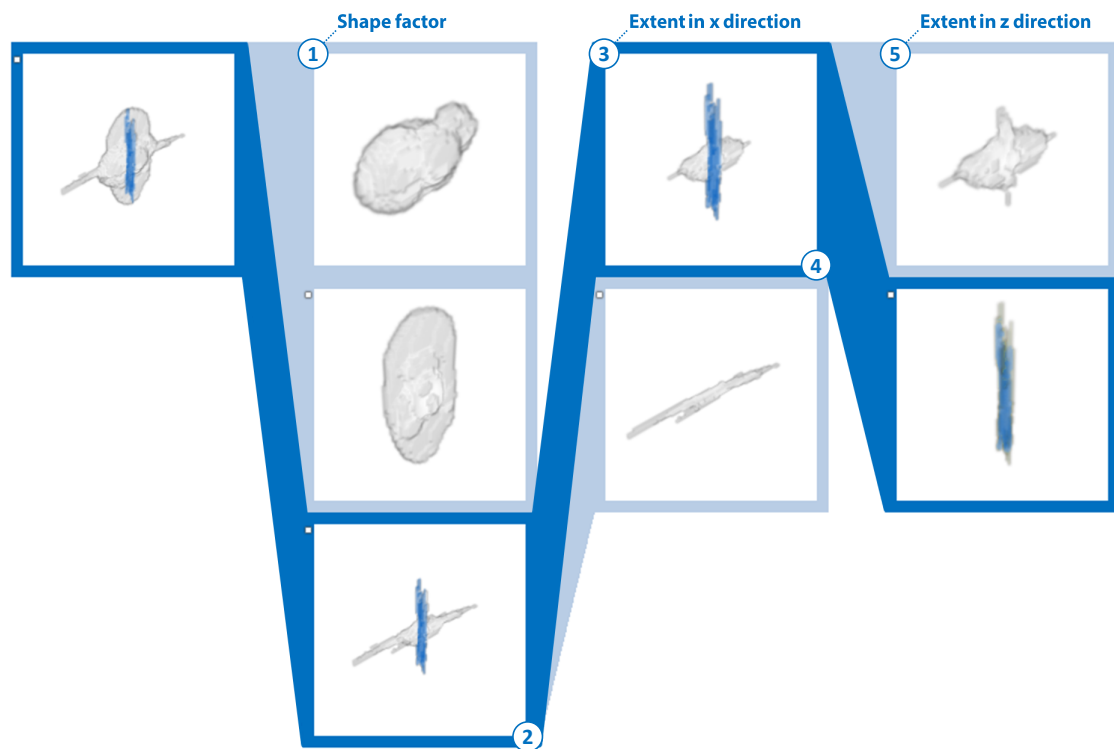
❖ Figure 4.15 — Parallel MObject Set visualization of a CFRP dataset showing the selected path without visual linking.

pores. Using this detailed pore overview as a preview, it is easier to parameterize the expert mode (see Section 4.5.3).

4.5.3 Parallel MObject Set Visualization

The parallel MObject Set visualization shows MObject Sets in a parallel arrangement. The user can interactively explore the MObjects. The results of a CFRP dataset are depicted in Figure 4.15 showing the selected path without visual linking and in Figure 4.16 using visual linking. First the parent MObject is split into three user-defined shape-factor classes (1). The three MObjects make up a new MObject Set. After the selection of the last MObject in this set (2), this MObject is split into two classes based on the extent in x direction (3). This step allows to separate the cross-shaped long and thin micro pores. Finally, the first class of the new MObject Set (4) is split into two classes based on the extent in z direction (5).

The parallel MObject Set visualization was used to find the representative mean pores in the CFRP dataset (see Figure 4.17). As a result of the manufacturing process nodular and disc-shaped pores propagate in the epoxy resin (1) and (2). Long and thin micro pores occur in x and z direction due to the twill-weave pattern of the fiber layers (3) and (4).

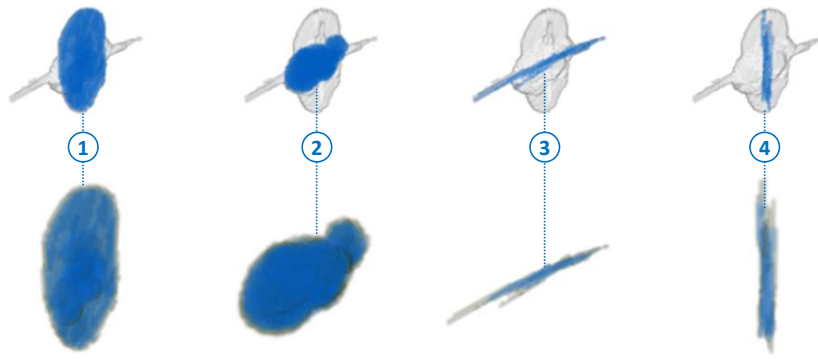


❖ Figure 4.16 — Parallel MObject Set visualization of a CFRP dataset showing the selected path with visual linking.

4.5.4 Evaluation Questionnaire

For the evaluation, a questionnaire (see Appendix B) was answered by 12 respondents which make up two groups. The first group consists of domain experts of a company manufacturing aircraft components, including non-destructive testing (NDT) practitioners and various engineers of the CFRP production process. They use the visualizations for gaining new insights into their components in order to draw conclusions about the manufacturing process (T1). Furthermore the domain experts employ the MObject Set visualization to explore the pores. The resulting representative mean pores are used to improve ultrasonic calibration (T3).

The second group of respondents consists of active thermography domain experts. They have a strong demand for a better understanding of the different pores in a CFRP component. Currently geometric primitives are used for mathematical simulations of a heat-conduction model. Based on the MObjects exploration and the resulting representative MObjects, the domain experts take the mean pores of a real dataset as input for the heat-conduction simulations. As their method assumes a homogenous distribution of the pores, the homogeneity visualization of the different pore properties is important (T2). These new possibilities aim to improve the simulations and finally the active-thermography method. The reference methods ultrasonic testing and active thermography only provide 2D images with lower resolutions than the used XCT data. Due to



❖ **Figure 4.17** — Representative mean pores of a CFRP dataset showing the visual-linking visualization (top row) and the MObjects (bottom row). (1 and 2) Nodular and disc-shaped pores. (3 and 4) Long and thin micro pores in x and z direction.

the missing 3D information, I was not able to directly compare the MObjects visualization to existing NDT methods. As the common XCT visualization is a 3D rendering of the dataset, the MObject visualizations were compared to 3D renderings of segmented pores instead. Until now there has not been an averaging approach available to visually explore the characteristics of defects in XCT datasets in 3D.

The questionnaire focuses on the evaluation of the three tasks concerning the MObjects visualization (T1), the homogeneity visualization (T2), and the MObjects exploration and extraction of representative MObjects (T3) in a dataset. A summary of the results from the evaluation-questionnaire is shown in Table 4.1.

T1: MObjects Visualization

Regarding the MObject visualization, the experts were shown 3D renderings of individual objects in isometric and xz views as well as 3D renderings of the corresponding MObject visualizations. Two different transfer-function settings influence the visual depiction of the uncertainty cloud. In the questionnaire the respondents were asked whether they can identify deviating structures in the visualizations. As the used dataset mainly contains nodular pores, apart from a few elongated objects with a different shape factor, the respondents were asked to identify deviating structures like non-nodular outliers. The feedback confirms that it is easier to find deviating structures in the MObject visualizations than in the 3D renderings showing the individual objects. This is due to the occlusion of the individual objects, so that deviating structures are hardly or not at all seen in a 3D rendering.

Considering the answers about the different transfer-function settings in the MObject visualizations, a slight trend is recognizable. Although the outliers can be clearly seen in both MObject visualizations ($\sigma = 0.15$ and $\sigma = 0.9$), due to perceptual reasons the respondents prefer a setting where the uncertainty cloud clearly separates the core from the outliers ($\sigma = 0.9$).

T2: Local MObjects Visualization

To evaluate the local MObjects visualization, the visualization of segmented pores in a CFRP dataset, the corresponding visualization of local MObjects in a 4 x 3 grid, and the color-coded homogeneity visualization of the same dataset were compared. The task for the respondents was to find the cells with lowest, highest positive, and highest negative deviation of the pore properties in the segmented pores and the color-coded homogeneity visualization. It was nearly impossible for the participants to see the pore homogeneity in the segmented pores visualization whereas they were able to properly classify all cells in the color-coded homogeneity visualization. Regarding the local MObjects visualization the respondents were asked to find the MObjects with lowest and highest average pore properties in the dataset as well as the lowest and highest pore homogeneity in the cells.

Generally the respondents judged the local MObjects visualization positively for perceiving the pore homogeneity inside the cells. To convey the pore homogeneity of the whole dataset across all the cells the color-coded homogeneity visualization was rated as a highly helpful visualization. Especially active-thermography experts gain new homogeneity information out of the visualization to evaluate and further develop their method.

T3: MObjects Exploration

Another part of the questionnaire addressed the interactive MObjects exploration approach. The respondents rated as high the need of the exploration to find nodular, long and thin as well as crack-shaped objects. Furthermore they agreed that the classifications based on the pore volume, the extents and the shape factors are very interesting. There is a slight preference to take the shape factors as the most important property. For each property the experts typically split up a MObject into two to five sub-classes.

All respondents were able to identify the selected path in a MObject Set visualization. The visual linking approach was positively received, as it allows the user to see the different scalings of the different MObjects along the selected path.

The last aspect of the evaluation comprises the exploration of representative mean pores in a CFRP dataset. The respondents were shown a 3D rendering of segmented pores in a CFRP specimen and the corresponding MObject visualization. They were hardly able to identify nodular, long and thin micro pores as well as cracks in the rendering of the segmented pores. On the other hand they positively valued the MObject visualization where it was easy for them to identify the different pore classifications. Furthermore renderings of MObjects with different pore classifications were shown to the respondents. These were found with the MObjects exploration approach. The respondents agreed that the MObjects convey the typical pore structures in a CFRP dataset.

Further Feedback

NDT practitioners mentioned that the MObjects visualization may have considerable practical relevance in future in-line XCT systems for 100 % testing in quality control. An automatic MObject evaluation tool may single out components with critical defects.

❖ Table 4.1 — Summary of the Evaluation Questionnaire

| | | |
|---|---|-------------|
| T1 | Identification of deviating (not nodular) structures - in a 3D rendering - in a MObject visualization | - ± |
| T2 | Pore homogeneity identification of the dataset - in the segmented pores visualization - in the local MObjects visualization - in the color-coded homogeneity visualization | ∓ ± + |
| | Pore homogeneity identification in the cells - in the segmented pores visualization - in the local MObjects visualization - in the color-coded homogeneity visualization | - ± ○ |
| T3 | Identification of the selected path and the different scalings through visual linking in a parallel MObject Set visualization | + |
| | Identification of representative pore classifications - in a 3D rendering - in a MObject visualization | ∓ + |
| - poor, ∓ fair, ○ average, ± very good, + excellent | | |

4.6 Summary

A novel method for the visualization and interactive exploration of MObjects was presented. MObjects from a set of individual objects were calculated and visualized by applying transfer functions. As the MObjects dataset stores probabilities, the transfer-function design is guided by a user-defined uncertainty filter. The approach includes the visualization of pore homogeneities as well. Local MObjects are visualized on a regular grid to show the pore homogeneity in individual cells. To visualize the pore homogeneity of the whole dataset, a color-coded homogeneity visualization was implemented which shows the deviation from the average pore properties. For the exploration with the MObject Set visualization a beginners mode in radial arrangement and an expert mode in parallel arrangement were proposed. Besides the interactive selection of MObjects, a scaling through visual linking approach along a selected path was introduced. Single MObjects hold probabilities for each voxel of belonging to the MObject and are visualized using transfer functions. They can be exported as volumetric dataset to drive subsequent calculations or simulations. The techniques were applied to cases of high practical relevance in the aeronautics industry. Representative pores of a CFRP dataset were found during an interactive exploration of the MObjects. Based on these results NDT practitioners calculate the most appropriate ultrasonic calibration-curve for each component to be tested in quality control. In active thermography the representative pores serve as input for the heat-conduction simulations to improve the underlying model. Domain experts of a company manufacturing aircraft components and active-thermography experts evaluated the MObjects approach with a questionnaire and found it to be a helpful tool with high practical relevance.

Fuzzy Feature Tracking - Visual Analysis of Industrial 4D-XCT Data

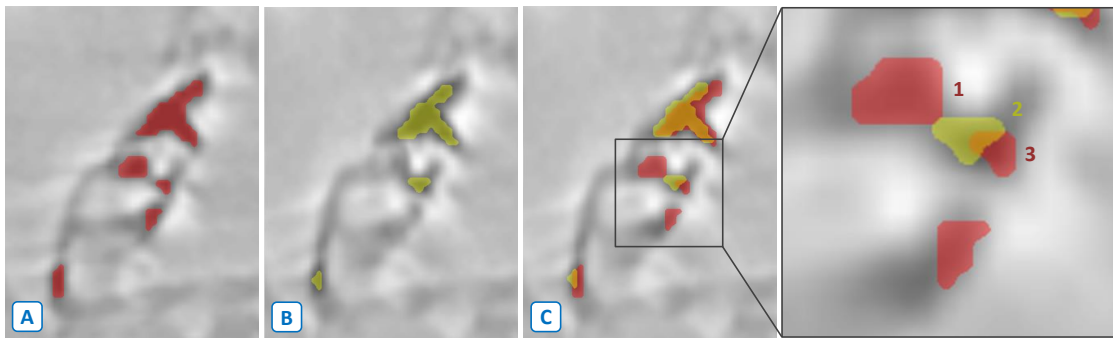
This chapter is based on the following publication:

A. Reh, A. Amirkhanov, J. Kastner, E. Gröller, and C. Heinzl. Fuzzy Feature Tracking: Visual Analysis of Industrial 4D-XCT Data. Technical Report TR-186-2-15-01, Institute of Computer Graphics and Algorithms, Vienna University of Technology, pp. 14, January 2015.

Two visual-analysis systems to explore pores and defects in industrial XCT data were presented in the previous chapters. Regarding the analysis and visualization of industrial XCT data, these systems are used for analyzing only a single condition or a single time-step of a specimen and not a *process* the specimen is exposed to. Thus, in this chapter I go one step further and consider a new dimension: the evolution of a specimen being subjected to an ongoing process over time. This additional dimension leads to new challenges for both analysis and visualization.

To the resulting *4D-XCT data* will also be referred as a *time-series* where each *time-step* corresponds to a single *dataset*, respectively a single XCT scan. To monitor a process using 4D-XCT an in-situ analysis can be used. During an in-situ analysis a scan is acquired at predefined stages (at regular or irregular time-steps) of a process. The process is continuing during the whole data acquisition without any interruptions, e.g., a specimen is heated up while XCT scans at predefined temperature steps are done. Analyzing these time-steps leads to an improved understanding of the material or its manufacturing procedure.

To do so, the main task [Task 4: Feature Tracking](#) (see Section 1.3) will be addressed. Therefore *features* have to be identified and tracked across the whole time-series. Such features can be voids, inclusions, particles, etc. Features may change over time, e.g., voids grow and merge under thermal loading. These changes are also called *events* which need to be determined from



❖ Figure 5.1 — Voids in SiC particle reinforced aluminum (AlSiC). (A and B) Cross-sectional images of two adjacent time-steps of the cooling down process from (A) 400 °C to (B) 300 °C. (C) Overlay of (A) and (B) showing a zoom-in indicating that void 2 has to be assigned either to void 1 or to void 3.

one time-step to the adjacent one regarding the *creation*, *continuation*, *split*, *merge* and *dissipation* of features. Thus an event can be seen as the connection of features from one time-step to another one. Since features also may move over time, an explicit tracking is not always possible. For example, Schöbel et al. [66] investigated voids in SiC particle reinforced aluminum (AlSiC) during a heating cycle. In this application it is of high interest, how the voids decrease during heating and increase while cooling down. Figure 5.1 shows cross-sectional images of two adjacent time-steps of the cooling down process from 400 °C (A) to 300 °C (B). The voids were extracted with a simple thresholding as described by Schöbel et al. [66] and colored in red (A) and yellow (B). Figure 5.1 (C) depicts an overlay of (A) and (B) as well as a zoom-in indicating that void 2 has to be assigned either to void 1 or to void 3. As void 2 touches void 1 and slightly overlaps with void 3, a distinct assignment to void 1 or 3 is not feasible. To solve this problem, the calculation of a *Tracking Uncertainty* will be introduced in this chapter. The Tracking Uncertainty is calculated for all potential features in a certain neighbourhood and is based on the features' volume overlap and volume ratio. As a result, the void tracking in Figure 5.1 (C) is fuzzy and void 2 is assigned to both voids 1 and 3, each with a specific Tracking Uncertainty. This tracking approach will be called *Fuzzy Feature Tracking*. To analyze the Fuzzy Feature Tracking results, novel visualization and interaction approaches are required.

In this chapter a visual-analysis tool will be presented to explore 4D-XCT data and to handle the different aspects of its spatial and time-specific information. The approach is applied to show results on real-world in-situ applications. One application area is the shrinkage of beech wood, where I focus on the voids between wood fibers during a drying-out process. In a second analysis I present results of a void formation in AlSiC alloys during a heating up and cooling down cycle.

Workflow Analysis

Below the workflow of analyzing 4D-XCT data and corresponding tasks for gaining new domain knowledge about a material or a component under load, its manufacturing procedure or any other process evolving over time will be discussed. Currently, users have to search interesting

features in 3D renderings or by scrolling through 2D cross-sectional images. If a feature of interest is found, the user has to search the corresponding features in all other datasets manually, mostly in the same way he has found the interesting feature (e.g., by scrolling through cross-sections). Feature properties such as extents are determined with ruler tools, depending on the used software. This procedure is imprecise and it is not guaranteed to find all features of interest. Apart from the subjectivity, such a workflow is rather time-consuming and error prone.

In this chapter, the aim is to overcome these drawbacks by designing a visual-analysis tool to interactively explore 4D-XCT time-series. During the collaborations with company partners and material scientists with application areas like composites, alloys, wood, etc. a detailed list of domain-specific requirements was defined. Although the applications and thus the material systems were different, the experts' requests converged to the following general questions:

Q1: *How are the feature properties (e.g., feature volume) distributed at a certain time-step?*

Q2: *How many features are created, continuing or dissipating at a time-step?*

Q3: *How many features are splitting or merging at a time-step?*

Q4: *Which features split and where are they located in the datasets?*

Q5: *Which features merge and where are they located in the datasets?*

Q6: *How does a feature evolve over time regarding its properties?*

Q7: *In which events is an evolving feature involved?*

5.1 Tasks and Contributions

Based on the domain experts' demands, the following tasks for the tool were derived:

T1: *Determination of Events*

Determine events (creation, continuation, split, merge and dissipation) from one time-step to another one.

T2: *Visualization of the Spatial Feature Information*

Visualize the spatial information including the extracted features for each time-step.

T3: *Visualization of the Temporal Overview of Events and Feature Properties*

Visualize the temporal overview of the events and corresponding feature properties.

T4: *Visualization of the Temporal Overview of Events and their Connections*

Visualize the temporal overview of the events and how they connect features from one time-step to another one.

Considering the domain experts' questions (Q1 - Q7) and the derived tasks (T1 - T4), a visual-analysis tool with the following contributions was implemented:

Fuzzy Feature Tracking

Features are tracked from one time-step to the next one (Q2, Q3 and T1). This step can be repeated for all time-steps to get feature-tracking information along the whole time-series data. It is determined, if features are created, continuing, splitting, merging or dissipating. As the events are not clearly distinguishable in all cases - this depends on the specific datasets and applications - a Tracking Uncertainty is calculated for each event, to quantify the quality of the results.

Volume Player

The need for a visualization of the spatial feature information (Q4, Q5 and T2) and the temporal overview of the events (T3) is combined. To do so, volume blending is used to visualize a smooth transition between two time-steps.

3D Data View

3D renderings from all time-steps in a row show the spatial information of all features (Q4, Q5 and T2). Individual features may be colored according to a determined event type.

Event Explorer

The combination of a temporal-event overview and the feature properties is achieved with an Event Explorer (Q1, Q2, Q3, Q4, Q5 and T3). The Event Explorer consists of a row of scatter plots, where each plot serves as snapshot for one time-step. Events can be plotted according to user-defined feature properties as well as their event type. As all views in the tool are linked together, a selection in the Event Explorer updates all other views and allows the user a detailed exploration of the data. For example, an interesting merged feature can be filtered in the scatter plot. Then its origin and how it evolves can be traced along all time-steps in the spatial domain as well as in the temporal domain.

Fuzzy Tracking Graph

The Fuzzy Tracking Graph visualizes the temporal evolution of the features combined with their events with respect to each other (Q6, Q7 and T4). The uncertainty information is integrated per event in the Fuzzy Feature Tracking by showing more than one assigned feature for an event. To do so, the opacity of the vertices and edges of the Fuzzy Tracking Graph are adjusted according to the Tracking Uncertainty of the events.

5.2 Related Work

For the visual analysis of industrial XCT data, several approaches exist in the literature. For example, Fritz et al. [28] presented a method to analyze graphite particles in ductile iron and fibers in steel fibers reinforced sprayed concrete. Two approaches [59, 60] were already introduced in Chapters 3 and 4 to explore pores in carbon fiber reinforced polymers. FiberScout [76] allows NDT practitioners the exploration of fibers in fiber reinforced polymers using parallel coordinates and a scatter plot matrix. However, these techniques only analyze a single condition of a specimen and not a process the specimen is exposed to. As time will be considered as fourth dimension in the data, a time-series of XCT scans will be analyzed in this chapter.

The analysis of such time-series shows a wide-spread variety of applications. Aigner et al. [4] overview time-oriented visualizations from many application domains. In the literature approaches such as ThemeRiver [36] or Stacked Graphs [21] cover research questions like the evolution of thematic variations over time within a large collection of documents or the presentation of large datasets to a general audience. Waser et al. [75] presented World Lines for steering multiple simulation runs. In their visualization, tracks which share a common time axis are shown in a tree. As these approaches are not purpose built for 3D volumetric data which are used in this chapter, these techniques are not applicable for analyzing 4D-XCT time-series.

In the medical domain several approaches are found for 4D data analysis. Köhler et al. [43] published an approach for the extraction of vortex flow in the aorta and pulmonary artery incorporating line predicates. Their technique is designed for the evaluation of time-resolved and spatial phase-contrast magnetic resonance imaging data (4D PC-MRI). It enables a reliable and time-resolved measuring of 3D flow for a qualitative and quantitative analysis of the patient-specific hemodynamics. A related method for pre-clinical cardiovascular research provides tools to interactively explore the 4D blood-flow data and depict essential blood-flow characteristics [72]. Both methods share the same imaging modality with temporal resolution varying from 14 to 21 time-steps with about 50 ms difference between each time-step. In the field of industrial XCT no visual-analysis techniques have been proposed regarding 4D-XCT data investigation so far. The closest related technique is seen in the work of Malik et al. [50] who proposed comparative visualization techniques for parameter studies of XCT scans. The 3D volumetric XCT dataset series in their work is generated by varying parameters of the XCT device for each scan. Using the proposed multi-view technique based on planar-reformatting, several datasets may be compared simultaneously in a single view.

The research questions of the domain experts and the corresponding tasks required the development of new approaches in the analysis of 4D-XCT time-series. To do so, features have to be extracted in the time-series. As the methods are applied on data of different industrial material applications such as AlSiC alloys and beech wood, feature extraction is considered as being out of scope for this chapter and the reader is referred to the used segmentation algorithms in the result sections of the corresponding papers [66, 70].

5.2.1 Fuzzy Feature Tracking

Based on the extracted features, an essential pre-processing stage is the tracking of the features along the time-series. Altendorfer [6] tracks voids in AlSiC alloys time-series. After registering the volumetric datasets and a subsequent segmentation of the voids he visualizes overlaid void contours. As this tracking is not automatic, it is insufficient for the domain experts' needs. For automatic tracking of features two general approaches are considered as most relevant for the presented chapter: One approach is to track features based on their voxel data. For instance, Silver et al. [68] track 3D features in computational fluid dynamics datasets. The spatial overlap of the features is calculated with boolean difference operations of the voxel data. The second approach is to calculate feature properties, e.g., size and position of each feature, and perform the tracking based on these properties. Samtaney et al. [62] introduced such a tracking method. In a pre-processing stage properties of features in 2D and 3D computational fluid dynamics simulations are calculated. Features are then tracked by finding potential correspondences in adjacent time-steps within a certain neighbourhood and by subsequently comparing their feature properties. As the voxel-based approach is more memory- and time-consuming, feature properties are used for the Fuzzy Feature Tracking and extended with the calculation of the Tracking Uncertainty.

5.2.2 Fuzzy Tracking Graph Visualization

After tracking features in time-series this tracking result needs to be visualized in an easy to understand and intuitive way. Besides coloring of tracked features along the time-steps [68], a directed acyclic graph is a common representation to show the evolution of a feature over time [62, 68]. For visualizing such graphs an appropriate graph layout which uses one spatial dimension to indicate time is called *tracking graph*. Each feature is represented by a track. Tracks may start, continue, merge, split or end at time-steps with respect to the corresponding feature event types creation, continuation, split, merge and dissipation. Thus a tracking graph is used in this chapter. If visualizing a tracking graph the main challenge can be found in minimizing the edge crossings between the time-steps. Widanagamaachchi et al. [79] used tracking graphs in a system for the exploration of combustion simulations. They implemented a median heuristic approach to solve their edge-crossing minimization-problem. As their solution showed satisfying results even for large graphs a median heuristic [29] for minimizing the edge crossings in the Fuzzy Tracking Graph was used.

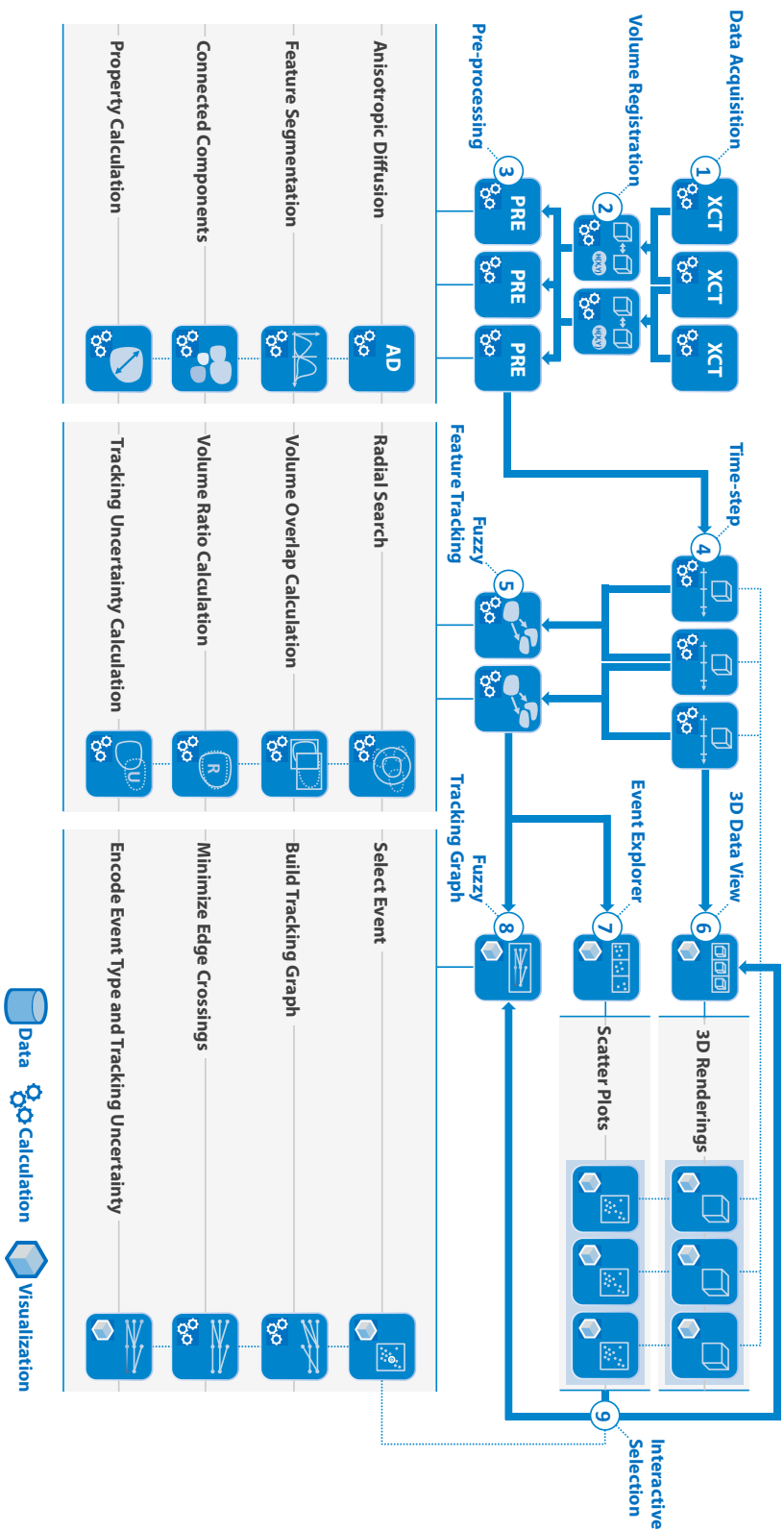
5.2.3 Uncertainty Visualization

In order to communicate information on the calculated Tracking Uncertainty, an adequate technique for uncertainty visualization is needed. In the domain of industrial X-ray computed tomography two approaches have been recently published with regard to uncertainty visualization. MObjects [59] have been introduced in Chapter 4 as an approach for the visualization of mean objects (MObjects) aggregating internal structures in carbon fiber reinforced polymer components. In order to generate a MObject an intermediate representation is created by aligning the extracted structures and aggregating them to a 3D uncertainty cloud. The uncertainty is encoded by setting opacity and colors in a transfer function. Amirkhanov et al. [7] focused in their work on fuzzy metrology of real-world components using XCT scans. As the component surface is not explicit due to artifacts and noise, a certain positional uncertainty in the data is given. The uncertainty is encoded by varying the thickness of reference shapes, as well as by using boxplots as extension to tolerance widgets.

One approach from a different domain encodes uncertainty in graphs. Collins et al. [23] presented a system to support decision-making concerning automated speech-recognition results. Typically such systems present a best-guess result to the user although deviating results may be correct. In their solution, Collins et al. [23] take these additional results into account. Therefore they visualize the recognized sentence as well as alternative words in a lattice graph. Each recognized word is represented by a vertex showing the word in the label. The uncertainty is then encoded by the vertex position, fill hue and a border transparency. For the Fuzzy Tracking Graph visualization the idea of encoding uncertainty on the vertices was adopted. Employing the graph layout with minimized edge crossings for the Fuzzy Tracking Graph, the uncertainty encoding was omitted by changing the vertex position. Vertices and edges are colored according to their event type and the Tracking Uncertainty is encoded by varying the opacity.

5.3 Visual-Analysis Pipeline

In this chapter, a general visual-analysis tool to interactively explore 4D-XCT time-series is presented. Therefore a visual-analysis pipeline is proposed (see Figure 5.2). In the data acquisition stage (1) a time-series is generated. The resulting datasets are registered (2) to compensate changes of features with respect to their size or position. Further pre-processing (3) steps are applied to enhance the data quality of the resulting time-steps (4). The time-steps are the basis for the Fuzzy Feature Tracking (5) where the change between the time-steps are detected regarding the creation, continuation, split, merge and dissipation of features. For the visualization of the time-steps and the Fuzzy Feature Tracking result, a 3D Data View (6) consisting of 3D renderings, an Event Explorer (7) showing scatter plots and a Fuzzy Tracking Graph (8) are used. Interactive selection (9) of an event in the Event Explorer leads to an update of the 3D Data View and the Fuzzy Tracking Graph.



❖ **Figure 5.2** — Pipeline for the visual analysis of 4D-XCT time-series. After the stages data acquisition (1) volume registration (2) is applied. Furthermore pre-processing (3) steps enhance the data. The acquired and enhanced time-series consists of time-steps (4) which are the basis for the Fuzzy Feature Tracking (5). For visualizing the time-steps and the Fuzzy Feature Tracking result, a 3D Data View (6) showing 3D renderings, an Event Explorer (7) consisting of scatter plots and a Fuzzy Tracking Graph (8) are used. Interactive selection (9) of an event in the Event Explorer leads to an update of the 3D Data View and the Fuzzy Tracking Graph.

5.3.1 Data Acquisition

As the experimental setup and the XCT scan parameters, e.g., tube voltage of the XCT device, differ for each application, the data acquisition and the feature extraction are described in Section 5.6 where 4D-XCT time-series analyses of wood shrinkage [70] and an AlSiC alloy under thermal load [66] are shown.

5.3.2 Pre-processing

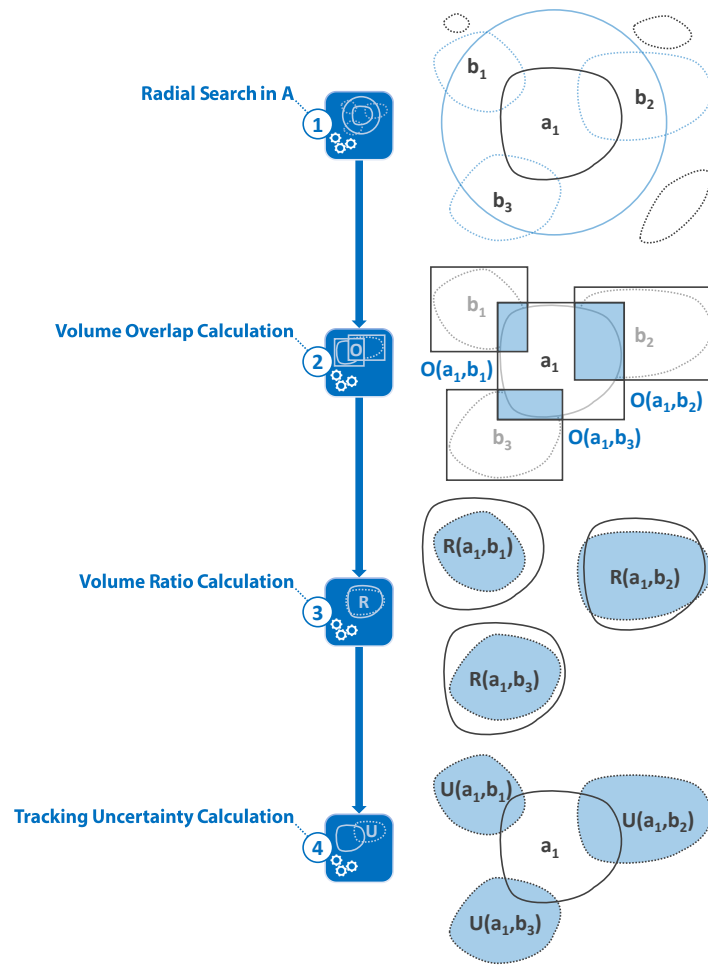
In this section, an overview of the essential pre-processing steps for 4D-XCT applications is presented. Specimens may change their size or move between the measurements. This depends on both, the measured process and the used testing method. For example, an alloy specimen expands under thermal load. Thus features may also change their size and position. To compensate these changes, a volume registration has to be applied. In general, if a registration requires affine transformations between a fixed and a moving image it is called rigid registration [78]. In contrast, non-rigid methods also deal with local feature deformations [52].

For the time-series which were analyzed in this work (wood shrinkage, AlSiC alloys), the underlying processes are global processes and thus the specimens and features are expected to move more or less uniformly in all directions. As the intervals between the time-steps in the time-series are short, the movement of specimens and features is either limited or does not exist at all. Thus a rigid registration is sufficient for the above mentioned applications. A mutual information registration is applied on the datasets. If however the process to be analyzed leads to features moving or expanding in one direction, i.e., in the case of tension tests, the registration component has to be replaced with a non-rigid registration method to compensate potential deformations.

After the registration, the features are extracted with thresholding methods [66,70]. A connected-components filter using a 26-connectivity labels the features uniquely. Thus the extracted features consist of sets of labeled voxels within a regular volumetric grid. Furthermore the properties of interest, **feature volume**, **extent**, and **centroid** have to be calculated for all features in a dataset. As these are analogous to the characteristics which were already calculated for pores, the pore-properties calculation from Section 2.3 can be used for this step. The pre-processing steps are executed for all time-steps.

5.4 Fuzzy Feature Tracking

One of the main tasks of this chapter is to track features within a 4D-XCT time-series. For each feature probable correspondences have to be found and one out of five events (creation, continuation, split, merge and dissipation) has to be assigned. To do so, a Fuzzy Feature Tracking algorithm is presented. The method is based on the feature properties where for each correspondence between two features a Tracking Uncertainty is calculated. The Tracking Uncertainty is based on the volume overlap and the volume ratio of a feature and its correspondences. Thus two



❖ **Figure 5.3** — Fuzzy Feature Tracking to find probable corresponding features for A in B . (1) Radial search at the centroid position of a_i in B . (2) Volume overlap calculation for each probable feature in B based on bounding boxes. (3) Volume ratio calculation for each probable feature in B . (4) Tracking Uncertainty calculation for each correspondence from a_1 to the probable features b_1, b_2 and b_3 in B .

features with the same volume at the same position have a low Tracking Uncertainty, whereas two features with different sizes at diverse positions lead to a high Tracking Uncertainty.

Consider A and B as two adjacent time-steps. Let a_i be a feature in dataset A with n_A features and b_j be a feature in dataset B containing n_B features. For each feature a_i in A a corresponding feature b_j in B has to be found and an event assigned. For each feature all corresponding features are stored in a list of *correspondences*. Figure 5.3 illustrates the proposed determination of correspondences for a feature a_1 . Solid lines show features in A whereas the dotted lines highlight features in B . To reduce complexity in the figure, it only shows two dimensions. For the used volumetric datasets in this work, the calculations are performed in 3D. The following four steps are processed in sequence:

1. Radial Search in A

A radial search with a radius r is performed at the center of a_i in dataset A , where r is user-defined. The found corresponding features for a_i are stored in *correspondences*.

2. Volume Overlap Calculation

As the algorithm is based on feature properties and in order to reduce calculation times, the volume overlap $O(a_i, b_j)$ is approximated using bounding boxes. The result is normalized to one.

3. Volume Ratio Calculation

The volume ratio $R(a_i, b_j)$ of two features a_i and b_j is calculated dividing the smaller volume of the features a_i and b_j by the larger one.

4. Tracking Uncertainty Calculation

Based on the volume overlap $O(a_i, b_j)$ and ratio $R(a_i, b_j)$ a Tracking Uncertainty $U(a_i, b_j)$ is calculated. As the behavior, of how features may change their size over time, is dependent on the used materials and application scenarios, $O(a_i, b_j)$ and $R(a_i, b_j)$ can be weighted with user-defined weights w_o and w_r , where $w_o + w_r = 1$. Thus the Tracking Uncertainty is calculated as follows:

$$U(a_i, b_j) = 1 - (O(a_i, b_j)w_o + R(a_i, b_j)w_r). \quad (5.1)$$

Following this sequence the probable correspondences for all features from A to B can be identified. For the following event assignment, the correspondences from B to A have to be identified. Thus the above steps are repeated in the other direction. Having all correspondences from A to B and from B to A , the event types can be assigned by traversing the correspondences. Algorithm 5.1 gives a description of the event assignment in pseudo code. The following event types can be distinguished:

- **Creation:** A creation event is assumed, if a feature is present in B without a corresponding feature in A . This is valid for a feature b_j if $b_j.correspondences().size() = 0$. In this case, a *creation* event is assigned.
- **Continuation:** Features which are present in A and have a correspondence in B *continue* from one time-step to the next. Here two options exist. If only one corresponding feature b_j for a_i exists, so $a_i.correspondences().size() = 1$ holds, the continuation event is assigned. If $a_i.correspondences().size() > 1$, either a split event or a continuation event is possible. As a feature may change its size or position from A to B , two user-defined thresholds t_O and t_R are introduced to consider these changes. If $t_O \leq O(a_i, b_j)$ and $t_R \leq R(a_i, b_j)$ is valid, a continuation event is assigned, otherwise a split event is chosen.

- **Split:** A feature in A can *split* into two or more features in B . This is valid if

$$\begin{aligned} a_i.correspondences().size() &> 1, \\ t_O &> O(a_i, b_j), \\ t_R &> R(a_i, b_j). \end{aligned} \tag{5.2}$$

Data: Datasets A, B with features and correspondences
Result: Assigned events

```

1 forall the Features  $a_i$  in  $A$  do
2   if  $a_i.correspondences().size() = 0$  then
3     SetEvent(Dissipation);
4   else if  $a_i.correspondences().size() = 1$  then
5     SetEvent(Continuation);
6   else if  $a_i.correspondences().size() > 1$  then
7     forall the Features  $b_j$  in  $a_i.correspondences()$  do
8       if  $t_O \leq O(a_i, b_j)$  and  $t_R \leq R(a_i, b_j)$  then
9         SetEvent(Continuation);
10      else
11        SetEvent(Split);
12      end
13    end
14  end
15 end
16 forall the Features  $b_j$  in  $B$  do
17   if  $b_j.correspondences().size() = 0$  then
18     SetEvent(Creation);
19   else if  $b_j.correspondences().size() = 1$  then
20     SetEvent(Continuation);
21   else if  $b_j.correspondences().size() > 1$  then
22     forall the Features  $a_i$  in  $b_j.correspondences()$  do
23       if  $t_O \leq O(a_i, b_j)$  and  $t_R \leq R(a_i, b_j)$  then
24         SetEvent(Continuation);
25       else
26         SetEvent(Merge);
27       end
28     end
29   end
30 end

```

Algorithm 5.1: Algorithm for assigning events.

- **Merge:** Two or more features from A merge to a feature in B if

$$\begin{aligned} b_j.correspondences().size() &> 1, \\ t_O &> O(a_i, b_j), \\ t_R &> R(a_i, b_j) \end{aligned} \quad (5.3)$$

is valid.

- **Dissipation:** A feature disappeared, if it is present in A and no correspondence is found in B . So if

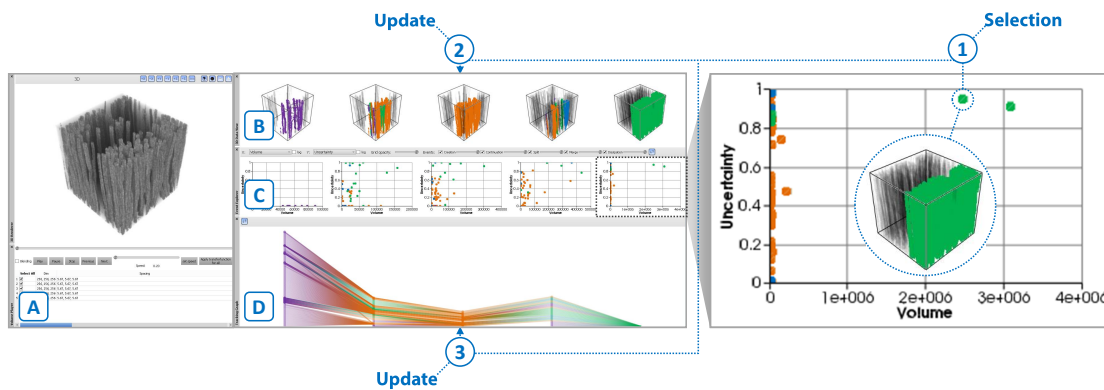
$$b_i.correspondences().size() = 0 \quad (5.4)$$

a *dissipation* event is assigned.

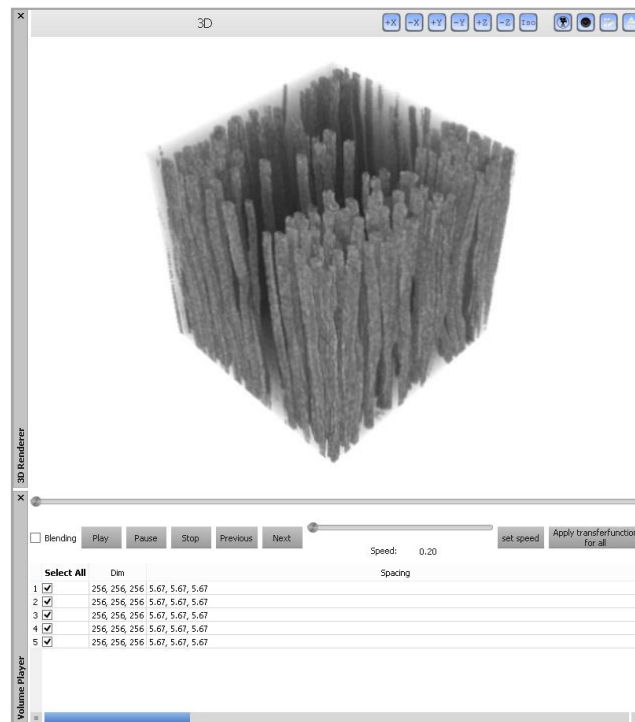
The Fuzzy Feature Tracking is applied on each time-step and its adjacent one. The found correspondences over the whole time-series are the basis of the visual-analysis system which is described in the next section.

5.5 Visual Analysis of 4D-XCT Data

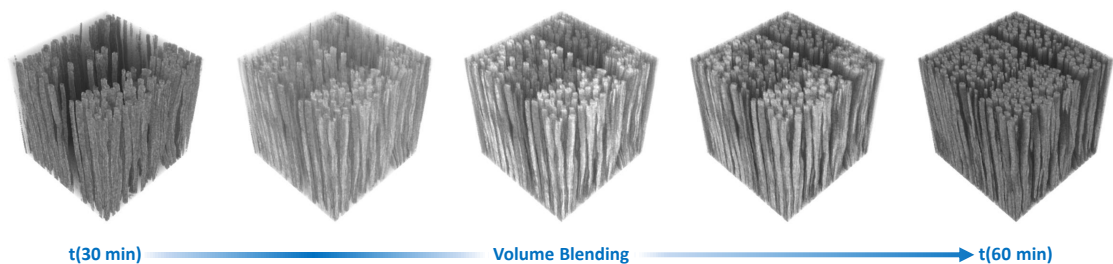
The tool is built of multiple linked-views to fulfill domain-specific 4D-XCT tasks. Each of the individual views emphasizes a certain aspect of the 4D-XCT time-series. Figure 5.4 (A-D) shows an overview of the different views. The tool is implemented in the custom analysis framework iAnalyse developed by the CT-group of the University of Applied Sciences Upper Austria, Wels Campus using VTK, ITK and Qt. For both time-series (wood shrinkage, AISic alloys) the Fuzzy Feature Tracking results are calculated within several seconds on an Intel Xeon E5-2667 workstation. The implementation achieves an interactive response with the time-series which were used in this work.



❖ **Figure 5.4** — 4D-XCT visual-analysis tool consisting of four linked views: (A) Volume Player. (B) 3D Data View. (C) Event Explorer. (D) Fuzzy Tracking Graph. (1) A selection in the Event Explorer leads to an update (2 and 3) of the 3D Data View and the Fuzzy Tracking Graph.

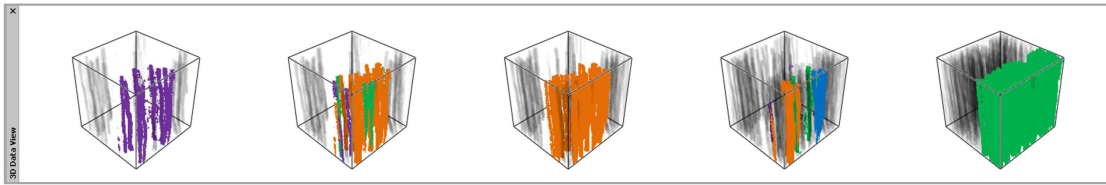


❖ Figure 5.5 — Volume Player.

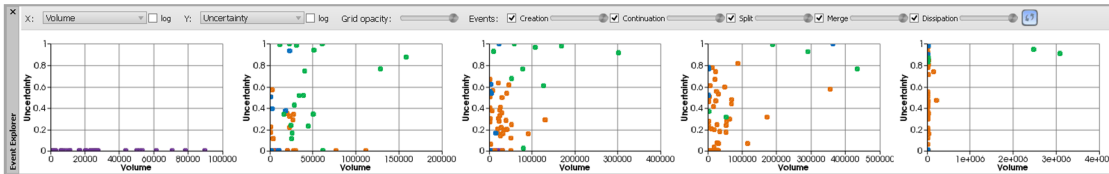
❖ Figure 5.6 — Five volume blending steps between the two time-steps $t(30 \text{ min})$ and $t(60 \text{ min})$ of the wood-shrinkage analysis.

5.5.1 Volume Player

The Volume Player shows control elements to traverse the time-steps of a time-series (see Figures 5.4 (A) and 5.5). In a list time-steps of interest can be selected. If the selected sequence is played, the corresponding volumetric datasets are shown in a 3D renderer above. As this may lead to coarse transitions in the rendering, a blending of two time-steps is integrated in order to emphasize a smoother transition between them. The method can be applied on both raw data and labeled data, already showing selected features. The volume blending is applied by setting



❖ Figure 5.7 — 3D Data View.



❖ Figure 5.8 — Event Explorer.

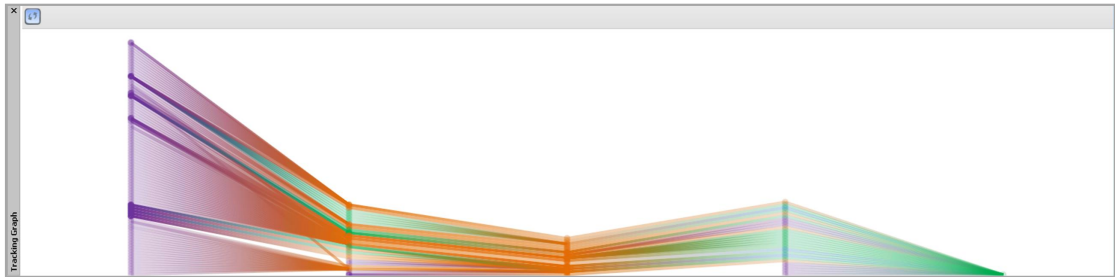
linear transition functions for two adjacent time-steps $t(n)$ and $t(n + 1)$. The opacity for $t(n)$ is decreased over time whereas the opacity for $t(n + 1)$ is increased. This approach leads to a smooth transition between time-steps $t(n)$ and $t(n + 1)$. Figure 5.6 shows an example of the wood-shrinkage analysis, namely five volume blending transitions between the two time-steps $t(30 \text{ min})$ and $t(60 \text{ min})$.

5.5.2 3D Data View

The 3D Data View depicts a time-series of labeled data as 3D renderings in a row mimicking a film-strip view of the time-series (see Figures 5.4 (B) and 5.7). In a 3D rendering, one for each time-step, the spatial information for all individual features is shown. For the interaction with the data, the basic methods rotation, translation and zooming are available. The interactions are connected along all renderers. For the visualization transfer functions are used. As event types were assigned to all features by the Fuzzy Feature Tracking algorithm, the features are colored according to the assigned event types. Shading is disabled in the renderings, as it would deteriorate the perception of small features. If a selection in the Event Explorer is done, the 3D Data View is updated and unselected features are either shown in gray with a low opacity as context information or they are completely hidden.

5.5.3 Event Explorer

In the Event Explorer a global temporal overview of events and feature properties is given. Therefore a row of scatter plots is used, one plot for each time-step (see Figures 5.4 (C) and 5.8). In a scatter plot events, which were assigned to features in the Fuzzy Feature Tracking, are visualized as colored points. Each event type has its own color. The scatter plots can then be



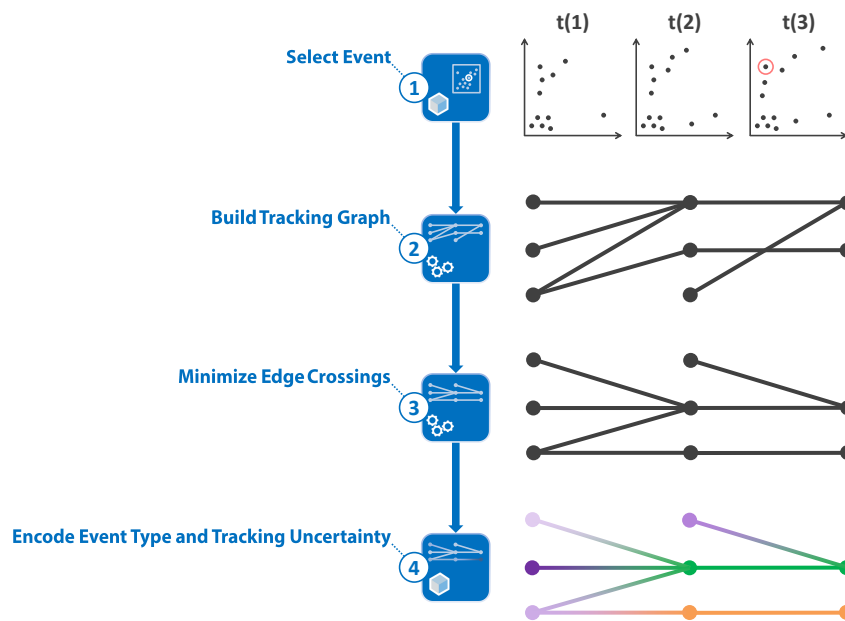
❖ Figure 5.9 — Fuzzy Tracking Graph.

tailored to the user's preferences and the analysis task. The axes are user-defined and show two feature properties, e.g., feature volume and Tracking Uncertainty. Furthermore they make use of log scales if needed. In the applications which are shown in Section 5.6 the number of features varies from 6 to 195 per time-step. As this number may be higher for other applications, the user can filter event types. This avoids information clutter of having too many points in the plots. In detail, the opacity of the plotted points is adjustable, separately for each event type. Regarding interaction techniques, selecting, panning and zooming into the plots is possible to analyze interesting clusters more accurately at a finer level of detail. Apart from that an interactive selection of events is provided to the user. As all views are linked, a selection of an event (see Figure 5.4 (1)) leads to an update of the 3D Data View and the Fuzzy Tracking Graph (see Figure 5.4 (2 and 3)).

5.5.4 Fuzzy Tracking Graph

The Event Explorer shows a temporal overview of events, which were assigned to features in the Fuzzy Feature Tracking. Now this temporal overview is expanded with the temporal evolution of how the features are tracked and connected over the whole time-series. Therefore a Fuzzy Tracking Graph (see Figures 5.4 (D) and 5.9) is introduced. Figure 5.10 illustrates, how this graph is calculated and visualized. One or more events can be selected in the Event Explorer (see Figure 5.10 (1)). Based on the selection, all corresponding features in the subsequent and adjacent time-steps are taken to build the graph. In the initial graph layout, all vertices of corresponding features are grouped by their time-step and stacked in y direction. The time-steps are arranged in discrete *layers* along the spatial dimension in x direction to indicate time. The spatial vertex position in a layer is called *rank* of the vertex. As the vertices have no specific rank order in y direction, edges may cross and thus deteriorate visual perception of how events are connected (see Figure 5.10 (2)). For this reason an edge-crossing minimization algorithm (see Figure 5.10 (3)) is employed. An approach which is based on mean heuristics by Gansner et al. [29] was implemented. Vertex positions in each layer are permuted to minimize edge crossings in the graph.

Gansner et al. [29] also calculated spline control points for the edges as their algorithm is for graphs where edges can connect vertices in layers that are not adjacent. Due to the time-series



❖ **Figure 5.10** — Calculation and visualization of the Fuzzy Tracking Graph: After an (1) event selection in the Event Explorer, (2) a tracking graph is built and the (3) edge crossings are minimized. Then (4) event types and Tracking Uncertainty are encoded.

used in this chapter a further constraint was added: Features can not skip one time-step and therefore edges can only connect vertices from adjacent layers. For that reason the spline control points were omitted.

In the last step, the event types and the Tracking Uncertainty (see Figure 5.10 (4)) is encoded. Therefore the same event-type colors as in the other views are used for coloring the vertices and the edges of the graph. If an edge connects events with different event types, a color gradient is used. The Tracking Uncertainty is visualized through the opacity of the vertices and edges.

5.6 Results and Evaluation

In the preceding section results from the visual-analysis tool for the exploration of 4D-XCT time-series is presented. The approach was applied on two real-world in-situ applications.

5.6.1 Wood-Shrinkage Analysis

Taylor et al. [70] observed the shrinkage behavior of European beech wood at a micro scale. Therefore they scanned a time-series of an in-situ dry-out process of wet wood with XCT. The XCT measurements were performed on a GE Phoenix|xray nanotom device with a 180 kV nano focus tube. The measurement current was 275 μ A and the voltage at the tube was 50 kV. With an

integration time of 125 ms and a number of 700 projections, a time-series of 25 datasets, with a resolution (voxel size) of 5.67 μm and a dataset size of 256 x 256 x 256 voxels was obtained. The relative humidity in the sample chamber was between 21 % and 19 % at a temperature between 21.8 ° C and 22.6 ° C. A 3 x 3 median filter was used for smoothing the data. For the analysis the time-steps of 15, 20, 25, 30 and 60 minutes of the dry-out process were available, as they show the most interesting changes of the voids between the wood fibers. These voids are the features of interest and were extracted with the automatic thresholding algorithm as proposed by Otsu [55]. After applying Fuzzy Feature Tracking on the time-series, the results were shown to the domain experts.

5.6.1.1 Case Study

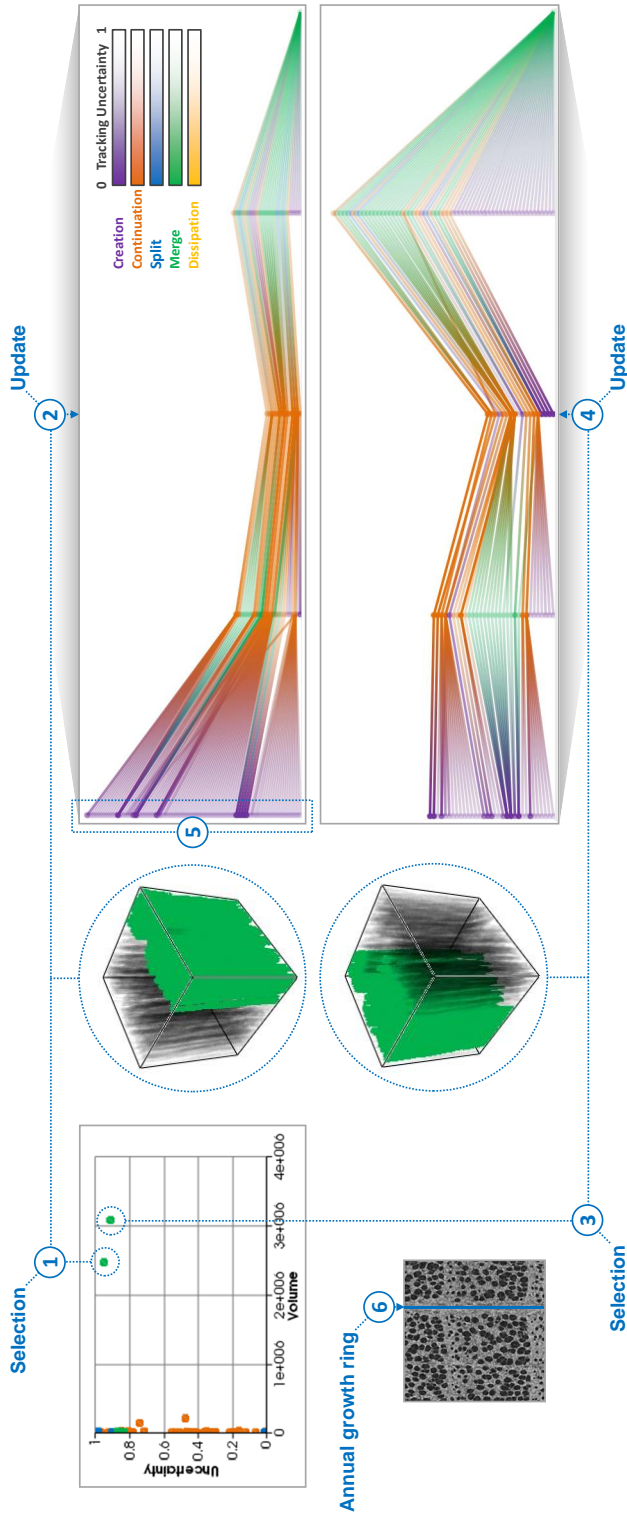
Wood consists of wood fibers. When drying out, voids in-between the fibers grow and merge through the cell walls of the fibers. The key aspect of the wood-shrinkage analysis is to track how these voids grow and merge over time. Figure 5.11 shows the results of the analysis. In the last time-step of the Event Explorer two merge events with a high volume were conspicuous. Thus both one after the other were selected (see Figure 5.11 (1 and 3)). Figure 5.11 (2 and 4) shows the updated Fuzzy Tracking Graphs which give an overview, of how the voids were created and merged over time. The maximum of 92 events in time-step $t(15 \text{ minutes})$ led to 92 stacked vertices in the Fuzzy Tracking Graph and thus to visual clutter (see Figure 5.11 (5)). Despite this the tracking results are traceable because of the used coloring of event types. The varying Tracking Uncertainty can be explained by the following combination: Voids only originate in-between a uniform arrangement of wood fibers and thus many of them have nearly the same size before merging with others. Furthermore a high number of voids appear within small regions.

5.6.1.2 Domain Experts Feedback

The results show how the voids grow in the time-series and thus fulfill the domain experts research questions. During the dry-out process the large features merge from many smaller voids between the wood fibers as expected. With the two selections (see Figure 5.11 (1 and 3)), domain experts further saw that voids are not able to merge across the barrier of an annual growth ring of the tree (see Figure 5.11 (6)).

5.6.2 AlSiC Alloys under Thermal Load

Schöbel et al. [66] inspected a heating cycle of SiC particle reinforced aluminum (AlSiC). This material is of high industrial interest as it offers the high thermal conductivity of a metal with the low thermal expansion of a ceramic. Therefore they analyzed a specimen under thermal load with synchrotron tomography at the ESRF ID15A beam-line in Grenoble. The specimen was heated up from 30 ° C to 400 ° C and cooled down to 50 ° C. As a result a time-series with the thermal cycle 30 ° C \rightarrow 200 ° C \rightarrow 300 ° C \rightarrow 400 ° C \rightarrow 300 ° C \rightarrow 190 ° C \rightarrow 50 ° C was acquired. The resulting scans with a resolution of 400 x 400 x 400 voxels were taken



❖ Figure 5.11 — Results of the wood-shrinkage time-series: Event Explorer of time-step $t(60 \text{ min})$ with two selections (1 and 3) of large merge events. Selections lead to updates (2 and 4) of the Fuzzy Tracking Graph. (5) Visual clutter in the Fuzzy Tracking Graph. (6) Annual growth ring in time-step $t(60 \text{ min})$.

using a voxel size of 1.4 μm . During this process the volume fraction of micro voids changes. Voids decrease during heating and increase while cooling down. As these voids influence the thermal expansion of the material, their changes in size are of high interest. Thus a region-of-interest with a size of 61 x 61 x 61 voxels was cut out showing one representative void for the analysis. For pre-processing, the seven datasets were registered by calculating their mutual information. As the specimen is expanding uniformly in all directions due to the isotropic material distribution, a rigid registration is sufficient. The micro voids as the features of interest, were extracted with a simple thresholding as described before [66]. Fuzzy Feature Tracking was applied on the time-series and the results were shown to the domain experts.

5.6.2.1 Case Study

In this application, the whole process of how the void splits and merges is of high interest for the domain experts. Thus the data was not filtered by selecting specific events. Figure 5.12 (A) shows the 3D Data View with all seven time-steps. The features are colored according to their assigned event type. Figure 5.12 (B) shows the Fuzzy Tracking Graph of the whole time-series. Two areas (see Figure 5.12 (1 and 4)) with encoded Tracking Uncertainty are highlighted. In the first time-step three features (see Figure 5.12 (1)) were created and assumed to take part in a merge event in the second time-step, each with a different Tracking Uncertainty. Figure 5.12 (4) shows how new micro voids are created and no continuing features in the adjacent time-steps are found. Regarding the application domain, Figures 5.12 (2 and 3) show an interesting split (2) and merge (3) event during the heating and cooling cycle from 300 ° C up to 400 ° C and down to 300 ° C.

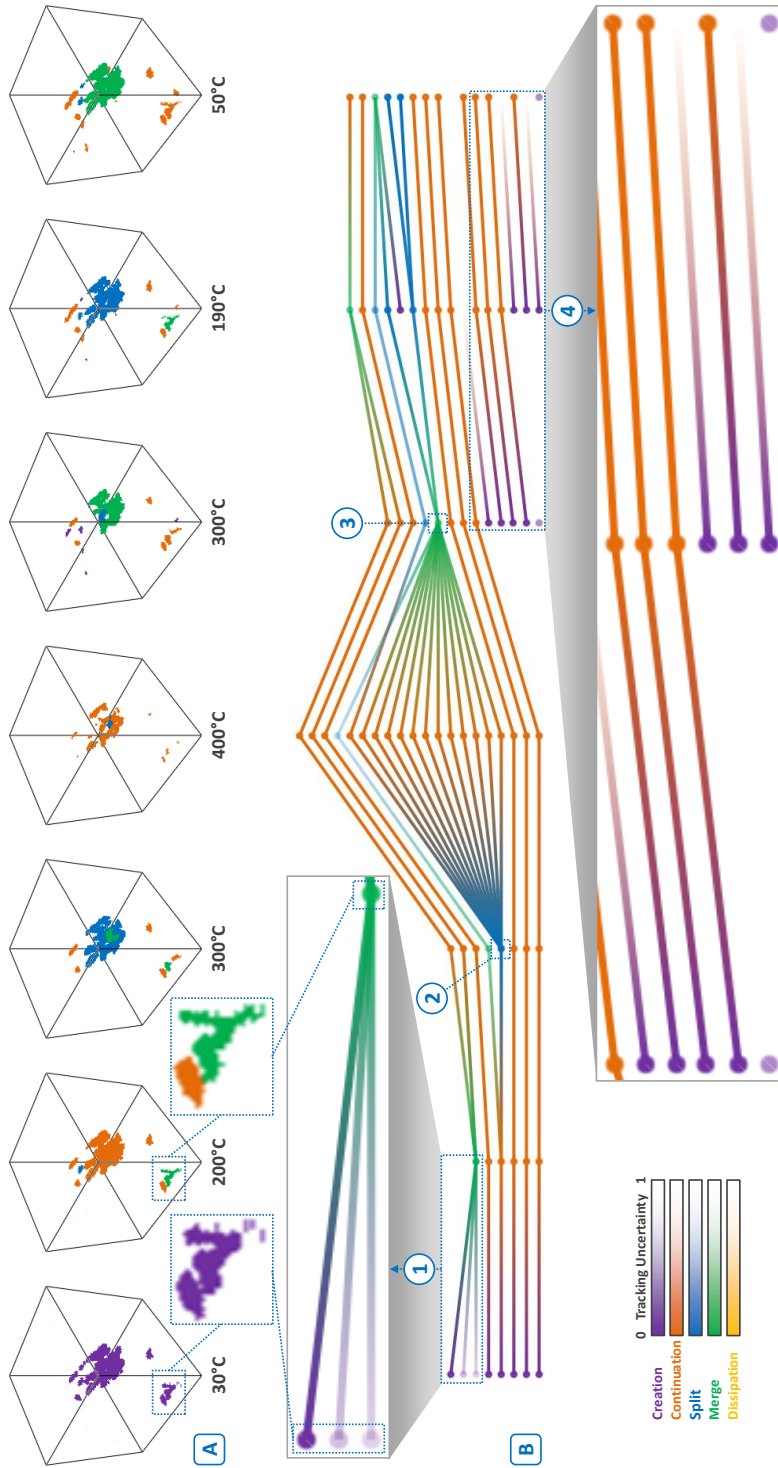
5.6.2.2 Domain Experts Feedback

In this case study, a need for selecting individual events in the Event Explorer was not necessary for the domain experts, as the number of micro voids in the time-series was low, i.e., resulting in 6 to 20 events in a time-step. Thus the 3D Data View and the Fuzzy Tracking Graph were sufficient. Especially the split event in Figure 5.12 (2) during heating and the merge event in Figure 5.12 (3) while cooling down, show exactly which micro voids are involved in this process and thus fully answer the research questions of the domain experts.

5.6.3 Design Lessons Learned

The initial idea was to analyze individual features in the time-series and track their temporal evolution over time. Therefore a tool with multiple linked-views was presented. The stacked arrangement of 3D Data View, Event Explorer and Fuzzy Tracking Graph in the tool emphasizes the connection between the linked views, as the same time-step is one upon the other in all views.

Regarding the Event Explorer, mostly the last time-step attracted attention. As it shows the final state of the underlying process, it was the starting point of the interaction. Scatter plots showed a large variety of information due to the user-defined axes.



❖ **Figure 5.12** — Results of the AISiC time-series: (A) 3D Data View of a void during a heating and cooling cycle (30 °C → 200 °C → 300 °C → 400 °C → 300 °C → 190 °C → 50 °C). (B) Fuzzy Tracking Graph showing two areas (1 and 4) with encoded Tracking Uncertainty. (2 and 3) Highlighting of an interesting split (2) and merge (3) event for the sequence (300 °C → 400 °C → 300 °C).

The Fuzzy Tracking Graph allows the domain experts to see the temporal evolution of how the features are tracked and connected over the whole time-series. In the two case studies it emerged, that the Fuzzy Tracking Graph is an appropriate visualization for small graphs, with a maximum of about 25 vertices per time-step when stacking the views in the tool. With more vertices per time-step, visual clutter of vertices and edges hinders the domain experts to see all details of the temporal evolution. However, even with visual clutter, a rough overview of the temporal evolution is given.

Encoding the Tracking Uncertainty was a first step to evaluate the tracking results of the Fuzzy Feature Tracking approach. Although visualizing the uncertainty by setting the opacity of vertices and edges clearly showed Tracking Uncertainty, for future work other visual encodings may be considered together with strategies to avoid visual clutter in the Fuzzy Tracking Graph.

5.7 Summary

In this chapter a visual-analysis tool for the exploration of 4D-XCT time-series was presented. Based on a detailed workflow and task analysis, the tool was designed to address the different aspects of the spatial and time-specific information of time-series. Therefore individual features and their properties were extracted to track them between the time-steps. As a result, the feature events creation, continuation, split, merge and dissipation are detected and a Tracking Uncertainty between adjacent time-steps is calculated. For the visualization and analysis of this data, a 3D Data View was proposed mimicking a filmstrip view of 3D renderings for each dataset in order to show the spatial feature information. An Event Explorer shows the global temporal overview implemented in the form of scatter plots, one for each time-step. A Fuzzy Tracking Graph gives the temporal overview of the events but with the extension of how they are linked between the time-steps. The Tracking Uncertainty was encoded by modulating the opacity of the vertices and edges. With the presented tool, the domain experts are able to interactively analyze a time-series by selecting events of interest in the Event Explorer which leads to an update of the 3D Data View and the Fuzzy Tracking Graph. As all views are linked, event selections highlight corresponding features in the 3D Data View. The solution further includes a Volume Player to cover the spatio-temporal domain. Using volume blending, the transition between two datasets can be visualized in a play-back fashion. The tool was illustrated on various real-world applications, such as wood-shrinkage analysis and AISiC alloys under thermal load.

Conclusion

I conclude this thesis by summing up the contributions which were developed in this thesis. After revisiting the research questions, I also give an outlook on possible research directions for the future and reflections on my four years of research.

6.1 Summary of the Contributions

To solve the four main tasks *Task 1: Quantitative Porosity*, *Task 2: Porosity Overview*, *Task 3: Exploration of Pores* and *Task 4: Feature Tracking* of this thesis, three visual-analysis tools were researched and integrated into the in-house framework iAnalyse of the CT-group of the University of Applied Sciences Upper Austria, Wels Campus:

Contribution 1 - Porosity Maps

Quantitative porosity determination of CFRP components is of high importance in the aeronautic industry. The presented quantification of pores showed satisfying results as the porosity values were in the range of inaccuracy of ultrasonic testing and acid digestion. On this basis local pore properties were calculated to serve as input for a two-stage drill-down approach to explore and visualize individual pores. For a fast porosity overview porosity maps were implemented and compared to active-thermography images. Due to the high-resolution XCT data the porosity maps showed significantly more details. A region-of-interest selection in the porosity maps was linked to a parallel-coordinates view for the classification of pores. In addition, a best-viewpoint widget allows the user to see the quality-varying viewing directions on a sphere. The results were demonstrated using real-world CFRP specimens.

Contribution 2 - MObjects

With the MObjects approach an alternative novel method for the visualization and interactive exploration of pores was introduced. Based on the segmented pores, a MObject was calculated. This global MObject shows the mean shape of all pores and thus a shape overview of all pores in a dataset. For further porosity overviews local MObjects were visualized on a regular grid to visualize the pore homogeneity in individual cells. A color-coded homogeneity visualization was implemented which shows the deviation from the average pore properties. To analyze the pores by interactively exploring the MObjects, a MObject Set visualization in a radial and parallel arrangement was presented. By exporting representative MObjects of interest as volumetric datasets, subsequent calculations and simulations, e.g., active-thermography simulations, may be enhanced. The techniques were applied to cases of high practical relevance in the aeronautics industry.

Contribution 3 - Fuzzy Feature Tracking

The presented tool allows for an interactive analysis of 4D-XCT data, respectively a time-series of XCT measurements showing a process over time. After extracting individual features and their properties, they were tracked between several time-steps. Feature events such as creation, continuation, split, merge, and dissipation were detected. A Tracking Uncertainty between adjacent time-steps was calculated. For visualizing the spatial feature information, 3D renderings for each time-step were presented. The global temporal overview was shown in an Event Explorer, where scatter plots served as snapshots for the time-steps. A Fuzzy Tracking Graph visualized the temporal overview of the events including the information of how they are linked between the time-steps. To cover the spatio-temporal domain of the data, a Volume Player used volume blending to display the transition between two time-steps. Due to missing data of a CFRP related process, e.g., a fatigue test of CFRP components, the results were demonstrated using various real-world applications, such as a wood-shrinkage analysis and AlSiC alloys under thermal load.

6.2 Revisiting the Research Questions

In Section 1.3, four main research questions were stated and main tasks were derived. Now I will reflect on these questions and show how they were addressed in the thesis.

Question 1: *What is the quantitative porosity?*

As porosity is a decisive factor if a component meets the specifications or if it needs to be reworked or rejected, porosity has to be quantified. Based on XCT data, porosity was determined by segmenting pores in the dataset with Otsu's thresholding technique. It was shown in this thesis, that porosity can be quantified adequately using XCT although no ground truth is available. Compared to the reference methods, the XCT results are in their range of inaccuracy.

Question 2: *How are the pores distributed?*

As XCT provides fully three-dimensional information of the scanned specimen and thus the exact spatial location of each pore, the proposed visualizations are crucial to show how the pores are distributed in the specimen. The presented approaches such as porosity maps, local MObjects, and the color-coded homogeneity visualization are crucial to show the pore distribution. Furthermore the exploration methods, e.g., ROI selection, parallel-coordinates interaction, and MObject Sets, allow the user a detailed analysis of the pores.

Question 3: *What are the shapes of the pores?*

The shapes are quantified by calculating shape factors of each pore. MObjects are crucial to visualize the average shape by aggregating the pores into an intermediate representation. It has further been shown that the mean shape of the pores changes with the degree of porosity [57].

Question 4: *How does a feature evolve over time?*

Fuzzy Feature Tracking and visual analysis of the tracking results are crucial to track features in 4D-XCT data. Since features also may move over time, an explicit tracking is not always possible. Calculating a Tracking Uncertainty solves this problem. The proposed visualizations are crucial to show which features are created, continuing, splitting, merging or dissipating at a certain time-step and how the corresponding features are tracked along the whole time-series. Visual clutter in large Fuzzy Tracking Graphs is still an open issue.

6.3 Outlook

The following potential research directions for enhancing the analysis of porosity in CFRP components may be considered in the future.

Accurate Porosity Determination

Compared to the reference methods ultrasonic testing and acid digestion, XCT results are in the range of inaccuracy (about ± 1 %) of these methods (see Section 3.5.1). Until now, no reference specimen with a ground truth is available, where the porosity is exactly known. Although a simulation can be used as reference point, the simulation result can not be applied to a real-world component. To allow the NDT practitioners an accurate determination of the quantitative porosity such a reference specimen has to be manufactured in the future.

Porosity Determination for Varying Data Quality

One of the main problems regarding an accurate porosity determination using XCT is the partial volume effect [30]. This discretization error of the scanned structures leads to inaccurate results.

With an increase of the voxel size, the partial volume effect has a growing impact on the data quality. As the voxel size depends on the size of the scanned component as well as on the used XCT device, segmentation results differ from each other, if the same component or material is scanned with varying voxel sizes. This problem has to be considered especially for scanning large components.

Porosity in Fiber Layers

In terms of material properties, the distribution of pores in a component is important. Porosity in a specific layer may be more critical than a homogenous distribution of pores as this may lead to a delamination of the affected layers. Several approaches for the analysis of the pore distribution were presented in this thesis. For example, with porosity maps the fiber layers and their weaving pattern can be estimated. For a quantification of the porosity per fiber layer, these fiber bundles have to be determined.

Reducing Visual Clutter

A high number of pores in a dataset leads to visual clutter in the 3D view. Therefore two methods were presented in this approach: First, exploring the pores with the data drill-down approach, reduces the number of visualized pores and thus the visual clutter. Second, the best-viewpoint widget helps the user to find viewpoints with reduced visual clutter. An open issue is the visual clutter in the Fuzzy Tracking Graph. Future work may focus on other visual encodings for the Tracking Uncertainty as well as strategies to avoid visual clutter in the Fuzzy Tracking Graph. For example, a magnification lens may be used for zooming into the Fuzzy Tracking Graph.

Additional Applications

Although I focused on the evaluation of pores in this work, the approaches can be used for all kinds of defects in material sciences. Interactive exploration with parallel coordinates was applied to fibers [76]. MObjects were also calculated for fibers [77]. In the future, the MObjects approach will be applied on cracks, inclusions, and particles. The methods may also be suitable for other applications from different domains.

6.4 Reflections

When finalizing this thesis, I critically reflect on the topic and the four years of research. Many interesting trends can be observed in the non-destructive testing, industrial X-ray Computed Tomography and aeronautics community.

The determination of quantitative porosity is the main task in quality control, especially in the aeronautics industry, where a 100 % testing is required. As a solution for this task, companies require a fully automatic approach. After scanning a component, the system should decide, if a component meets the specifications or if it needs to be reworked or rejected. Therefore several in-line XCT systems are currently brought to the market. Although the need for a fully automatic

approach is understandable, several objections arise. To specify the accuracy of XCT with respect to quantitative porosity determination, a reference specimen with a ground truth is needed. In addition, a high resolution with a voxel size below 20 μm is necessary. Besides quantitative porosity, the structural analysis of each component has to be considered. Thus I believe that human interaction is always needed as the porosity and the pore distribution in relation to the structural analysis has to be evaluated for each component and material type individually. This is particularly essential for complex components. Concerning quality control in the aeronautics industry, the authorization cycle for non-destructive testing methods may take years or decades. At the moment also other methods like active thermography and laser-ultrasonic testing are also available and under development. Because of all these issues, I believe that ultrasonic testing will not be fully replaced as state-of-the-art method in quality control in the aeronautics industry in the next years.

Nevertheless, XCT is the most advanced method for the domain experts as it non-destructively offers insights into the components by providing three-dimensional data of the internal structures, whereas the other methods only provide two-dimensional result images. In my opinion, XCT is a powerful method for specific analysis tasks or for the evaluation of components which can not be clearly evaluated with ultrasonic testing. Furthermore detailed investigations of small reference samples by XCT can serve as input to enhance other methods such as active thermography.

This is the point, where we as the visualization community should support the user with advanced visualizations and visual-analysis techniques. The trend can already be seen in the community where more and more visual-analysis tools are presented to solve increasingly more detailed analysis tasks. Thereby one of the main challenges can be seen in the dataset sizes and the high number of features in these datasets. In my opinion specifically tailored visualizations combined with data drill-down techniques will be the key to cope with visual complexity and visual clutter.



Porosity-Maps Evaluation-Questionnaire

The aim of this evaluation questionnaire is to get feedback about the software prototype for porosity determination and visualization. Your feedback will be part of an application/design paper submission for the EuroVis 2012 - 14th Eurographics / IEEE Conference on Visualization. In the paper a visualization pipeline that is customized for the specific application of interactive exploration and visual analysis of CFRP specimens is developed to enhance the evaluation workflow for non-destructive testing (NDT) practitioners based on specified tasks. Besides quantitative porosity determination and the calculation of local pore properties, i.e., volume, extent and shape factors, a drill down approach to explore pores in a CFRP specimen is employed. This questionnaire will focus on:

- The porosity overview
- The comparison of active thermography, porosity maps, and ultrasonic images

A.1 Previous Work

1a. Have you ever used one of the following methods?

- Ultrasonic testing
- Acid digestion
- Active thermography
- Computed tomography

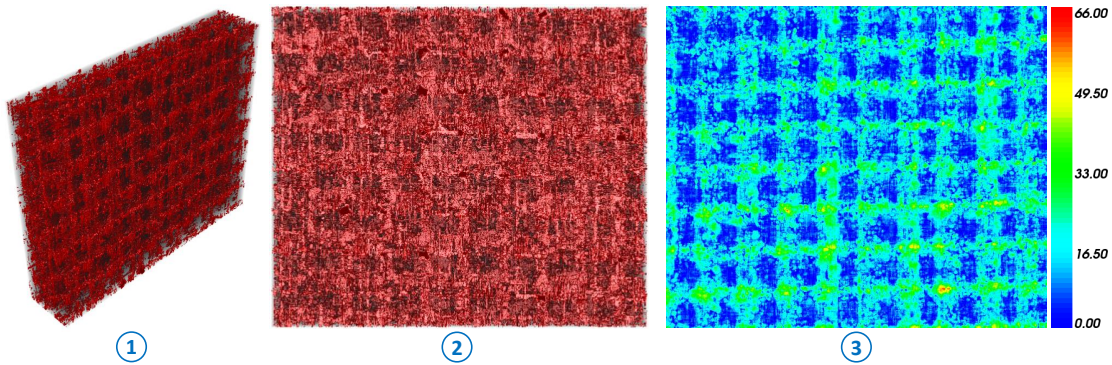
1b. If yes, how many years of experience do you have using these methods?
_____ year(s)

1c. Have you ever done testing in the field of carbon fiber reinforced polymers?

- Yes
- No

1d. If yes, which methods did you use?

A.2 Porosity Overview



❖ Figure A.1 — (1) PrePreg component after porosity determination in 3D iso view (2) in 3D xz view (3) and porosity map xz view.

2a. Task: Mark areas with high porosity in Figure A.1.

2b. How well can you locate areas with high porosity for further investigations using a 3D iso view (see Figure A.1 (1))?
 poor fair average very good excellent

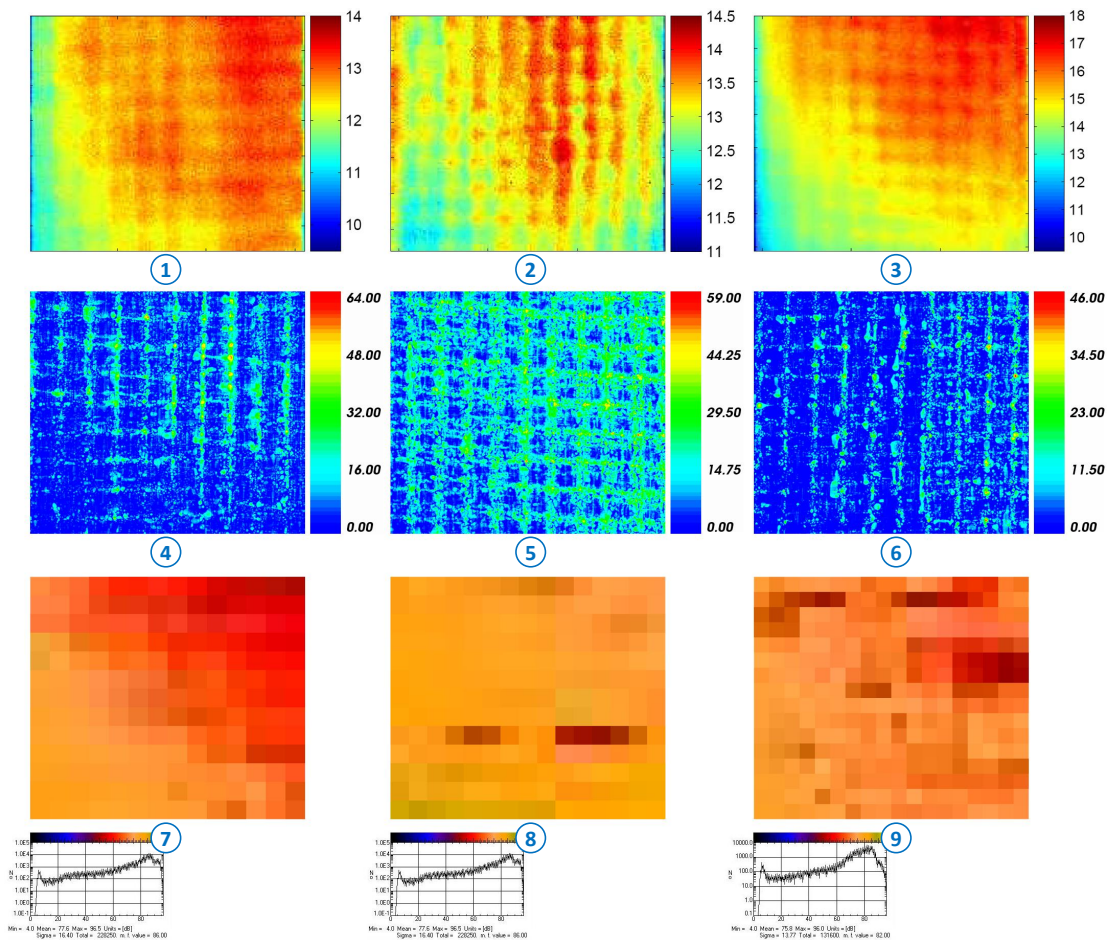
2c. How well can you locate areas with high porosity for further investigations using a 3D xz view (see Figure A.1 (2))?
 poor fair average very good excellent

2d. How well can you locate areas with high porosity for further investigations using a porosity map (see Figure A.1 (3))?
 poor fair average very good excellent

2e. Remarks concerning the porosity overview using porosity maps (benefits / drawbacks):

A.3 Comparison of Active Thermography, Porosity Maps, and Ultrasonic Testing

The currently used state-of-the-art method for porosity determination in aeronautics, where all critical parts have to be inspected completely, is ultrasonic testing. It can be easily used for quality control, thus it is a NDT method. The porosity level can be estimated by the ultrasonic velocity and attenuation because of a bilinear correlation between the porosity and the ultrasonic attenuation coefficient.



❖ **Figure A.2** — Comparison of active thermography images (1-3), porosity maps (4-6), and ultrasonic images (7-9). Based on the thermal diffusivity model high values in the active thermography images depict a high porosity, which is encoded as the observation time in seconds.

3a. Task: Mark areas with high porosity in Figure A.2.

3b. How well can you locate areas with high porosity using active thermography images (see Figure A.2 (1-3))?

- poor fair average very good excellent

3c. How well can you locate areas with high porosity using porosity maps (see Figure A.2 (4-6))?

- poor fair average very good excellent

3d. How well can you locate areas with high porosity using ultrasonic images (see Figure A.2 (7-9))?

- poor fair average very good excellent

3e. Which image best depicts the twill weave pattern of the fiber bundles in the specimens (see Figure A.2 (1-6))?

- (1) (2) (3) (4) (5) (6)

3f. Task: Identify related specimens in Figure A.2:

Figure A.2 (1) belongs to ...

- (4) (5) (6) (7) (8) (9)

Figure A.2 (2) belongs to ...

- (4) (5) (6) (7) (8) (9)

Figure A.2 (3) belongs to ...

- (4) (5) (6) (7) (8) (9)

3g. Remarks concerning the porosity overview using porosity maps (benefits / drawbacks):

MObjects Evaluation-Questionnaire

The aim of this evaluation questionnaire is to get feedback about the software prototype for the interactive exploration and visualization of defects in industrial XCT data. Your feedback will be part of an application/design paper submission for SciVis 2013. In this work mean objects (MObjects) are introduced. A MObject represents the summation of a set of individual objects in a dataset. To create a MObject, the centroids of all individual objects are aligned. After summing up the individual objects, the resulting MObject is visualized. A set of MObjects is called mean object set (MObject Set). They are used to explore the parameter space of the calculated MObjects. This questionnaire will focus on the evaluation of the following tasks:

- MObject Visualization (T1)
- Local MObject Visualization (T2)
- MObjects Exploration (T3)

B.1 Previous Work

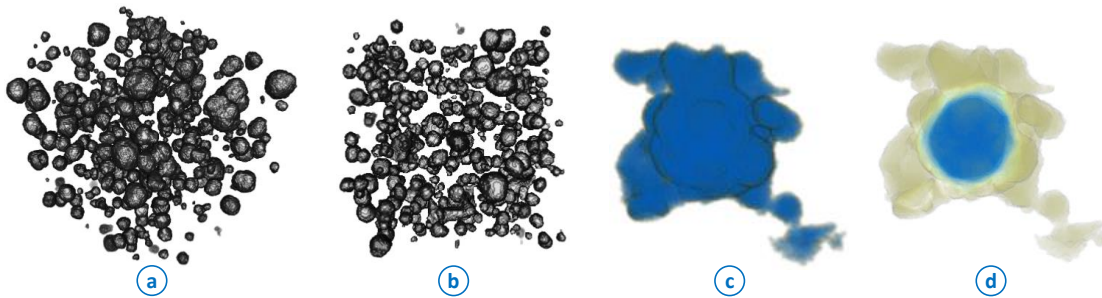
Non-destructive testing methods

| |
|---|
| <p>1a. Have you ever worked with computed tomography data? <input type="checkbox"/> Yes <input type="checkbox"/> No</p> |
| <p>1b. If yes, how many years of experience do you have using computed tomography? _____ year(s)</p> |
| <p>1c. Have you ever used active thermography? <input type="checkbox"/> Yes <input type="checkbox"/> No</p> |
| <p>1d. If yes, how many years of experience do you have using active thermography? _____ year(s)</p> |
| <p>1e. Have you ever used ultrasonic testing? <input type="checkbox"/> Yes <input type="checkbox"/> No</p> |
| <p>1f. If yes, how many years of experience do you have using ultrasonic testing? _____ year(s)</p> |

Materials

| |
|---|
| <p>1g. Are you experienced with carbon fiber reinforced polymers? <input type="checkbox"/> no experience <input type="checkbox"/> hardly any <input type="checkbox"/> moderate <input type="checkbox"/> plenty of <input type="checkbox"/> high level of experience</p> |
| <p>1f. How many years of experience do you have with carbon fiber reinforced polymers? _____ year(s)</p> |
| <p>1g. Are you experienced with light metals? <input type="checkbox"/> no experience <input type="checkbox"/> hardly any <input type="checkbox"/> moderate <input type="checkbox"/> plenty of <input type="checkbox"/> high level of experience</p> |
| <p>1f. How many years of experience do you have with light metals? _____ year(s)</p> |
| <p>1g. Are you experienced with steel? <input type="checkbox"/> no experience <input type="checkbox"/> hardly any <input type="checkbox"/> moderate <input type="checkbox"/> plenty of <input type="checkbox"/> high level of experience</p> |
| <p>1f. How many years of experience do you have with steel? _____ year(s)</p> |

B.2 MObject Visualization (T1)



❖ **Figure B.1** — 3D renderings of individual objects in (a) isometric view, (b) xy view. (c and d) 3D rendering of MObject visualization generated from the input of image (a) using two different transfer function settings.

2a. Can you identify deviating (not nodular) structures in Figure B.1 (a)?

poor fair average very good excellent

2b. Can you identify deviating (not nodular) structures in Figure B.1 (b)?

poor fair average very good excellent

2c. Can you identify deviating (not nodular) structures in Figure B.1 (c)?

poor fair average very good excellent

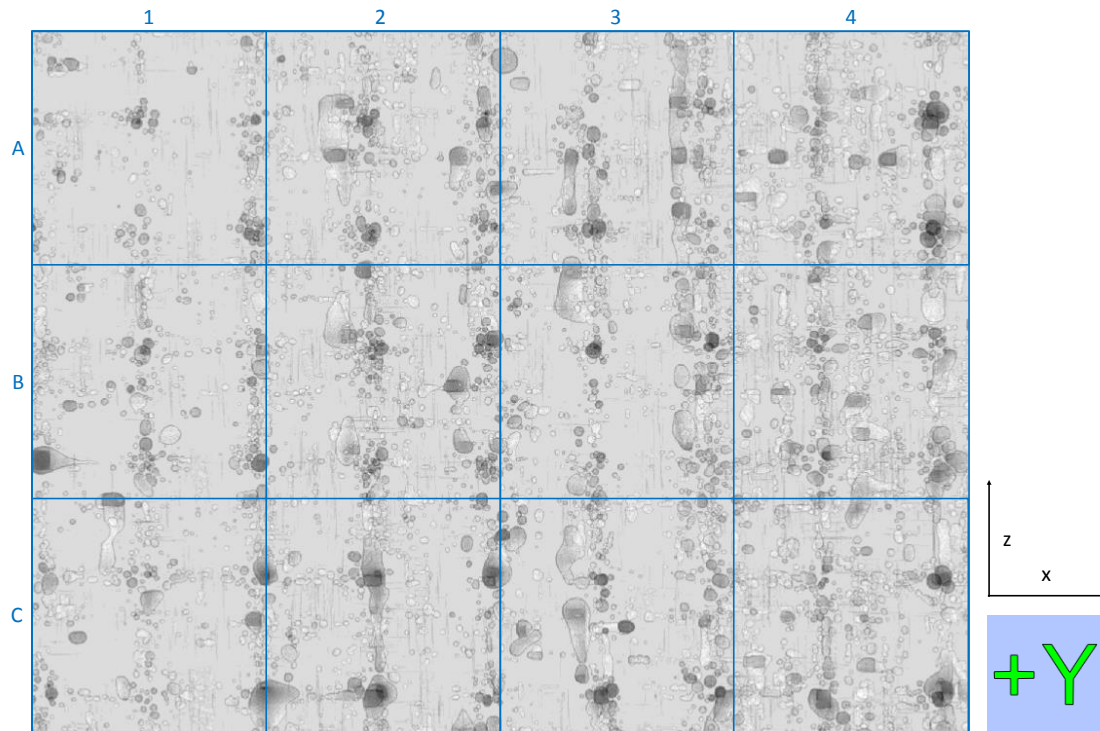
2d. Can you identify deviating (not nodular) structures in Figure B.1 (d)?

poor fair average very good excellent

2e. Remarks concerning the mean objects visualization (benefits / drawbacks):

B.3 Local MObject Visualization (T2)

For a fast homogeneity overview of the specimen the dataset is divided into regular sub-volumes (cells). Figure B.2 shows the partitioning of a CFRP dataset with segmented pores in the cells.



❖ Figure B.2 — Visualization of segmented pores in a CFRP dataset.

3a. Which cell in Figure B.2 has the lowest deviation from the average pore volume?

3b. Which cell in Figure B.2 has the highest positive deviation from the average pore volume?

3c. Which cell in Figure B.2 has the highest negative deviation from the average pore volume?

3d. Which cell in Figure B.2 has the lowest deviation from the average pore shape factor?

3e. Which cell in Figure B.2 has the highest positive deviation from the average pore shape factor?

3f. Which cell in Figure B.2 has the highest negative deviation from the average pore shape factor?

3g. Which cell in Figure B.2 has the lowest deviation from the average pore extent in x direction?

3h. Which cell in Figure B.2 has the highest positive deviation from the average pore extent in x direction?

3i. Which cell in Figure B.2 has the highest negative deviation from the average pore extent in x direction?

3j. Which cell in Figure B.2 has the lowest deviation from the average pore extent in y direction?

3k. Which cell in Figure B.2 has the highest positive deviation from the average pore extent in y direction?

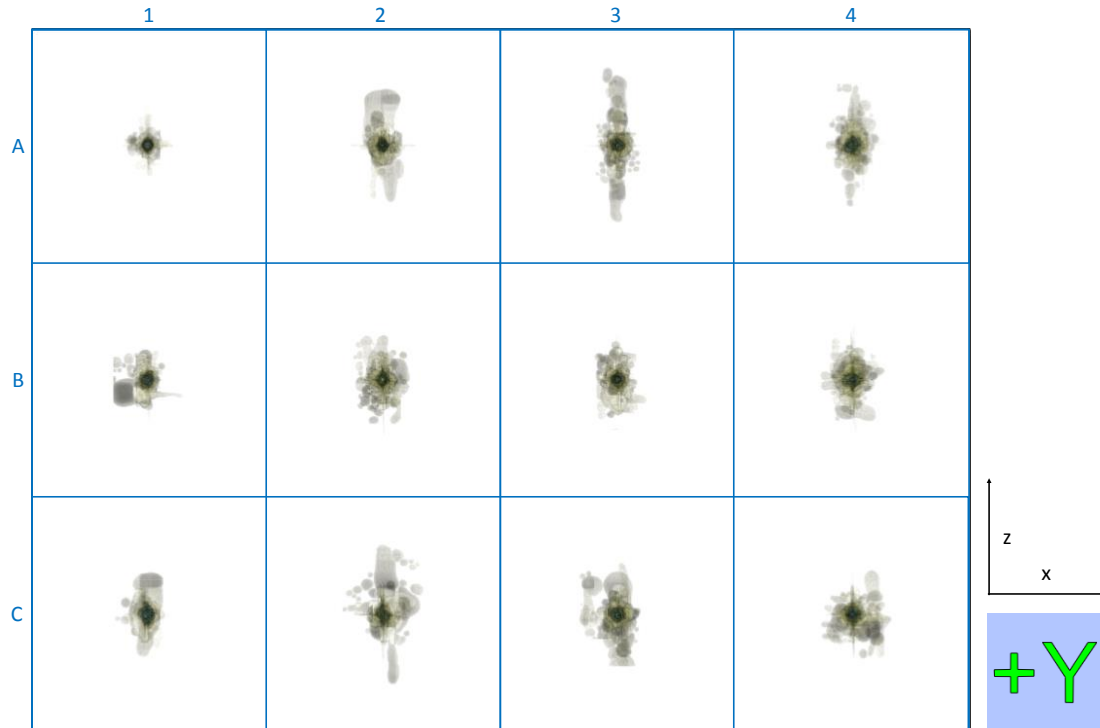
3l. Which cell in Figure B.2 has the highest negative deviation from the average pore extent in y direction?

3m. Which cell in Figure B.2 has the lowest deviation from the average pore extent in z direction?

3n. Which cell in Figure B.2 has the highest positive deviation from the average pore extent in z direction?

3o. Which cell in Figure B.2 has the highest negative deviation from the average pore extent in z direction?

For each cell a local MObject is calculated. In this calculation an individual pore belongs to the cell, in which the center of the pore is located. Figure B.3 shows the local MObjects visualization using the segmented pores dataset from Figure B.2.



❖ Figure B.3 — Local MObjects visualization of the CFRP dataset from Figure B.2.

- 4a. Which MObject in Figure B.3 represents the lowest average pore volume in the dataset?

- 4b. Which MObject in Figure B.3 represents the highest average pore volume in the dataset?

- 4c. Which MObject in Figure B.3 represents the lowest average pore shape factor in the dataset?

- 4d. Which MObject in Figure B.3 represents the highest average pore shape factor in the dataset?

- 4e. Which MObject in Figure B.3 represents the lowest average pore extent in x direction in the dataset?

- 4f. Which MObject in Figure B.3 represents the highest average pore extent in x direction in the dataset?

4g. Which MObject in Figure B.3 represents the lowest average pore extent in z direction in the dataset?

4h. Which MObject in Figure B.3 represents the highest average pore extent in z direction in the dataset?

4i. Which MObject in Figure B.3 has the lowest pore volume homogeneity in its cell?

4j. Which MObject in Figure B.3 has the highest pore volume homogeneity in its cell?

4k. Which MObject in Figure B.3 has the lowest pore shape factor homogeneity in its cell?

4l. Which MObject in Figure B.3 has the highest pore shape factor homogeneity in its cell?

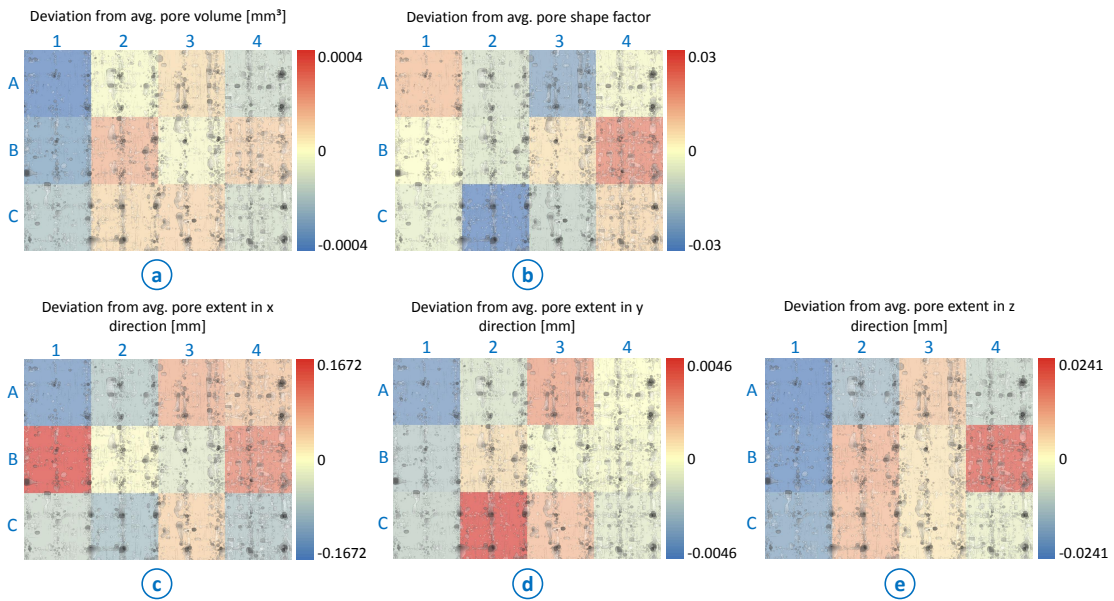
4m. Which MObject in Figure B.3 has the lowest homogeneity regarding the pore extent in x direction in its cell?

4n. Which MObject in Figure B.3 has the highest homogeneity regarding the pore extent in x direction in its cell?

4o. Which MObject in Figure B.3 has the lowest homogeneity regarding the pore extent in z direction in its cell?

4p. Which MObject in Figure B.3 has the highest homogeneity regarding the pore extent in z direction in its cell?

Figure B.4 shows a color-coded cell visualization. Each cell is colored regarding its deviation of the average individual pore properties volume, shape factor, extent in x, y and z direction.



❖ Figure B.4 — Color-coded visualization of the deviation from the average pore (a) volume, (b) shape factor, (c) extent in x direction, (d) extent in y direction, and (e) extent in z direction.

- 5a. Which cell in Figure B.4 has the lowest deviation from the average pore volume?

- 5b. Which cell in Figure B.4 has the highest positive deviation from the average pore volume?

- 5c. Which cell in Figure B.4 has the highest negative deviation from the average pore volume?

- 5d. Which cell in Figure B.4 has the lowest deviation from the average pore shape factor?

- 5e. Which cell in Figure B.4 has the highest positive deviation from the average pore shape factor?

- 5f. Which cell in Figure B.4 has the highest negative deviation from the average pore shape factor?

- 5g. Which cell in Figure B.4 has the lowest deviation from the average pore extent in x direction?

5h. Which cell in Figure B.4 has the highest positive deviation from the average pore extent in x direction?

5i. Which cell in Figure B.4 has the highest negative deviation from the average pore extent in x direction?

5j. Which cell in Figure B.4 has the lowest deviation from the average pore extent in y direction?

5k. Which cell in Figure B.4 has the highest positive deviation from the average pore extent in y direction?

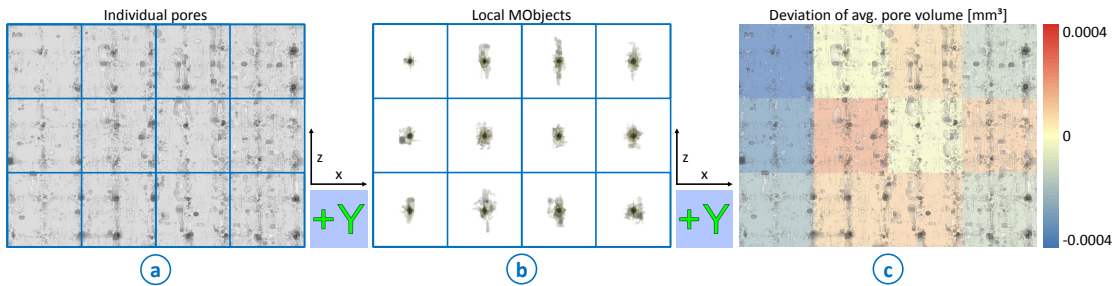
5l. Which cell in Figure B.4 has the highest negative deviation from the average pore extent in y direction?

5m. Which cell in Figure B.4 has the lowest deviation from the average pore extent in z direction?

5n. Which cell in Figure B.4 has the highest positive deviation from the average pore extent in z direction?

5o. Which cell in Figure B.4 has the highest negative deviation from the average pore extent in z direction?

Figure B.5 compares the before evaluated visualizations of individual pores, local MObjects and the color-coded cells.



❖ Figure B.5 — Visualization of (a) segmented pores (b) local MObjects, and (c) the color-coded cell visualization.

6a. Can you identify the pore homogeneity of the whole dataset in Figure B.5 (a)?
 poor fair average very good excellent

6b. Can you identify the pore homogeneity in the individual cells in Figure B.5 (a)?
 poor fair average very good excellent

6c. Can you identify the pore homogeneity of the whole dataset in Figure B.5 (b)?
 poor fair average very good excellent

6d. Can you identify the pore homogeneity in the individual cells in Figure B.5 (b)?
 poor fair average very good excellent

6e. Can you identify the pore homogeneity of the whole dataset in Figure B.5 (c)?
 poor fair average very good excellent

6f. Can you identify the pore homogeneity in the individual cells in Figure B.5 (c)?
 poor fair average very good excellent

6g. Remarks concerning the mean objects visualization (benefits / drawbacks):

B.4 MObjects Exploration (T3)

For the interactive exploration of the MObjects, MObject Sets are calculated by clustering the individual objects regarding their calculated properties, e.g., volume, extent, or shape factors.

7a. Are you interested in nodular objects?

not interested hardly interested little interested interested very interested

7b. Are you interested in long and thin objects?

not interested hardly interested little interested interested very interested

7c. Are you interested in crack-shaped objects?

not interested hardly interested little interested interested very interested

7d. Are you interested in classifications based on the volume of the individual objects?

not interested hardly interested little interested interested very interested

7e. Are you interested in classifications based on the dimensions of the individual objects?

not interested hardly interested little interested interested very interested

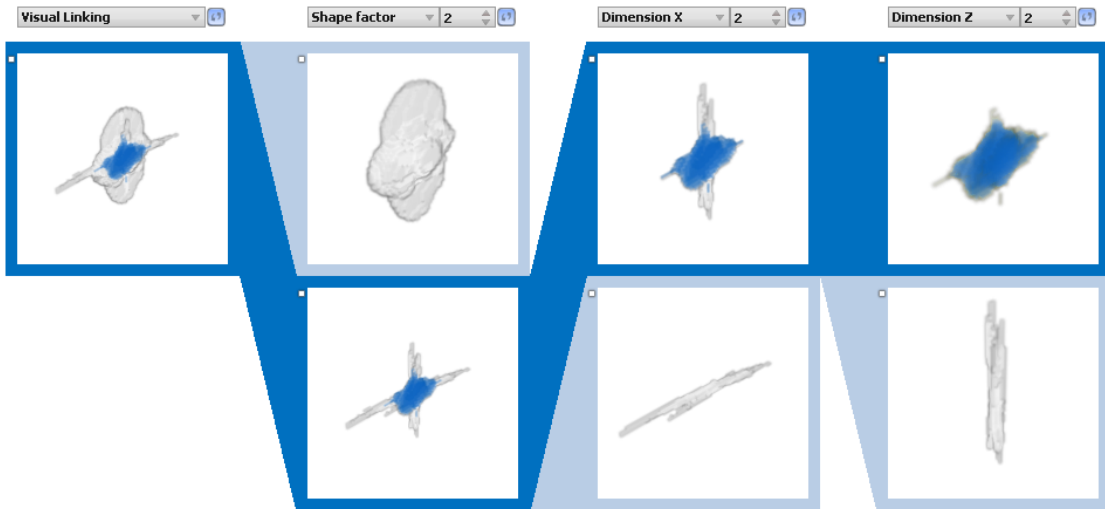
7f. Are you interested in classifications based on the shape factors of the individual objects?

not interested hardly interested little interested interested very interested

7g. Into how many sub-classes would you split the individual objects regarding the volume?
_____ classes

7h. Into how many sub-classes would you split the individual objects regarding the dimensions?
_____ classes

7i. Into how many sub-classes would you split the individual objects regarding the shape factors?
_____ classes



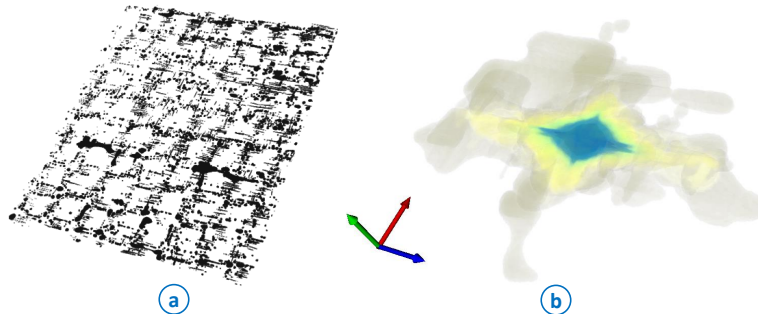
❖ Figure B.6 — MObject Set visualization showing the selected path and the visual linking approach of the rendered MObjects.

8a. Can you identify the selected path of the interactive exploration in Figure B.6?
 poor fair average very good excellent

8b. Can you identify the different scaling of the MObjects through visual linking in Figure B.6?
 poor fair average very good excellent

8c. Remarks concerning the mean objects visualization (benefits / drawbacks):

The visualization was tested with a dataset of a carbon fiber reinforced polymer specimen, showing a MObject of the whole dataset (see Figure B.7) as well as some exported MObjects after the interactive exploration of a ROI (see Figure B.8).



❖ Figure B.7 — (a) Rendering of individual objects (pores) of a CFRP dataset. (b) Mean object (MObject) visualization of the individual objects from (a).

9a. Can you identify nodular pores in Figure B.7 (a)?
 poor fair average very good excellent

9b. Can you identify long and thin pores in Figure B.7 (a)?
 poor fair average very good excellent

9c. Can you identify crack-shaped pores in Figure B.7 (a)?
 poor fair average very good excellent

9d. Can you identify nodular pores in Figure B.7 (b)?
 poor fair average very good excellent

9e. Can you identify long and thin pores in Figure B.7 (b)?
 poor fair average very good excellent

9f. Can you identify crack-shaped pores in Figure B.7 (b)?
 poor fair average very good excellent



❖ Figure B.8 — Rendering of mean objects (MOjects) of a CFRP dataset.

9g. Do the mean objects in Figure B.8 represent the typical pore structures in a CFRP dataset?

poor fair average very good excellent

9h. Remarks concerning representative mean objects (benefits / drawbacks):

Bibliography

- [1] Aerospace series - carbon fibre laminates - determination of the fibre-, resin- and void contents, August 1998. DIN EN 2564:1998-08 (German Industrial Norm). [page 7]
- [2] R. Adams and L. Bischof. Seeded Region Growing. *IEEE Transactions on Pattern Analysis and Machine Intelligence*, 16:641–647, June 1994. [pages 13 and 14]
- [3] J. Ahrens, K. Heitmann, M. Petersen, J. Woodring, S. Williams, P. Fasel, C. Ahrens, C.-H. Hsu, and B. Geveci. Verifying Scientific Simulations via Comparative and Quantitative Visualization. *IEEE Computer Graphics and Applications*, 30(6):16–28, November/December 2010. [page 43]
- [4] W. Aigner, S. Miksch, H. Schumann, and C. Tominski. *Visualization of Time-Oriented Data*. Human-Computer Interaction. Springer Verlag, 2011. [page 69]
- [5] R. Al-Raoush and A. Papadopoulos. Representative elementary volume analysis of porous media using x-ray computed tomography. *Powder Technology*, 200(1-2):69–77, June 2010. [page 14]
- [6] W. Altendorfer. Void Tracking in SiC Particle Reinforced Al. Master’s thesis, Institute of Computer Graphics and Algorithms, Vienna University of Technology, Favoritenstrasse 9-11/186, A-1040 Vienna, Austria, March 2008. [page 70]
- [7] A. Amirkhanov, C. Heinzl, C. Kuhn, J. Kastner, and E. Gröller. Fuzzy CT Metrology: Dimensional Measurements on Uncertain Data. In *Proceedings of the 29th Spring conference on Computer Graphics (SCCG 2013)*, pages 93–101, May 2013. [page 71]
- [8] A. Amirkhanov, C. Heinzl, M. Reiter, and E. Gröller. Visual Optimality and Stability Analysis of 3DCT Scan Positions. *IEEE Transactions on Visualization and Computer Graphics (TVCG)*, 16(6):1477–1487, November/December 2010. [page 41]
- [9] C.L. Bajaj, V. Pascucci, and D.R. Schikore. The Contour Spectrum. In *Proceedings of IEEE Visualization '97 (VIS '97)*, pages 167–173, October 1997. [page 41]
- [10] J.-P. Balabanian, I. Viola, and E. Gröller. Interactive Illustrative Visualization of Hierarchical Volume Data. In *Proceedings of Graphics Interface 2010*, pages 137–144, June 2010. [page 42]

- [11] W. Berger, H. Piringer, P. Filzmoser, and E. Gröller. Uncertainty-Aware Exploration of Continuous Parameter Spaces Using Multivariate Prediction. *Computer Graphics Forum*, 30(3):911–920, June 2011. [page 41]
- [12] S. Beucher. The Watershed Transformation Applied To Image Segmentation. In *Proceedings of the 10th Pfefferkorn Conference on Signal and Image Processing in Microscopy and Microanalysis*, pages 299–314, September 1991. [page 14]
- [13] E. A. Birt and R. A. Smith. A review of NDE methods for porosity measurement in fibre-reinforced polymer composites. *Insight - Non-Destructive Testing and Condition Monitoring*, 46(11):681–686, November 2004. [pages 2 and 5]
- [14] J. Blaas, C.P. Botha, and F.H. Post. Extensions of Parallel Coordinates for Interactive Exploration of Large Multi-Timepoint Data Sets. *IEEE Transactions on Visualization and Computer Graphics (TVCG)*, 14(6):1436–1451, November/December 2008. [page 20]
- [15] U.D. Bordoloi and H.-W. Shen. View Selection for Volume Rendering. In *Proceedings of IEEE Visualization 2005 (VIS 2005)*, pages 487–494, October 2005. [page 20]
- [16] D. Borland and R.M. Taylor. Rainbow Color Map (Still) Considered Harmful. *IEEE Computer Graphics and Applications*, 27(2):14–17, March/April 2007. [page 24]
- [17] A. Brambilla, I. Viola, and H. Hauser. A Hierarchical Splitting Scheme to Reveal Insight into Highly Self-Occluded Integral Surfaces. *Journal of WSCG*, 20(1):57–64, July 2012. [page 42]
- [18] H.M. Britz, J. Jokihaara, O.V. Leppänen, T. Järvinen, and D.M. Cooper. 3D visualization and quantification of rat cortical bone porosity using a desktop micro-CT system: a case study in the tibia. *Journal of Microscopy*, 240(1):32–37, October 2010. [page 19]
- [19] S. Bruckner and T. Möller. Result-Driven Exploration of Simulation Parameter Spaces for Visual Effects Design. *IEEE Transactions on Visualization and Computer Graphics (TVCG)*, 16(6):1467–1475, November/December 2010. [page 41]
- [20] S. Bruckner, V. Šoltészová, E. Gröller, J. Hladůvka, K. Bühler, J. Yu, and B. Dickson. BrainGazer - Visual Queries for Neurobiology Research. *IEEE Transactions on Visualization and Computer Graphics (TVCG)*, 15(6):1497–1504, November/December 2009. [page 41]
- [21] L. Byron and M. Wattenberg. Stacked Graphs - Geometry & Aesthetics. *IEEE Transactions on Visualization and Computer Graphics (TVCG)*, 14(6):1245–1252, November/December 2008. [page 69]
- [22] J. Canny. A Computational Approach to Edge Detection. *IEEE Transactions on Pattern Analysis and Machine Intelligence*, 8(6):679–698, November 1986. [page 14]
- [23] C. Collins, S. Carpendale, and G. Penn. Visualization of Uncertainty in Lattices to Support Decision-making. In *Proceedings of the 9th Joint Eurographics / IEEE VGTC Conference on Visualization 2007 (EuroVis 2007)*, pages 51–58, 2007. [page 71]

- [24] H. Doleisch. SimVis: Interactive visual analysis of large and time-dependent 3D simulation data. In *Proceedings of 2007 Winter Simulation Conference*, pages 712–720, December 2007. [page 20]
- [25] C.C. Dumitrescu and L. Lines. Seismic Attributes used for Reservoir Simulation: Application to a Heavy Oil Reservoir in Canada. *SEG Technical Program Expanded Abstracts*, 27(1):1471–1475, January 2008. [page 19]
- [26] P. Felkel, M. Bruckschwaiger, and R. Wegenkittl. Implementation and Complexity of the Watershed-from-Markers Algorithm Computed as a Minimal Cost Forest. *Computer Graphics Forum*, 20(3):26–35, September 2001. [page 14]
- [27] N. Fout and K.-L. Ma. Fuzzy Volume Rendering. *IEEE Transactions on Visualization and Computer Graphics (TVCG)*, 18(12):2335–2344, December 2012. [page 42]
- [28] L. Fritz, M. Hadwiger, G. Geier, G. Pittino, and E. Gröller. A Visual Approach to Efficient Analysis and Quantification of Ductile Iron and Reinforced Sprayed Concrete. *IEEE Transactions on Visualization and Computer Graphics (TVCG)*, 15(6):1343–1350, November/December 2009. [pages 41 and 69]
- [29] E.R. Gansner, E. Koutsofios, S.C. North, and K.-P. Vo. A technique for drawing directed graphs. *IEEE Transactions on Software Engineering*, 19(3):214–230, March 1993. [pages 70 and 80]
- [30] T. Géraud, L. Plurdal, H. Maître, and I. Bloch. Estimation of Partial Volume Effect using Spatial Context. Application to Morphometry in Cerebral Imaging. In *Nuclear Science Symposium and Medical Imaging Conference Record*, volume 3, pages 1485–1487, October 1995. [pages 7 and 89]
- [31] G. Grigoryan and P. Rheingans. Point-Based Probabilistic Surfaces to Show Surface Uncertainty. *IEEE Transactions on Visualization and Computer Graphics (TVCG)*, 10(5):564–573, September/October 2004. [page 42]
- [32] M. Hadwiger, L. Fritz, C. Rezk-Salama, T. Höllt, G. Geier, and T. Pabel. Interactive Volume Exploration for Feature Detection and Quantification in Industrial CT Data. *IEEE Transactions on Visualization and Computer Graphics (TVCG)*, 14:1507–1514, November/December 2008. [page 20]
- [33] M. Hadwiger, C. Langer, H. Scharsach, and K. Bühler. State of the Art Report 2004 on GPU-Based Segmentation. VRVis Research Center. 2004. [page 13]
- [34] J. Hale. Boeing 787 from the Ground Up. *AERO*, 24:17–23, 2006. [pages xv, 1 and 2]
- [35] M. Harrower and C.A. Brewer. ColorBrewer.org: An Online Tool for Selecting Color Schemes for Maps. *The Cartographic Journal*, 40(1):27–37, June 2003. [pages 24 and 49]
- [36] S. Havre, B. Hetzler, and L. Nowell. ThemeRiver: Visualizing Theme Changes over Time. In *Proceedings of IEEE Symposium on Information Visualization 2000 (InfoVis 2000)*, pages 115–123, 2000. [page 69]

- [37] C. Heinzl, J. Kastner, and E. Gröller. Surface Extraction from Multi-Material Components for Metrology using Dual Energy CT. *IEEE Transaction on Visualization and Computer Graphics (TVCG)*, 13(6):1520–1527, November/December 2007. [page 13]
- [38] C. Heinzl, J. Kastner, T. Möller, and E. Gröller. Statistical Analysis of Multi-Material Components using Dual Energy CT. In *Proceedings of Vision, Modeling and Visualization 2008 (VMV 2008)*, pages 179–188, October 2008. [page 42]
- [39] A. Inselberg. *Parallel Coordinates: Visual Multidimensional Geometry and Its Applications*. Springer Verlag, 2009. [pages 19 and 43]
- [40] C.Y. Ip, A. Varshney, and J.F. Jaja. Hierarchical Exploration of Volumes Using Multilevel Segmentation of the Intensity-Gradient Histograms. *IEEE Transactions on Visualization and Computer Graphics (TVCG)*, 18(12):2355–2363, December 2012. [page 42]
- [41] J. Kastner, B. Plank, D. Salaberger, and J. Sekelja. Defect and Porosity Determination of Fibre Reinforced Polymers by X-ray Computed Tomography. In *Proceedings of the 2nd International Symposium on NDT in Aerospace 2010*, pp. 12, November 2010. [page 2]
- [42] J.M. Kniss, R. Van Uitert, A. Stephens, G.-S. Li, T. Tasdizen, and C. Hansen. Statistically Quantitative Volume Visualization. In *Proceedings of IEEE Visualization 2005 (VIS 2005)*, pages 287–294, October 2005. [page 42]
- [43] B. Kohler, R. Gasteiger, U. Preim, H. Theisel, M. Gutberlet, and B. Preim. Semi-Automatic Vortex Extraction in 4D PC-MRI Cardiac Blood Flow Data using Line Predicates. *IEEE Transactions on Visualization and Computer Graphics (TVCG)*, 19(12):2773–2782, December 2013. [page 69]
- [44] P. Kohlmann, S. Bruckner, A. Kanitsar, and E. Gröller. LiveSync: Deformed Viewing Spheres for Knowledge-Based Navigation. *IEEE Transactions on Visualization and Computer Graphics (TVCG)*, 13:1544–1551, October 2007. [page 20]
- [45] R. Kosara, F. Bendix, and H. Hauser. Parallel Sets: Interactive Exploration and Visual Analysis of Categorical Data. *IEEE Transactions on Visualization and Computer Graphics (TVCG)*, 12(4):558–568, July/August 2006. [page 43]
- [46] A. Lex, M. Streit, C. Partl, K. Kashofer, and D. Schmalstieg. Comparative Analysis of Multidimensional, Quantitative Data. *IEEE Transactions on Visualization and Computer Graphics (TVCG)*, 16(6):1027–1035, November/December 2010. [page 20]
- [47] A. Lex, M. Streit, H.-J. Schulz, C. Partl, D. Schmalstieg, P.J. Park, and N. Gehlenborg. StratomeX: Visual Analysis of Large-Scale Heterogeneous Genomics Data for Cancer Subtype Characterization. *Computer Graphics Forum*, 31(3):1175–1184, June 2012. [page 43]
- [48] L. Lin, M. Luo, H.T. Tian, X.M. Li, and G.P. Guo. Experimental investigation on porosity of carbon fiber-reinforced composite using ultrasonic attenuation coefficient. In *Proceedings of the 17th World Conference on Nondestructive Testing*, October 2008. [page 5]

- [49] K.-L. Ma. Image Graphs - A Novel Approach to Visual Data Exploration. In *Proceedings of IEEE Visualization '99 (VIS '99)*, pages 81–88, 1999. [page 41]
- [50] M.M. Malik, C. Heinzl, and E. Gröller. Comparative Visualization for Parameter Studies of Dataset Series. *IEEE Transactions on Visualization and Computer Graphics (TVCG)*, 16(5):829–840, September/October 2010. [pages 43 and 69]
- [51] J. Marks, B. Andalman, P.A. Beardsley, W. Freeman, S. Gibson, J. Hodgins, T. Kang, B. Mirtich, H. Pfister, W. Ruml, K. Ryall, J. Seims, and S. Shieber. Design Galleries: A General Approach to Setting Parameters for Computer Graphics and Animation. In *Proceedings of the 24th annual conference on Computer graphics and interactive techniques '97 (SIGGRAPH '97)*, pages 389–400, 1997. [page 41]
- [52] D. Mattes, D.R. Haynor, H. Vesselle, T.K. Lewellen, and W. Eubank. Nonrigid Multimodality Image Registration. In *Proceedings of Medical Imaging 2001: Image Processing*, volume 4322, pages 1609–1620, July 2001. [pages 20 and 73]
- [53] G. Mayr, B. Plank, J. Šekelja, and G. Hendorfer. Active thermography as a quantitative method for non-destructive evaluation of porous carbon fiber reinforced polymers. *NDT & E International*, 44(7):537–543, 2011. [pages 5 and 16]
- [54] J.R. Miller. Attribute Blocks: Visualizing Multiple Continuously Defined Attributes. *IEEE Computer Graphics and Applications*, 27(3):57–69, May/June 2007. [page 43]
- [55] N. Otsu. A Threshold Selection Method from Gray-Level Histograms. *IEEE Transactions on Systems, Man and Cybernetics*, 9(1):62–66, March 1979. [pages 14 and 82]
- [56] P. Perona and J. Malik. Scale-Space and Edge Detection Using Anisotropic Diffusion. *IEEE Transactions on Pattern Analysis and Machine Intelligence*, 12(7):629–639, July 1990. [page 13]
- [57] B. Plank, G. Mayr, A. Reh, D. Kiefel, R. Stössel, and J. Kastner. Evaluation and Visualisation of Shape Factors in Dependence of the Void Content within CFRP by Means of X-ray Computed Tomography. In *Proceedings of the 11th European Conference on Non-Destructive Testing (ECNDT 2014)*, pp. 9, October 2014. [page 89]
- [58] A. Reh, A. Amirkhanov, J. Kastner, and C. Gröller, E. Heinzl. Fuzzy Feature Tracking: Visual Analysis of Industrial 4D-XCT Data. Technical Report TR-186-2-15-01, Vienna University of Technology, January 2015. [page 11]
- [59] A. Reh, C. Gusenbauer, J. Kastner, E. Gröller, and C. Heinzl. MObjects - A Novel Method for the Visualization and Interactive Exploration of Defects in Industrial XCT Data. *IEEE Transactions on Visualization and Computer Graphics (TVCG)*, 19(12):2906–2915, December 2013. [pages 11, 69 and 71]
- [60] A. Reh, B. Plank, J. Kastner, E. Gröller, and C. Heinzl. Porosity Maps - Interactive Exploration and Visual Analysis of Porosity in Carbon Fiber Reinforced Polymers. *Computer Graphics Forum*, 31(3):1185–1194, June 2012. [pages 11, 47 and 69]

- [61] M. Reiter, C. Heinzl, D. Salaberger, D. Weiss, and J. Kastner. Study on parameter variation of an industrial computed tomography simulation tool concerning dimensional measurement deviations. In *Proceedings of the 10th Conference on Non-Destructive Testing*, pp. 8, June 2010. [page 30]
- [62] R. Samtaney, D. Silver, N. Zabusky, and J. Cao. Visualizing Features and Tracking Their Evolution. *Computer*, 27(7):20–27, 1994. [page 70]
- [63] J.S.U. Schell, M. Renggli, G.H. van Lenthe, R. Müller, and P. Ermanni. Micro-computed tomography determination of glass fibre reinforced polymer meso-structure. *Composites Science and Technology*, 66(13):2016–2022, October 2006. [page 2]
- [64] J. Schmidt, E. Gröller, and S. Bruckner. Vaico: Visual analysis for image comparison. *IEEE Transactions on Visualization and Computer Graphics (TVCG)*, 19(12):2090–2099, December 2013. [page 43]
- [65] J. Schmidt, R. Preiner, T. Auzinger, M. Wimmer, E. Gröller, and S. Bruckner. YMCA - Your Mesh Comparison Application. In *Proceedings of IEEE Conference on Visual Analytics Science and Technology 2014 (VAST 2014)*, pages 153–162, November 2014. [page 43]
- [66] M. Schöbel, W. Altendorfer, H.P. Degischer, S. Vaucher, T. Buslaps, M. Di Michiel, and M. Hofmann. Internal stresses and voids in SiC particle reinforced aluminum composites for heat sink applications. *Composites Science and Technology*, 71:724–733, February 2011. [pages 66, 70, 73, 82 and 84]
- [67] M. Sezgin and B. Sankur. Survey over image thresholding techniques and quantitative performance evaluation. *Journal of Electronic Imaging*, 13(1):146–165, January 2004. [page 13]
- [68] D. Silver and X. Wang. Tracking and Visualizing Turbulent 3D Features. *IEEE Transactions on Visualization and Computer Graphics (TVCG)*, 3(2):129–141, April 1997. [page 70]
- [69] Rik Stokking, I. George Zubal, and M.A. Viergever. Display of fused images: Methods, interpretation, and diagnostic improvements. *Seminars in Nuclear Medicine*, 33(3):219–227, July 2003. [page 43]
- [70] A. Taylor, B. Plank, G. Standfest, and A. Petutschnigg. Beech wood shrinkage observed at the micro-scale by a time series of X-ray computed tomographs (μ XCT). *Holzforschung*, 67(2):201–205, September 2013. [pages 70, 73 and 81]
- [71] T. Torsney-Weir, A. Saad, T. Möller, H. Hege, B. Weber, J. Verbavatz, and S. Bergner. Tuner: Principled Parameter Finding for Image Segmentation Algorithms Using Visual Response Surface Exploration. *IEEE Transactions on Visualization and Computer Graphics (TVCG)*, 17(12):1892–1901, December 2011. [page 41]

- [72] R. van Pelt, J. Olivan Bescos, M. Breeuwer, R.E. Clough, E. Gröller, B. ter Haar Romenij, and A. Vilanova. Exploration of 4D MRI Blood Flow using Stylistic Visualization. *IEEE Transactions on Visualization and Computer Graphics (TVCG)*, 16(6):1339–1347, November/December 2010. [page 69]
- [73] J. van Wijk and R. van Liere. HyperSlice: Visualization of scalar functions of many variables. In *Proceedings of IEEE Visualization '93 (VIS '93)*, pages 119–125, October 1993. [page 41]
- [74] P. Viola and W.M. Wells III. Alignment by Maximization of Mutual Information. *International Journal of Computer Vision*, 24(2):16–23, June 1997. [page 20]
- [75] J. Waser, R. Fuchs, H. Ribičić, B. Schindler, G. Blöschl, and E. Gröller. World Lines. *IEEE Transactions on Visualization and Computer Graphics (TVCG)*, 16(6):1458–1467, November/December 2010. [page 69]
- [76] J. Weissenböck, A. Amirkhanov, W. Li, A. Reh, A. Amirkhanov, E. Gröller, J. Kastner, and C. Heinzl. FiberScout: An Interactive Tool for Exploring and Analyzing Fiber Reinforced Polymers. In *Proceedings of IEEE Pacific Visualization 2014 (PacificVis 2014)*, pages 153–160, March 2014. [pages 31, 69 and 90]
- [77] J. Weissenböck, D. Salaberger, A. Reh, C. Heinzl, and J. Kastner. Advanced Visualization and Exploration Techniques for Fiber Reinforced Polymers. In *Proceedings of the 11th European Conference on Non-Destructive Testing (ECNDT 2014)*, pp. 10, October 2014. [page 90]
- [78] W.M. Wells III, P. Viola, H. Atsumi, S. Nakajima, and R. Kikinis. Multi-modal volume registration by maximization of mutual information. *Medical Image Analysis*, 1(1):35–51, March 1996. [page 73]
- [79] W. Widanagamaachchi, C. Christensen, P.-T. Bremer, and V. Pascucci. Interactive Exploration of Large-scale Time-varying Data using Dynamic Tracking Graphs. In *Proceedings of IEEE Symposium on Large Data Analysis and Visualization 2012 (LDAV 2012)*, pages 9–17, October 2012. [page 70]
- [80] J. Woodring and H.-W. Shen. Multiscale Time Activity Data Exploration via Temporal Clustering Visualization Spreadsheet. *IEEE Transactions on Visualization and Computer Graphics (TVCG)*, 15(1):123–137, January/February 2009. [page 41]
- [81] R. Xu and D. Wunsch II. Survey of Clustering Algorithms. *IEEE Transactions on Neural Networks*, 16(3):645–678, May 2005. [page 42]
- [82] X. Yuan, H. Xiao, H. Guo, P. Guo, W. Kendall, J. Huang, and Y. Zhang. Scalable Multivariate Analytics of Seismic and Satellite-based Observational Data. *IEEE Transactions on Visualization and Computer Graphics (TVCG)*, 16(6):1413–1420, November/December 2010. [page 20]

- [83] P. Zhigeng and L. Jianfeng. A Bayes-Based Region-Growing Algorithm for Medical Image Segmentation. *Computing in Science and Engineering*, 9(4):32–38, July 2007. [page 14]

Curriculum Vitae

Personal Details

| | |
|----------------|------------------------------|
| Name | Andreas Reh |
| Date of Birth | March 3 rd , 1986 |
| Place of Birth | Linz, Austria |
| Citizenship | Austrian |
| Languages | German, English |

Education

| | |
|-------------------|---|
| since 03/2011 | Doctoral Programme in Technical Sciences (Dr. techn.) Vienna University of Technology, Vienna, Austria Institute of Computer Graphics and Algorithms |
| 10/2008 – 09/2010 | Master's Degree Programme in Software Engineering (M.Sc.) University of Applied Sciences Upper Austria, Hagenberg, Austria School of Informatics, Communications and Media |
| 10/2005 – 07/2008 | Bachelor's Degree Programme in Software Engineering (B.Sc.) University of Applied Sciences Upper Austria, Hagenberg, Austria School of Informatics, Communications and Media |
| 09/2000 – 07/2005 | University-entrance diploma Upper Secondary Technical and Vocational College, Leonding, Austria Department for Informatics and Software Engineering |
| 09/1996 – 07/2000 | High School Landwiedstraße, Linz, Austria |
| 09/1992 – 07/1996 | Elementary School Langholzfeld, Pasching, Austria |

Work and Research Experience

| | |
|-------------------|--|
| since 12/2010 | Research Associate University of Applied Sciences Upper Austria, Wels, Austria School of Engineering and Environmental Sciences Research Group Computed Tomography |
| 11/2009 – 04/2010 | Internship Salzburg Research Forschungsgesellschaft mbH, Salzburg, Austria |
| 04/2008 – 09/2008 | Internship Continental Automotive GmbH, Regensburg, Germany |

Publications

A. Reh, A. Amirkhanov, J. Kastner, E. Gröller, C. Heinzl. Fuzzy Feature Tracking: Visual Analysis of 4D Industrial X-Ray Computed Tomography Data. Technical report TR-186-2-15-01, Institute of Computer Graphics and Algorithms, Vienna University of Technology, pp. 14, January 2015.

C. Heinzl, J. Weissenböck, **A. Reh**, J. Kastner, T. Dierig, T. Günther, R. Stössel. Software tools for robust extraction, analysis and visualization of porosities in XCT scans of fiber-reinforced polymers. 6th Symposium for NDT in Aerospace, Madrid, Spain, November 2014 (Extended abstract reviewed, pp. 8).

J. Weissenböck, **A. Reh**, D. Salaberger, C. Heinzl, J. Kastner. Advanced Visualization and Exploration Techniques for Fiber Reinforced Polymers. 11th European Conference on Non-Destructive Testing (ECNDT 2014), Prague, Czech Republic, October 2014 (Extended abstract reviewed, pp. 9).

B. Plank, G. Mayr, **A. Reh**, D. Kiefel, R. Stössel, J. Kastner. Evaluation and Visualisation of Shape Factors in Dependence of the Void Content within CFRP by Means of X-ray Computed Tomography. 11th European Conference on Non-Destructive Testing (ECNDT 2014), Prague, Czech Republic, October 2014 (Extended abstract reviewed, pp. 9).

J. Weissenböck, A. Amirkhanov, W. Li, **A. Reh**, A. Amirkhanov, J. Kastner, E. Gröller, C. Heinzl. FiberScout: An Interactive Tool for Exploring and Analyzing Fiber Reinforced Polymers. In Proceedings of IEEE Pacific Visualization Symposium 2014 (PacificVis), pages 153-160. March 2014.

A. Reh, C. Gusenbauer, J. Kastner, E. Gröller, C. Heinzl. MObjects - A Novel Method for the Visualization and Interactive Exploration of Defects in Industrial XCT Data. *IEEE Transactions on Visualization and Computer Graphics*, 19(12), pages 2906-2915, December 2013.

A. Reh, B. Plank, J. Kastner, E. Gröller, C. Heinzl. Advanced Visualization Methods for Porosity in Carbon Fiber Reinforced Polymers. *1st International Conference on Tomography of Materials and Structures (ICTMS 2013)*, Ghent, Belgium, July 2013 (Extended abstract reviewed, pp. 4).

J. Kastner, B. Plank, **A. Reh**, D. Salaberger, C. Heinzl. Advanced X-ray tomographic methods for quantitative characterisation of carbon fibre reinforced polymers. *4th International Symposium on NDT in Aerospace*, Augsburg, Germany, October 2012 (Extended abstract reviewed, pp. 9).

A. Reh, B. Plank, J. Kastner, E. Gröller, C. Heinzl. Interactive Exploration and Visual Analysis of Porosity in Carbon Fiber Reinforced Polymers. *4th International Conference on Industrial Computed Tomography (ICT 2012)*, Wels, Austria, September 2012 (Poster).

A. Reh, B. Plank, J. Kastner, E. Gröller, C. Heinzl. Porosity Maps - Interactive Exploration and Visual Analysis of Porosity in Carbon Fiber Reinforced Polymers. *Computer Graphics Forum*, 31(3), pages 1185-1194, June 2012.

M. Vesely, C. Novak, **A. Reh**, H. Mayr. Incremental Navigation Map Enhancement with GPS Tracks from Heterogeneous Sources. In *Proceedings of The 2008 International Conference on Machine Learning; Models, Technologies and Applications in the frame of WORLDCOMP'08-The World Congress in Computer Science, Computer Engineering, and Applied Computing*, pages 787-793, Las Vegas (NV), USA, July 2008.

*When shall we three meet again
in thunder, lightning, or in rain?
When the hurlyburly's done,
when the battle's lost and won.*

SHAKESPEARE, MACBETH